

**PREPARATION AND
CHARACTERIZATION OF
POLYANILINE AND TiO₂ BASED
NANOCOMPOSITE MEMBRANES FOR
WATER PURIFICATION**

Thesis

Submitted in partial fulfillment of the requirements for the degree of
DOCTOR OF PHILOSOPHY

by

VALEEN RASHMI PEREIRA



DEPARTMENT OF CHEMISTRY
NATIONAL INSTITUTE OF TECHNOLOGY KARNATAKA
SURATHKAL, MANGALORE – 575025

December, 2015

DECLARATION

I hereby *declare* that the Research Thesis entitled “**Preparation and characterization of Polyaniline and TiO₂ based nanocomposite membranes for water purification**” which is being submitted to the National Institute of Technology Karnataka, Surathkal in partial fulfillment of the requirements for the award of the Degree of *Doctor of Philosophy* in Chemistry is a *bonafide report of the research work carried out by me*. The material contained in this Research Thesis has not been submitted to any University or Institution for the award of any degree.

Reg. No. 121167CY12F05, Valeen Rashmi Pereira
Department of Chemistry

Place: NITK, Surathkal

Date:

CERTIFICATE

This is to *certify* that the Research Thesis entitled “**Preparation and characterization of Polyaniline and TiO₂ based nanocomposite membranes for water purification**” submitted by **Valeen Rashmi Pereira (Register Number: 121167CY12F05)** as the record of the research work carried out by her is *accepted as the Research Thesis submission* in partial fulfillment of the requirements for the award of degree of **Doctor of Philosophy**.

Dr. Arun M. Isloor
Research Guide

Chairman- DRPC

ACKNOWLEDGEMENTS

No venture can be a success without help, support, guidance, encouragement and contributions of a number of people making it possible. It is my overwhelming pleasure to express my deep felt gratitude towards them.

I express my deep sense of gratitude to my research guide Dr. Arun M. Isloor, Associate Professor, Department of Chemistry, NITK, Surathkal for his inspiration, constant supervision, encouragement throughout the research work and for providing me an exposure to the field of Membrane Technology. I am greatly being owed to him for his support throughout the work.

I thank with pride NITK, Surathkal for providing me the infrastructure and fellowship required to carry out the doctoral research work.

My sincere gratitude towards my RPAC members, Prof. K. Rajendra Udupa, Department of Metallurgical and Materials Engineering and Prof. D. Krishna Bhat, Department of Chemistry, for spending their precious time in evaluating my progress and providing thoughtful suggestions and valuable feedback throughout the research work.

I am very grateful to the present Head of the Department, Prof. B. Ramachandra Bhat, and former Head of the Department, Prof. A. Chitharanjan Hegde for providing the laboratory facilities. I am also thankful to Prof. A. Nithyananda Shetty, Prof. A. Vasudeva Adhikari, Prof. D. Krishna Bhat, Dr. D. Udayakumar, Dr. Darshak R. Trivedi, Dr. Sib Sankar Mal, Dr. Beneesh P.B., Dr. Debashree Chakraborty, Dr. Saikat Dutta, Dr. Noufal Kandoth for their assistance and moral support.

I wish to express my great appreciation to Prof. K. Rajendra Udupa, Prof. K. Narayan Prabhu, Dr. Uday Bhat and Dr. Anandhan Srinivasan (Department of Metallurgical and Materials Engineering, NITK) for allowing me to avail the instrument facility during my research. I am also thankful to Ms. Rashmi (SEM analyst), Mr. Vinayak, Ms. Mrunali Sona for their help in analysis.

I am very thankful to Prof. Ahmed Fauzi Ismail, Advanced Membrane Technology Centre (AMTEC), Universiti Teknologi Malaysia for the analytical support. Special thanks to Dr. Lau Woie Jye, AMTEC, Universiti Teknologi Malaysia

for permitting me to carry out a part of my research work in his laboratory in Malaysia.

I appreciate the support extended by my research group at NITK, including Dr. Rajesh, Dr. Ganesh, Dr. Seema, Mr. Harikrishna, Ms. Irfana, Mr. Raghavendra Hebbar and Mr. Chandrashekar for making my days at NITK during my research a memorable one.

I owe my special thanks to the non-teaching staff of Department of Chemistry, Mrs. Shamila, Mrs. Kasthuri, Mr. Prashanth, Mr. Pradeep, Mr. Harish, Mr. Santhosh, Mrs. Sharmila Mrs. Deepa, Mr. Gopal and Mrs. Reshma who have promptly lent me a helping hand when needed.

I am greatly indebted to my parents, sister and my family for their cooperation, encouragement, support, love and affection. My heartfelt thanks to my friends and all the people who have shared their knowledge, experience, time and assisted me to complete my research work successfully.

VALEEN RASHMI PEREIRA

ABSTRACT

Membrane based separation has proved its efficiency over other traditional techniques of water purification. Significant research had been done in this area, still the abundant scope of membrane technology has driven many scientists to further explore the field. The current research work is one such attempt to study the efficiency of nanomaterials in the polymeric membranes.

This research work is focused on incorporating Polyaniline and TiO₂ based nanocomposites into the polymer membranes and to study the properties and performance of the prepared polymer nanocomposite membranes. Polyvinylidene fluoride and Polysulfone were the two polymers used in this study. The different nanomaterials prepared for this study include Polyaniline nanofibers, Polyaniline coated TiO₂, sulfated TiO₂, Aminated TiO₂. The properties and performance of the membranes was analyzed by cross sectional morphology, surface hydrophilicity, water uptake capacity, surface topography studies, permeation properties, antifouling ability. The self-cleaning ability of the membranes was determined by evaluating the flux recovery ratio. The water purification ability of the membranes was evaluated in terms of heavy metal ion rejection and dye removal studies.

Polyvinylidene fluoride membrane containing 1.0 wt.% of Polyaniline nanofibers exhibited a maximum rejection of 98.52% and 97.38% for Pb²⁺ and Cd²⁺ respectively. Polysulfone membranes containing sulfated TiO₂ were successful in removing Methylene Blue dye up to 90.4% under Ultraviolet radiation. Polyaniline-TiO₂ incorporated Polysulfone hollow fibre membranes showed maximum rejection of 81.5% and 96.5% for Reactive Black 5 and Reactive Orange 16 dyes respectively.

Keywords: *Polyaniline, nanocomposites, heavy metal ion, dye removal*

CONTENTS

CHAPTER 1

INTRODUCTION

1.1 INTRODUCTION TO MEMBRANE TECHNOLOGY	1
1.2 HISTORY OF MEMBRANES	3
1.3 MEMBRANE SEPARATION BASICS	4
1.3.1 Basic Terms in Membrane Science	5
1.4 MERITS AND DEMERITS OF MEMBRANE TECHNOLOGY	7
1.5 CLASSIFICATION OF MEMBRANES	8
1.5.1 Classification of Membranes Based on Driving Force.....	8
1.5.2 Classification of Membranes Based on Morphology	9
1.5.3 Classification of Membranes Based on Pore Size	10
1.6 MEMBRANE PROPERTIES AND MATERIALS.....	11
1.6.1 Nanoparticles in Membranes	13
1.7 MEMBRANE PREPARATION	16
1.8 APPLICATION OF MEMBRANE TECHNOLOGY	18
1.9 LITERATURE SURVEY	19
1.10 AIM AND SCOPE OF THE WORK.....	23
1.11 OBJECTIVES OF THE WORK	24

CHAPTER 2

PREPARATION AND ANTIFOULING PROPERTIES OF POLYVINYLIDENE FLUORIDE (PVDF) ULTRAFILTRATION MEMBRANES WITH POLYANILINE (PANI) NANOFIBRE AND HYDROLYSED PSMA (H-PSMA) AS ADDITIVES

2.1 INTRODUCTION.....	25
2.2 EXPERIMENTAL	28
2.2.1 Materials	28
2.2.2 Preparation of PANI nanofibers	28
2.2.3 Hydrolysis of Polystyrene-co-maleic anhydride (PSMA).....	28
2.2.4 Preparation of PVDF–H-PSMA–PANI membrane.....	29
2.3 CHARACTERIZATION	30
2.3.1 Characterization of PANI nanofibers	30
2.3.2 Characterization of PSMA and H-PSMA.....	30

2.3.3	Characterization of membranes	30
2.3.3.1	Membrane morphology	30
2.3.3.2	Contact angle measurement	31
2.3.3.3	Water uptake measurements	31
2.3.3.4	Water flux study.....	31
2.3.3.5	Antifouling study	32
2.3.3.6	Heavy metal ion rejection	33
2.4	RESULTS AND DISCUSSIONS	34
2.4.1	Characterization of PANI nanofibers	34
2.4.2	FTIR analysis of PSMA and H-PSMA.....	36
2.4.3	Membrane characterization	37
2.4.3.1	Membrane morphology.....	37
2.4.3.2	Contact angle	39
2.4.3.3	Water uptake measurement.....	40
2.4.3.4	Water flux study.....	40
2.4.3.5	Antifouling study	42
2.4.3.6	Heavy metal ion rejection	43
2.5	CONCLUSIONS	45
 CHAPTER 3		
PREPARATION, CHARACTERIZATION AND THE EFFECT OF POLYANILINE (PANI) COATED TiO ₂ NANOCOMPOSITES ON THE PERFORMANCE OF POLYSULFONE ULTRAFILTRATION MEMBRANES		
3.1	INTRODUCTION.....	47
3.2	EXPERIMENTAL	49
3.2.1	Materials	49
3.2.2	Preparation of PANI coated TiO ₂ nanotubes.....	50
3.2.3	Preparation of membranes	50
3.3	CHARACTERIZATION	51
3.3.1	Characterization of PANI coated TiO ₂ nanotubes.....	51
3.3.2	Membrane Characterization	51
3.3.2.1	Morphology of membranes.....	51
3.3.2.2	Atomic Force Microscopy (AFM) measurements	51

3.3.2.3 Porosity and pore size	52
3.3.2.4 Water Uptake and contact angle measurement	52
3.3.2.5 Permeation studies	52
3.3.2.6 Heavy metal ion rejection	53
3.4 RESULTS AND DISCUSSION	53
3.4.1 PANI coated TiO ₂ nanotubes characteristics	53
3.4.2 Membrane characterization	56
3.4.2.1 Membrane morphology	56
3.4.2.2 Surface topography of membranes	57
3.4.2.3 Porosity and pore size of membranes	59
3.4.2.4 Water Uptake	60
3.4.2.5 Contact Angle of membrane surfaces	61
3.4.2.6 Permeation properties	62
3.4.2.7 Antifouling properties	63
3.4.2.8 Heavy Metal Ion Rejection	65
3.5 CONCLUSIONS	67

CHAPTER 4

PREPARATION AND PERFORMANCE STUDIES OF POLYSULFONE-SULFATED NANO-TITANIA (S-TiO₂) NANOFILTRATION MEMBRANES FOR DYE REMOVAL

4.1 INTRODUCTION.....	69
4.2 EXPERIMENTAL	71
4.2.1 Materials	71
4.2.2 Preparation of sulfated TiO ₂	72
4.2.3 Preparation of membranes	72
4.3 CHARACTERIZATION	72
4.3.1 Characterization of S-TiO ₂	72
4.3.2 Characterization of membranes	73
4.3.2.1 Morphology of membranes.....	73
4.3.2.2 Porosity and water uptake of membranes	73
4.3.2.3 Mechanical property of membranes.....	73
4.3.2.4 AFM analysis	73

4.3.2.5 Contact angle of membranes.....	73
4.3.2.6 Water Permeability	74
4.3.2.7 Antifouling ability of membranes.....	74
4.3.2.8 Dye Removal by membranes	74
4.4 RESULTS AND DISCUSSIONS	75
4.4.1 Characterization of S-TiO ₂ nanoparticles.....	75
4.4.2 Membrane characteristics	77
4.4.2.1 Membrane morphology.....	77
4.4.2.2 Porosity and Water Uptake of membranes	80
4.4.2.3 Mechanical strength analysis	80
4.4.2.4 AFM analysis	81
4.4.2.5 Contact Angle of membranes.....	82
4.4.2.6 Water Permeability of membranes.....	84
4.4.2.7 Antifouling nature of membranes	85
4.4.2.8 Dye Removal by membranes	88
4.5 CONCLUSIONS	93

CHAPTER 5

PREPARATION AND CHARACTERIZATION OF POLYSULFONE MEMBRANES CONTAINING TiO₂, SiO₂ 3-AMINOPROPYLTRIETHOXYSILANE (APTES) MODIFIED TiO₂ AND SiO₂ NANOCOMPOSITES

5.1 INTRODUCTION.....	95
5.2 EXPERIMENTAL	97
5.2.1 Materials	97
5.2.2 Modification of TiO ₂ and SiO ₂ nanoparticles	97
5.2.3 Preparation of membranes	97
5.3 CHARACTERIZATION	98
5.3.1 Characterization of aminated TiO ₂ and aminated SiO ₂	98
5.3.2 Characterization of membranes	98
5.4 RESULTS AND DISCUSSIONS	99
5.4.1 FTIR analysis.....	99
5.4.2 Characterization of membranes	101

5.4.2.1 Morphology of membranes.....	101
5.4.2.2 Contact angle and water uptake of membranes	102
5.4.2.4 Permeability of membranes	105
5.4.2.5 Antifouling property of membranes.....	106
5.4.2.6 Heavy metal ion rejection by membranes.....	107
5.5 CONCLUSIONS.....	108
CHAPTER 6	
PREPARATION OF PANI-TiO₂ NANOCOMPOSITE POLYSULFONE HOLLOW FIBER MEMBRANES FOR DYE REMOVAL APPLICATION	
6.1 INTRODUCTION.....	109
6.2 EXPERIMENTAL	111
6.2.1 Materials	111
6.2.2 Preparation of PANI coated TiO ₂ nanotubes	111
6.2.3 Membrane Preparation	112
6.3 CHARACTERIZATION	113
6.3.1 Characterization of PANI coated TiO ₂ nanotubes.....	113
6.3.2 Characterization of membranes	114
6.3.2.1 Membrane Morphology	114
6.3.2.2 Porosity and pore size of membranes	114
6.3.2.3 Water Uptake study.....	114
6.3.2.4 Contact Angle of membranes.....	114
6.3.2.5 Atomic Force Microscopy of membranes.....	115
6.3.2.6 Pure Water Flux measurements	115
6.3.2.7 Antifouling studies.....	115
6.3.2.8 Dye Rejection.....	116
6.4 RESULTS AND DISCUSSIONS	116
6.4.1 PANI coated TiO ₂ nanotubes characteristics	116
6.4.2 Membrane Morphology	116
6.4.3 Porosity, pore size and water uptake of membranes	121
6.4.4 Contact Angle of membranes	122
6.4.5 Surface roughness of membranes	123
6.4.6 Permeation Studies	125

6.4.7 Antifouling property	125
6.4.8 Dye removal by membranes	127
6.5 CONCLUSIONS	129
CHAPTER 7	
SUMMARY AND CONCLUSIONS	
7.1 SUMMARY	131
7.2 CONCLUSIONS	134
LIST OF PUBLICATIONS	137
LIST OF CONFERENCES ATTENDED	137
REFERENCES.....	139
BIODATA.....	158

LIST OF ABBREVIATIONS

AFM	: Atomic Force Microscopy
APS	: Ammonium peroxydisulfate
APTES	: 3-Aminopropyltriethoxysilane
FTIR	: Fourier Transform Infrared Spectroscopy
BER	: Bore Extrusion Rate
BSA	: Bovine Serum Albumin
CDH	: Central Drug House
CTAB	: Cetyltrimethyl ammonium bromide
DER	: Dope Extrusion Rate
DMFC	: Direct Methanol Fuel Cell
EDX	: Energy dispersive X-ray spectroscopy
EIPS	: Evaporation Induced Phase Separation
EY	: Eosin Yellow
FRR	: Fouling Resistance Ratio
GO	: Graphene Oxide
H-PSMA	: Hydrolysed Poly(styrene-co-maleic anhydride)
MB	: Methylene blue
MF	: Microfiltration
M_w	: Average Molecular Weight
NBB	: Naphthol Blue Black
NF	: Nanofiltration
NIPS	: Non-solvent Induced Phase Separation
NMP	: N-methyl-2-pyrrolidone
PAN	: Poly(acrylonitrile)
PANI	: Polyaniline
PEG	: Polyethylene Glycol
PEI	: Polyethyleneimine
PEMFC	: Proton Exchange Membrane Fuel Cell
PES	: Polyethersulfone
PEUF	: Polymer Enhanced Ultrafiltration

ppm	: parts per million
PSf	: Polysulfone
PSMA	: Poly(styrene-co-maleic anhydride)
PVDF	: Polyvinylidene difluoride
PVA	: Polyvinyl alcohol
PVP	: Poly(1-vinylpyrrolidone)
PWF	: Pure water flux
RB-5	: Reactive Black 5
RO	: Reverse Osmosis
RO-16	: Reactive Orange 16
SEM	: Scanning Electron Microscope
SPES	: Sulfonated Polyethersulfone
SWCT	: Single walled carbon tube
TEM	: Transmission Electron Microscope
T _g	: Glass Transition Temperature
TIPS	: Thermally Induced Phase Separation
TMP	: Transmembrane Pressure
VIPS	: Vapor Induced Phase Separation
XRD	: X-ray Diffraction
UF	: Ultrafiltration
UV	: Ultraviolet
UV-Vis	: Ultraviolet-Visible

CHAPTER 1

INTRODUCTION

Abstract

This is an introductory chapter which outlines the need and importance of the current research work on water purification. It deals with the important aspects of polymeric membrane technology, such as membrane separation basics, membrane fabrication process, merits and demerits of membranes, different types of membranes and their applications. The chapter also gives a literature review which justifies the use of nanomaterials as a membrane additive for the present work.

1.1 INTRODUCTION TO MEMBRANE TECHNOLOGY

Water is one of the nature's precious gifts to mankind and is a source of prime importance. Water is very essential for the existence of life on earth. In the 21st century, the most crucial problem afflicting people around the world is global water scarcity. Majority of the earth's water i.e., over 97% of all water on earth is in the oceans. The remaining 3% of the water is available as freshwater out of which 68.7% is locked up in glaciers and icecaps, 30.1% as groundwater and remaining 1% in lakes and rivers which is accessible to human use (Figure 1.1). However the rapid growth in population and economy have resulted in greater demand on the quantity and quality of drinking water, leading to catastrophic water shortage in arid and water-stressed areas. Various organizations report that about 1.2 billion people will be short of access to clean fresh water and about 66% of the world's population may live in water stressed countries by 2025. It is projected that by year 2030, the global needs of water would increase to 6900 billion m³ from the current 4500 billion m³ (Misdan et al. 2012). As a result, the present surface water resources will no longer be sufficient to meet the future needs for mankind.

Many freshwater bodies are being contaminated by industries and human use. Over 1.2 billion people lack access to safe drinking water, 2.6 billion have little or no sanitation, millions of people die annually, 3,900 children a day, from diseases transmitted through unsafe water or human excreta. Countless more are sickened from disease and contamination (Shannon et al. 2008).

Water contamination and scarcity also strongly affects energy and food production, industrial output, and the quality of our environment, affecting the

economies of both developing and industrialized nations. With the increasing water scarcity and rise in wastewater generation each day, treatment of waste water has become inevitable.

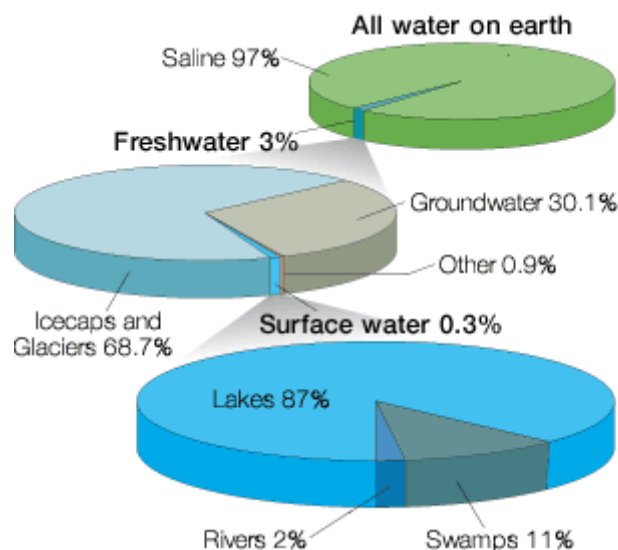


Figure 1.1 Distribution of water on earth (SOPAC Water, Sanitation and Hygiene)

Water reuse continues to rise as demand for fresh water supplies increases worldwide. By recycling and reusing treated wastewater, communities and industries can save on the costs of clean water, ensure adequate supplies and help to preserve a diminishing natural resource. Fortunately, a recent flurry of activity in water treatment research offers hope in mitigating the impact of impaired waters around the world. Numerous researches have been conducted in an effort to develop sustainable technological solutions that would meet increasing water consumption. Some of the alternative sources that have been studied to tackle the fresh water scarcity are the treatment of brackish water, waste water and seawater into clean water. Among them, desalination technology, which converts seawater into clean water, has been regarded as an effective approach due to their abundance in nature (Subramanian and Seeram 2013). Membranes are used for desalination of sea water and brackish water, production of potable water and also for treating industrial effluents.

Thus pollution and scarcity of fresh water around the world, accompanying increasing population and stringent standards of drinking water or wastewater

discharge, make membrane filtration emerge as a competitive alternative in future water treatment processes.

1.2 HISTORY OF MEMBRANES

The first study of membrane phenomena dates back to 1748, when Abbe Nollet placed spirit of wine in a vessel closed with animal bladder, permeation was observed. In 1820, Dutrechet introduced the phenomenon osmosis to characterise flow of liquid through permeable barrier. The first synthetic membrane was developed by Fick in 1855, from nitrocellulose. In some years, i.e., in 1861, Graham carried out first dialysis process using synthetic membranes. For the next 30 years, Traube and Pfeffer worked with osmotic process using artificial membranes.

In 1906, scientist Bechold coined the term Ultrafiltration (UF) and these membranes were used as filters (Singh 2006). Membrane filters were then commercialized in 1927 in Germany. Around 1920s, Reverse Osmosis (RO) was first observed and experimented. However it was not much noticed, until it was rediscovered by Ried and his workers after 30 years. In 1940, Kolff first demonstrated hemodialysis using membranes.

By 1960, membrane science had developed but only at laboratory scale and at industrial application in small scale. A milestone in membrane technology was discovery in 1960, that transformed membrane separation from laboratory scale to industrial production i.e., Loeb and Sourirajan process for making Cellulose Acetate RO membrane by phase inversion. The flux of the first Loeb Sourirajan RO membrane was nearly 10 times higher than any membrane available till then. The work of Loeb and Sourirajan led to the commercialization of RO membranes and also paved a way for the development of Ultrafiltration (UF) and Microfiltration (MF) membrane processes.

With the industrial application of membranes, development of membranes for medical separation processes also progressed individually. By 1960, membrane technology was used in medical field on a large scale. More than a million people are now treated by artificial kidneys, membrane blood oxygenator and controlled drug delivery system.

During 1960 to 1980, major growth was observed in membrane technology. On the basis of L-S method, new methods of membrane preparation like interfacial polymerisation, multilayer composite membranes and also different modules membranes like spiral wound, hollow fibre, capillary modules were developed (Richard 2004). Hence by the end of 1980, UF, MF and RO membranes were well established worldwide.

The major discovery after 1980s was the development of membranes for gas separation process. Most important development was hydrogen separation using membrane introduced in 1980. Within few years gas separation technology evolved and expanded rapidly. In late 1980s, pervaporation technique for dehydration of alcohol was developed which are now at commercial stage.

1.3 MEMBRANE SEPARATION BASICS

Membrane is the heart of every membrane process. Membrane can be defined as a semipermeable active or passive barrier which, under a certain driving force, permits preferential passage of one or more selected species or components of a gaseous and/or liquid mixture or solution (Hsieh 1996).

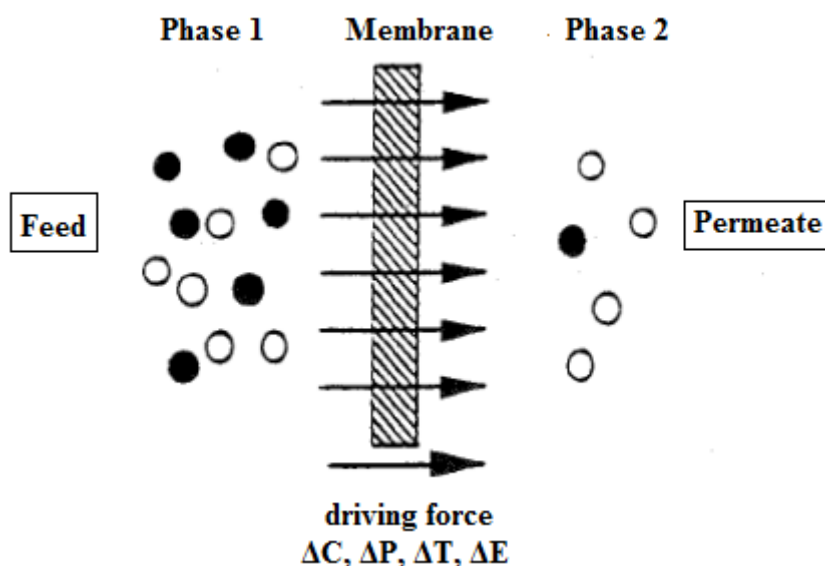


Figure 1.2 Schematic representation of membrane separation

The schematic representation of membrane separation is given in the Figure 1.2. Phase 1 represents the feed and phase 2 represents the permeate. The stream to be treated by the membrane is called the feed. The species passing through the

membrane is called the permeate whereas the species rejected by the membrane is called retentate. Separation through the membrane is achieved because of the ability of the membrane to transport one component from the feed mixture more readily than the other component or components. This separation takes place through different mechanisms for different membrane processes and also depends on the type of membrane used.

Transport through porous membranes occurs through pores by diffusion flow and the selectivity is based on size exclusion (sieving mechanism). The selectivity of the membranes depends on the differences between the particle and pore size. Molecules with size larger than the pore size of the membrane are completely rejected and molecules with smaller size than the pore size can pass through the barrier.

Transport through nonporous membranes is based on solution-diffusion mechanism in which the permeate dissolve in the membrane material and then diffuse through the membrane. Therefore the interactions between the permeate and the membrane material dominate the mass transport and selectivity. Selectivity in these membranes is mainly determined by differences in solubility and/or differences in diffusivity.

The transport rate of a component through a membrane is determined by driving forces such as concentration (ΔC), pressure (ΔP), temperature (ΔT) and electrical potential (ΔE) gradients and the concentration and mobility of the component in the membrane matrix.

1.3.1 Basic Terms in Membrane Science

Flux: Flux is defined as the amount of water passing through unit area of the membrane per unit time. The productivity of the membrane is expressed in terms of flux.

$$J = \frac{Q}{\Delta t \times A} \dots \dots \dots \text{eqn 1.1}$$

where,

'J' is water flux expressed in L/m²h

'Q' is amount of water passing through the membrane in Liter (L)

' Δt ' is the time in hours (h)

' A ' is the effective membrane area responsible for the filtration, expressed in (m^2).

Solute Rejection: The selectivity of a membrane is given in terms of rejection which is expressed as

$$\text{Percent Rejection (\%R)} = \left(1 - \frac{C_p}{C_f}\right) \times 100 \dots \dots \dots \text{eqn1.2}$$

where,

' C_p ' is the concentration of the solute in permeate (can be expressed in M, mM, %)

' C_f ' is the concentration of the solute in feed solution.

- **Fouling:** Fouling is a process in which the suspended or dissolved substances from the feed deposit on the external surface of the membrane, at its pore openings or within the pores (Figure 1.3). This leads to an accumulation of retained material and depletion of the permeating components in the boundary layers adjacent to the membrane surface. Membrane fouling results in flux decline and eventually effects the performance of the membrane over a period of time.

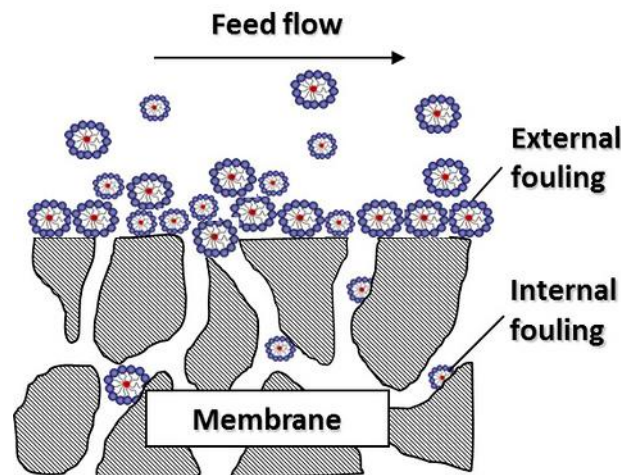


Figure 1.3 Fouling on membrane (The University of Texas, Austin)

- **Water Uptake:** Water uptake capacity of the membrane is expressed as

$$\text{Water uptake (\%)} = \left(\frac{W_w - W_d}{W_w}\right) \times 100 \dots \dots \dots \text{eqn 1.3}$$

where,

'W_w' is the weight of wet membrane

'W_d' is the weight of dry membrane

The water uptake property of a membrane reflects its bulk hydrophilic nature which is a very essential parameter that affects its permeability and antifouling property.

- **Porosity:** Porosity of a membrane is defined as the ratio of the pore volume to geometrical volume. It is given as

$$Porosity \ \varepsilon \ (\%) = \left(\frac{W_w - W_d}{Al\rho} \right) \dots \dots \dots \text{eqn 1.4}$$

where,

'W_w' and 'W_d' are the weights (g) of wet and dry membrane samples respectively, A is the area of the sample (cm²), 'l' is the thickness (cm) and 'ρ' is the density of water (0.998 g/cm³).

1.4 MERITS AND DEMERITS OF MEMBRANE TECHNOLOGY

Benefits

- Membrane processes are energy efficient
- Simple in operation
- Membrane processes can easily be combined with other separation processes
- Separation can be carried out under mild conditions
- Membrane properties are variable and can be adjusted
- Easy to control and scale up

Drawbacks

- The long term reliability is not yet proven
- Membranes may require extensive pretreatment owing to their sensitivity towards concentration polarisation and fouling
- Membranes are not mechanically very robust and can be damaged under the operating conditions (Mulder 1996)

Nevertheless, progress has been done in the recent years, in preparing membranes which have better performance, better chemical and thermal stability and which are less sensitive to operation conditions.

1.5 CLASSIFICATION OF MEMBRANES

A very precise classification of membranes is rather difficult to make, since they can be broadly classified on the basis of their origin, nature, morphology, and application as,

- Biological or synthetic membranes
- Organic or inorganic membranes
- Symmetric or asymmetric membranes
- Porous or non-porous membranes
- Solid, liquid or gel membranes
- Neutral, positive, negative or bipolar membranes

1.5.1 Classification of Membranes Based on Driving Force

The physical and chemical properties of the membrane govern the mechanism by which the separation of solutes is brought about. If the solution contains two or more components, the separation is determined by their transport rate through the interphase. The driving force for this transportation can be concentration gradient ΔC , electrical potential gradient ΔE , pressure gradient ΔP or temperature gradient ΔT (Table 1.1).

- ΔP acts as a driving force and leads to separation of chemical species when the hydrodynamic permeability of the membrane is different for different materials
- When the diffusivity and concentration of various chemical species in the membrane are different for different components, ΔC acts as the driving force
- Difference in electrical potential between two phases separated by membrane, leads to separation of various chemical species when different charged particles show different mobility in the membrane (Porter 1989)

Table 1.1 Classification of membranes on the basis of driving force

ΔP	ΔC	ΔT	ΔE
Microfiltration	Pervaporation	Thermo osmosis	Electrodialysis
Ultrafiltration	Gas separation	Membrane distillation	Membrane electrolysis
Nanofiltration	Dialysis		
Reverse osmosis			

1.5.2 Classification of Membranes Based on Morphology

Membranes can be classified as symmetric and asymmetric membranes depending on their structure and morphology.

- **Symmetric Membrane:** They are characterized by uniform pore size distribution across the membrane (Figure 1.4). They may have either porous or dense structure which can be tuned as per the requirement. These types of membranes are generally prepared by sintering or track etching method.

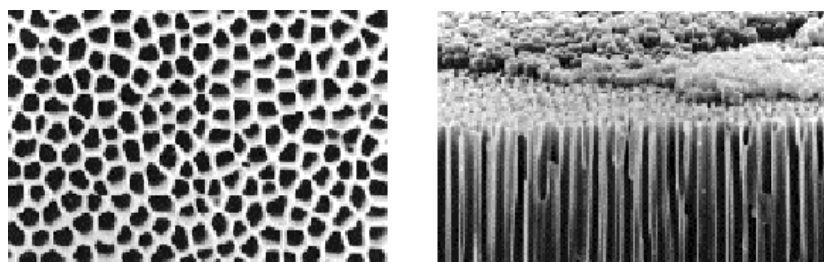


Figure 1.4 Surface and cross section of symmetric membranes

- **Asymmetric Membrane:** Asymmetric membranes form the most widely adopted category of membranes today. The distinguishing features of these membranes lie in their morphology, which comprises of thin-dense surface layer on a porous sub-layer

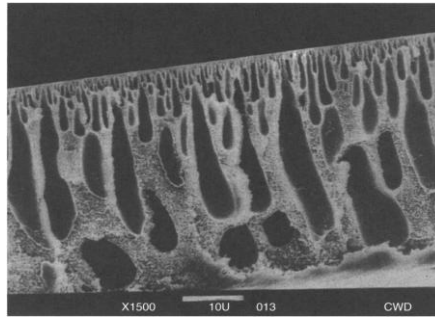


Figure 1.5 Cross section morphology of asymmetric membranes

They are further classified as

- *Integrally skinned asymmetric membrane*: The dense top layer and the porous support are composed of the same material. This type of structure is generally obtained by phase inversion process.
- *Thin film composite membrane*: In this case, an ultra-thin layer of a polymer is deposited on the top of a porous support. The dense active thin layer and the porous support are made up of two different materials. Thus, the thin barrier and the support layers are physically separated.

1.5.3 Classification of Membranes Based on Pore Size

TYPE OF MEMBRANES AND CHARACTERISTICS

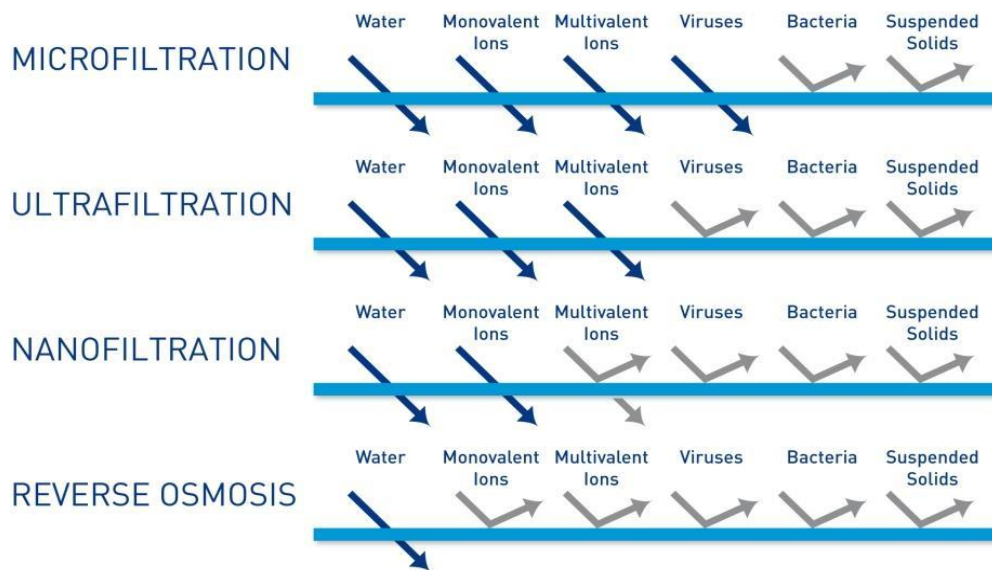


Figure 1.6 Types of membranes based on pore size (Pentair X-Flow)

Membranes are classified into four types depending on their pore size.

1. Microfiltration (MF): The average pore size of these membranes ranges from 0.05 to 2 μm . They operate at a low pressure, below 2 bar. These membranes retain particles by means of sieving. MF are used to remove microorganisms, separate particles, bacteria from other smaller solutes.
2. Ultrafiltration (UF): UF membranes have pore size ranging from 2 nm to 0.05 μm and operating pressure ranging from 2 to 10 bar. They retain particles and macromolecules by sieving mechanism as in MF.
3. Nanofiltration (NF): NF membranes are membranes having pore size less than 2 nm and which operate between the pressures 5 and 40 bar. NF membranes are well known for rejecting organics, multivalent ions.
4. Reverse Osmosis (RO): RO membranes operate at a higher pressure up to 100 bar and having pore size less than 1 nm. They are mainly used in desalination of brackish water and sea water. The mechanism of separation by these membranes is solution diffusion.

1.6 MEMBRANE PROPERTIES AND MATERIALS

Membranes can be prepared from different materials such as polymers, ceramics, glass, metals etc. Commercially used synthetic membranes are prepared using either organic or inorganic materials. However the most important class of materials in membrane preparation are organic i.e. polymers (Mulder 1996). Though all polymers can be used for membrane fabrication only a limited number of polymers are practically used for membrane preparation, taking into account their physical and chemical properties.

Membrane material decides the properties of a membrane. Each material has its own characteristic nature with respect to degree of hydrophilicity, chemical resistance, mechanical strength and flexibility. A good membrane material exhibits following characteristics

1. Film forming ability of the material which results in the formation of cohesive film.

2. Good mechanical strength of the material which can provide strength, flexibility and stability to the film to sustain high operating pressures.
3. Tolerance to temperature variation i.e. T_g of membrane material should be higher than that of the process temperature
4. Tolerance to all feed stream i.e. the material must have the ability to withstand extreme pH conditions and other chemical environment
5. Good hydrophilic and hydrophobic balance to obtain higher flux, better rejection and overall good performance.
6. Minimal fouling during operation

Many membrane materials are now available which satisfy most of the above mentioned properties. Some of them are Polysulfone (PSf), Poly(vinylidene difluoride) (PVDF), Poly(acrylonitrile) (PAN), Polyethersulfone (PES) (Figure 1.7). These materials are hydrophobic but exhibit excellent thermal, chemical and mechanical stability required for a membrane. It may be difficult to have all the above mentioned properties in one single polymer. The polymers can be mixed with inorganic materials such as nanomaterials to enhance the membrane properties.

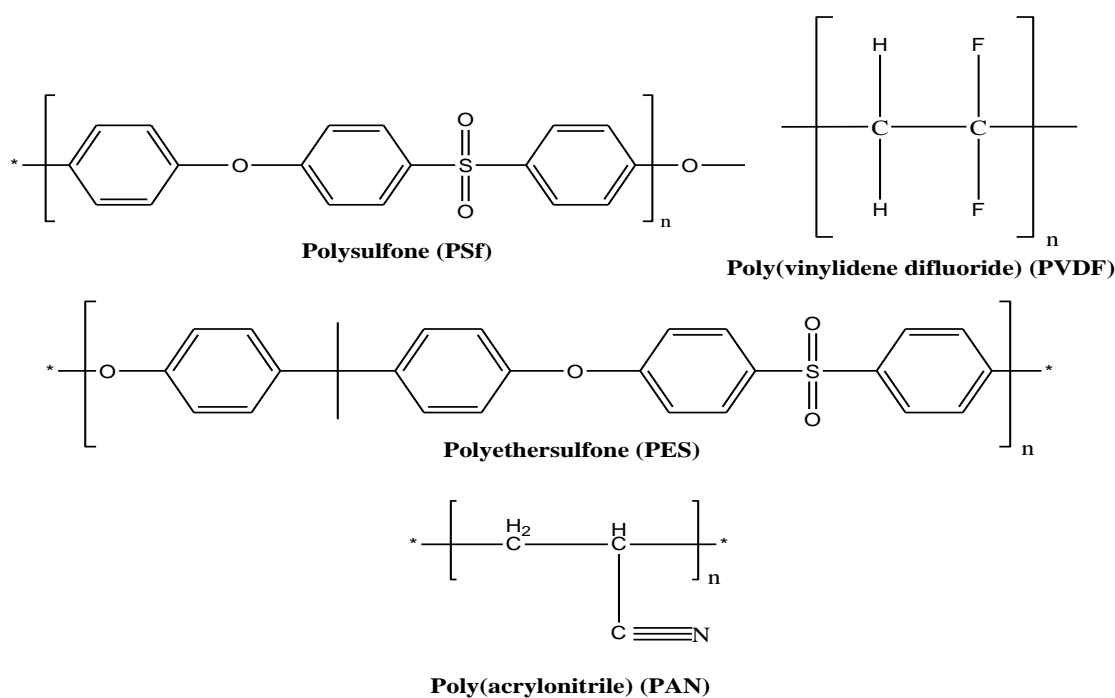


Figure 1.7 Structures of some commonly used polymers in membrane technology

1.6.1 Nanoparticles in Membranes

Synthetic membranes have become the focus of separation processes in different industries. But the common problems faced by polymeric membranes, such as high hydrophobicity, fouling, low fluxes and low mechanical strength have become the focus of researchers in order to improve these disadvantages.

The most common disadvantage associated with the application of the polymer membrane is membrane fouling. The consequence of fouling is the reduction of membrane performance. Severe membrane fouling may require intense chemical cleaning, higher energy demand or membrane replacement. Membrane fouling originates from the attachment of solutes onto the membrane surface or into the internal structure of the membrane. Membrane fouling has usually been explained by pore blocking, cake formation or hydrophobic interaction. However, membrane material is accepted as one of the predominant fouling modulators, with membrane fouling expected to be more severe with hydrophobic than hydrophilic membranes. The fouling materials set up an additional barrier or block the membrane pores preventing the solvent from transporting through the membrane, hence raising the transmembrane pressure and lowering the permeate productivity. There are various solutions available to overcome this disadvantage, such as pre-treatment process installation, membrane surface modifications, chemical and physical membrane cleaning and so on.

However, membrane surface modification has become one of the most important fields in the research. In membrane surface modification, the techniques commonly used are blending, grafting, surface chemical reaction, and nanoparticle incorporation. Although many attempts have been made to modify membrane surfaces by chemical modification such as by grafting hydrophilic monomers on the membrane, the effect is still too small to obtain satisfactory reduction of membrane fouling (Ng et al. 2013). An emerging technology, polymer-nanomaterial composite membranes, dispersing nanoscale fillers into the large polymer matrix, has been attempted to solve some of the issues of permeability, selectivity, fouling, and mechanical strength in the application of water treatment. The presence of finely

dispersed inorganic nanoparticles in the polymer matrix has been proven to be very useful in the improvement of membrane performance.

Polymer-nanomaterial composites, consisting of different couplings of polymers and inorganic nanoparticles, are promising systems for varieties of applications. A lot of combination moieties (polymers and nanomaterials) and methods (*in situ* and *ex situ*) contribute to the extraordinary properties of these polymer-nanomaterial composites. The incorporation of nanoparticles into polymeric membranes has been the trend in the field of membrane research recently.

The nanoparticles can be incorporated with most of the polymeric materials available, in order to produce membranes with specific characteristics, as a result of the synergism of properties between the polymeric materials and nanoparticles. Nanoparticles can affect the selectivity, hydrophilicity, conductivity, mechanical strength, antiviral and antibacterial properties of the polymeric membranes, increased skin layer thickness, a higher surface porosity of the skin, suppress macrovoid formation, permeability of the membrane (although a decreased permeability may also been observed, or a maximum permeability at intermediate nanoparticles loadings) (Kim and Bruggenb 2010). However, the main objective of using nanoparticles is often the fouling mitigation, sometimes combined with water flux enhancement.

Though nanoparticles usually improve the performances of the membranes, they also might change or even deteriorate the performances of the membranes. Incorporation of nanoparticles into polymeric membranes has some disadvantages. An increment in concentration of nanoparticles could lead to an increase in nanoparticles agglomeration. Thus, careful study needs to be done in order to choose the most appropriate types and composition of nanoparticles to be incorporated into polymeric membranes.

The reason behind this approach can be mainly related to the interaction between the two phases: by using well-distributed smaller particles, an enhanced interaction is to be expected, so that the nanoparticles sites are used more effectively for flux enhancement or fouling mitigation. Various characters of these nanomaterials have resulted in different structures and performances of the prepared nanocomposite

membranes. The first challenge for development of nanoparticle enhanced membranes is in the manufacturing process. The simplest approach is to add a well-chosen amount of nanoparticles to the casting solution. However, higher weight percentage of nanoparticles in membranes might deteriorate the performances of membranes and cause losses.

The addition of inorganic oxide nanoparticles causes an increase in tensile strength to some extent. The reason reported was that the free motion of polymeric chains is partly restricted by the intermolecular forces between the polymeric chains and the inorganic oxide nanoparticles. At the same time inorganic oxide nanoparticles are packed by polymeric chains twisting mutually, so the tensile strength of membranes is also improved.

The increased permeability has been ascribed to increased free volume in the polymer matrix caused by the nanoparticles disrupting the packing of the polymer chains. The enhancement in permeability obtained for a given filler loading increases as the primary particle size of the filler decreases. This result is likely related to smaller particles yielding larger polymer/particle interfacial area, since at a fixed volume fraction of particles there are a large number of small particles per unit volume of nanocomposites, which gives them a greater capacity disrupt chain packing, thereby affecting transport property. The macrovoids grow and become run-through at low filler concentration and then are suppressed or disappear at higher filler concentration (Wang et al. 2013). The thickness of skin layer increases with the increase of filler concentration. These findings indicate that the addition of nanoparticles has a large effect on membrane structure.

Whether polymer-nanomaterial composite casting solutions need other additives has been always controversial in recent research. The nanoparticles are apt to aggregate to each other. Therefore, varieties of dispersants or porogens are added to the casting system of the polymer solution to overcome their aggregation and to increase their dispersibility in the casting solution. Dispersion methods of nanomaterials in polymer membranes include differing additions of original nanomaterials, modified nanomaterials, dispersants, and porogens, etc. to overcome their aggregation and to increase their dispersibility in the casting solution.

Threshold content, good dispersion and pore-forming agent (porogen) have become dominating factors during the preparation process of polymer-nanoparticle mixed matrix membranes by the classical phase inversion method. Good dispersion of all the nanomaterials, interlinking with threshold content, is greatly important to the development of membrane structures. Threshold contents of the nanomaterials are different, based on their characters. Beyond the threshold content, all nanomaterials could increase the viscosities of the casting solution and in turn inhibit the development of pore-structures and active layers.

Thus polymer-nanomaterial composite membranes prepared from the classical phase inversion method are of great interest and have been researched extensively in the fields of membrane and water treatment, although the varieties of complexities and controversies are still to be studied.

1.7 MEMBRANE PREPARATION

Various techniques have been developed to prepare permeable films. The selection of a technique for polymer membrane preparation depends on the choice of the polymer, desired structure of the membrane and also application of the membrane (Lalia et al. 2013). The performance of a membrane strongly depends on the membrane structure. Various techniques are used for the preparation of membranes namely

1. Sintering of pressed powder
2. Stretching of films
3. Track etching
4. Phase inversion
5. Template leaching
6. Coating

The most important and frequently used technique is phase inversion. Phase inversion can be described as demixing process where the homogenous polymer

solution is transformed from liquid to solid state in a controlled manner. Phase inversion process involves a ternary system, which contains at least one polymer component, one solvent and a non solvent, where the solvent and the solvent are miscible. During phase inversion, solvent containing polymer solution undergoes transition from one phase to two phase system i.e. liquid-liquid demixing takes place. The two phase system will be consisting of polymer rich phase and solvent-rich or polymer lean phase. At some stage of demixing (as the nonsolvent content increases), the solution becomes thermodynamically unstable and the polymer rich phase gets solidified and hence phase separation takes place. This phase inversion can be achieved by different techniques given below:

1. Non-solvent Induced Phase Separation (NIPS): In this method, the polymer solution is immersed in a coagulation bath containing non solvent usually water. Demixing and precipitation takes place due to exchange of solvent from polymer solution and non solvent from coagulation bath.

2. Thermally Induced Phase Separation (TIPS): In this method, a solvent at elevated temperature and a nonsolvent at lower temperature are used. Thermal energy is used to produce phase separation which on cooling results in the formation of the membrane.

3. Evaporation Induced Phase Separation (EIPS): This method consists of a polymer dissolved in a mixture of volatile solvent and a less volatile nonsolvent. As the evaporation of volatile solvent takes place, polymer solubility decreases leading to phase separation.

4. Vapor Induced Phase Separation (VIPS): In this method, polymer solution is exposed to an atmosphere containing non-solvent, where the demixing is induced because of the absorption of non solvent.

In a membrane process, the performance of a membrane depends strongly on the morphology formed during the phase inversion and subsequent precipitation or

solidification. The phase inversion methods usually result in the formation of asymmetric membranes which are commercially used worldwide.

1.8 APPLICATION OF MEMBRANE TECHNOLOGY

Membranes are used in a broad range of applications. Generally membranes are used for a variety of applications such as for water purification, dyes separation, food processing, pharmaceutical industries etc. However each type of membrane has its own applications as given below.

RO membranes are used for potable water production, municipal water treatment, water/organic separation, food processing industries, removal of environmental pollutants from water. RO membranes are used in textile industries for chemicals recovery and in pulp and paper industry for water reuse.

NF membranes are used in softening of surface and ground water, for removal of organics, removal of pesticides and treatment of textile effluents. NF membranes are good candidates for waste water treatments as they are capable of removing inorganic as well as organic foulants.

UF membranes are used to remove proteins, suspended colloids. They are commonly used for product concentration, treatment of industrial waste water containing heavy metal ions.

MF membranes are used for clarifying liquids. They are used to remove yeast from alcoholic beverages. MF membranes are also used to remove long chain traces of saturated fat from food oils.

Membranes are used in pervaporation process to separate solvent water mixtures or organic solvent mixtures.

Membranes are used in gas and vapour separation equipments for oxygen/nitrogen separation, helium recovery, separation of organic vapors from air.

Energy applications of membranes include their use in fuel cells. Polymeric cation exchange membranes are used in Proton Exchange Membrane Fuel Cell (PEMFC) and Direct Methanol Fuel Cell (DMFC).

Membranes are used in medicine for therapeutic purposes like hemodialysis, hemofiltration and others (Li et al. 2011). More than 1 million uremic patients are treated worldwide by hemodialysis using artificial membranes.

Thus separations using synthetic membranes have been extensively adopted for environmental, energy and biomedical applications

1.9 LITERATURE SURVEY

A significant amount of research has been conducted in the field of water treatment using membrane technology. The use of nanoparticles in the manufacturing process of polymeric membranes has received much attention during the last years. Hybrid membranes comprising inorganic fillers i.e., nanoparticles in a polymer matrix are well known, some of which are given below.

Fan et al. (2008) prepared novel nanocomposite membrane by filtration of polyaniline (PANI) nanofiber aqueous dispersion with Polysulfone (PSf) ultrafiltration (UF) membrane. The nanocomposite membrane showed better permeability due to the hydrophilicity of PANI nanofiber layer when compared with the PSf substrate membrane. In addition, the nanocomposite membrane had positive surface potential under acidic condition because PANI could be protonated easily by acid. During the filtration of Bovine Serum Albumin (BSA) solution, the nanocomposite membrane showed much better antifouling performance than the substrate membrane for the hydrophilicity and steric hindrance effect because of its nanofiber layer.

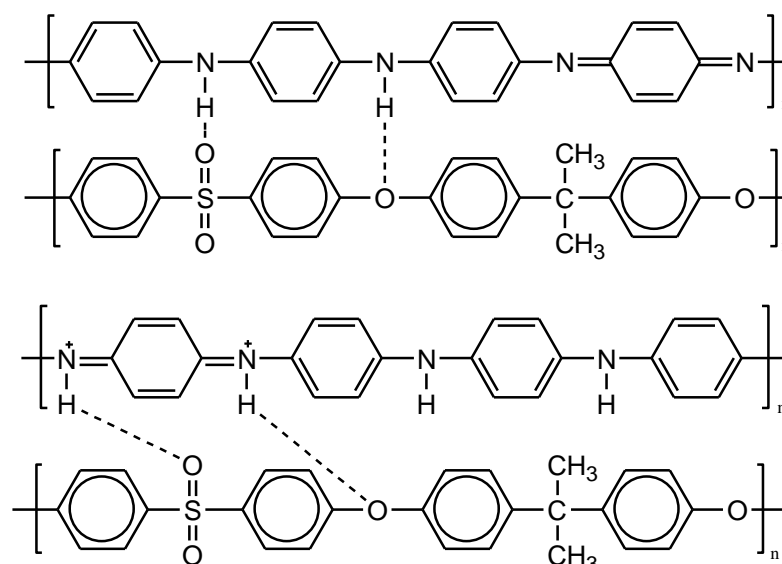


Figure 1.8 Assembly of PANI nanofibers on Polysulfone membranes

Zhang et al. (2012) prepared TiO₂ nanoparticles entrapped poly(vinylidene fluoride) (PVDF) hybrid membranes by impregnating the pre-treated PVDF film in the TiO₂ suspension. The pre-treatment of PVDF with cetyltrimethyl ammonium bromide (CTAB) enhanced the TiO₂ loading. The adsorption behavior of Cu²⁺ on the hybrid membranes was studied, and a promoted adsorption and elution efficiency of PVDF/TiO₂ hybrid membranes were observed compared with that of the pristine PVDF film. It was found that the TiO₂ nanoparticles improved the surface hydrophilicity and permeability of PVDF membranes, and the decreased adsorption capacity of BSA indicated the promoted antifouling ability of PVDF membranes. Also the PVDF/TiO₂ hybrid membranes exhibited potential applications in the separation and pre-concentration of metal ions.

Kim et al. (2012) synthesized sulfonated SiO₂ nanoparticles with uniform core-shell structure and were used as functional fillers for preparing composite proton conducting membranes for direct methanol fuel cells (DMFCs). Poly(4-styrenesulfonic acid) in the shell of SiO₂ nanoparticle contributed well-dispersion of the SiO₂ nanoparticle in the Nafion membrane. The addition of core-shell SiO₂ nanoparticles into Nafion matrix effectively improved membrane performance, including ion exchange capacity, proton conductivity, mechanical strength and methanol permeability.



Figure 1.9 Core-shell structured SiO₂ nanoparticles containing poly(sodium 4-styrenesulfonate)

Vatanpour et al. (2012) studied the influence of boehmite nanoparticles as innovative nanofiller on fabrication of polyethersulfone (PES) blended membrane.

Boehmite is an aluminum oxide hydroxide (γ -AlOOH) particle, containing hydroxyl groups on its surface. The hydrophilicity and pure water flux of the membranes were

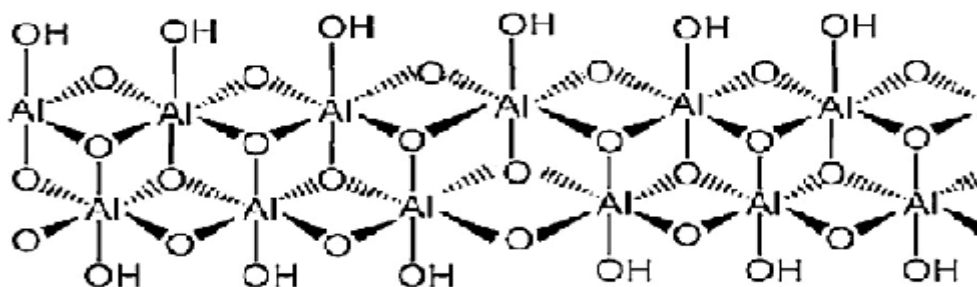


Figure 1.10 Structure of Boehmite (Vatanpour, V., Madaeni, S. S., Rajabi, L., Zinadini, S. and Derakhshan, A. A. 2012)

improved by incorporating of boehmite nanoparticles. Scanning electron microscope (SEM) images showed that the nanoboehmite embedded membranes possessed a typical asymmetric structure. These membranes also showed improved the flux recovery ratio (FRR).

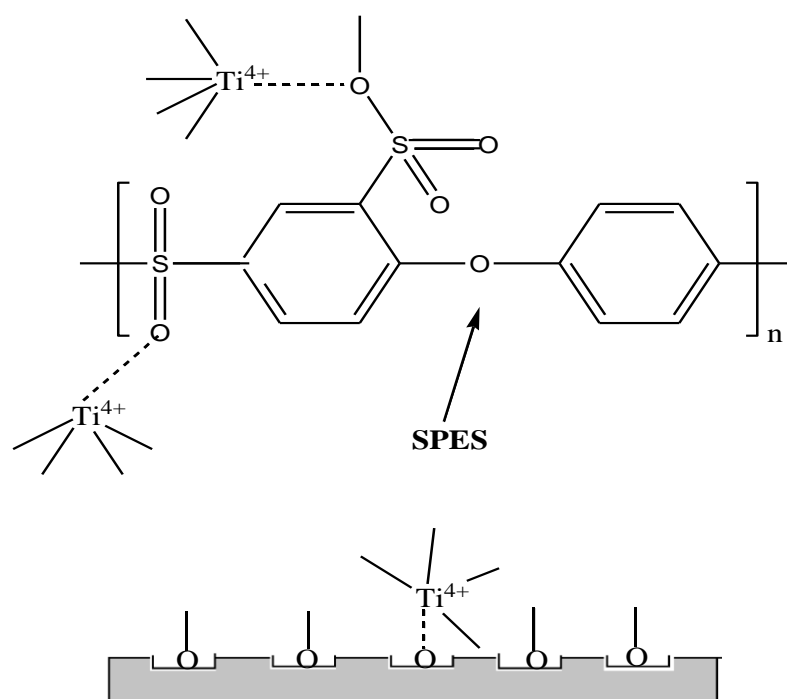


Figure 1.11 Assembly of TiO₂ nanoparticles on the surface of PVDF/PES membrane

Rahimpour et al. (2012) prepared poly (vinylidene fluoride) (PVDF)/sulfonated polyethersulfone (SPES) blend membrane via immersion precipitation. The membranes were modified by depositing of TiO_2 nano-particles followed by UV irradiation to activate their photocatalytic property. The FTIR spectrum confirmed the presence of OH functional groups on the PVDF/SPES membrane structure, which was the key factor for deposition, and self-assembly of TiO_2 nanoparticles on the membrane surface. The contact angle measurements showed that the hydrophilicity of PVDF/SPES membrane was strongly improved by TiO_2 deposition and UV irradiation. UV irradiated TiO_2 deposited PVDF/SPES membranes possess high antibacterial property.

Song and Kim (2013) prepared membranes for ultrafiltration from polysulfone (PSf) composites with poly(1-vinylpyrrolidone) grafted silica nanoparticles (PVP-g-silica). PSf/PVP-g-silica membranes exhibited higher water flux than PSf membranes. The water flux of the membrane containing 1 wt% PVP-g-silica was 2.3 times higher than that of PSf membrane. The hydrophilicity of the PSf/PVP-g-silica membrane also increased with increasing PVP-g-silica content. PSf/PVP-g-silica membranes exhibited enhanced fouling resistance in fouling experiments using nonionic surfactants.

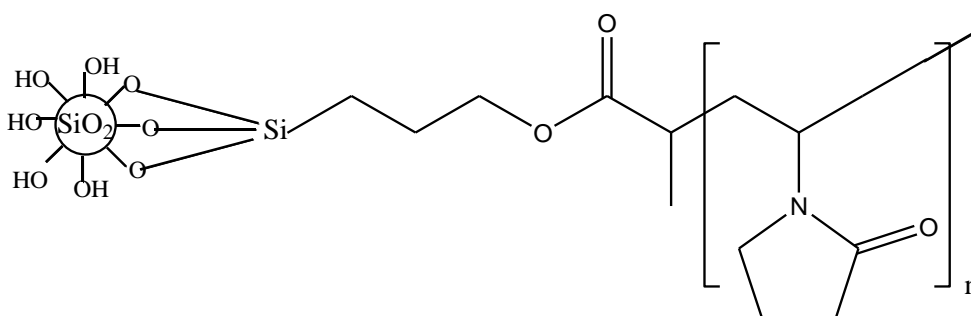


Figure 1.12 Structure of poly(1-vinylpyrrolidone) grafted silica nanoparticles (PVP-g-silica)

Zhao et al. (2013) synthesized poly(vinylidene fluoride) (PVDF)/graphene oxide (GO) ultrafiltration (UF) membranes. SEM images showed that the PVDF/GO UF membranes developed finger-like pore substructure along with the increased

porosity and mean pore size. As revealed by FTIR spectra, large amount of -OH groups appeared due to the introduction of GO nanosheets that improve the surface hydrophilicity of the modified membrane. In permeation experiment, the water flux is improved after blending GO. The flux recovery ratio (FRR) and the fouling resistance results suggested that PVDF/GO UF membranes had better antifouling properties than pure PVDF due to the changes of surface hydrophilicity and membrane morphologies.

Wu et al. (2014) prepared PANI nanofibers and carbonised them. After carbonization, Polyaniline nanofibers were grafted with sulfonic acid groups using concentrated H_2SO_4 . The resultant sulfonated carbonised PANI nanofibers had high conductivity and good hydrophilicity which was able to load 18% of Pt on the surface. These modified nanofibers were tested for PEMFC (Proton Exchange Membrane Fuel Cell). The single cell performance testing showed that an increasing maximum power and maximum current density was achieved with sulfonation time.

Jyothi et al. (2016) prepared aminated Polysulfone– TiO_2 composite membranes. Amine group was introduced into PSf using $\text{Na}_2\text{S}_2\text{O}_4$ and nitrating mixture. Membranes were decorated with different dosages of TiO_2 nanoparticles and the performance of the membranes was studied for chromium removal. The membrane containing 0.4 g of TiO_2 nanoparticles was able to remove chromium (IV) completely from solution at pH 4.

From the above literature survey, it is observed that, nanomaterials have wide scope as membrane materials and can be used for various applications. Keeping these factors in mind the current research work was proposed.

1.10 AIM AND SCOPE OF THE WORK

The aim of the research work is to incorporate different nanoparticles into the polymer membranes and to study the performance of the prepared polymer nanocomposite membranes in water treatment.

From the literature survey, it is found that the incorporation of nanomaterials in the membranes has given interesting and extraordinary results in the water-treatment applications. Even though new fabrication methods using nanomaterials are available, better understanding of the membrane fouling with nanoparticle-enhanced

membranes in water purification and wastewater treatment is still lacking. Further investigation of the properties of various polymeric membranes incorporated with nanoparticles should be carried out in order to find the most appropriate combinations and applications of the membranes fabricated.

1.11 OBJECTIVES OF THE WORK

- To synthesize the nanomaterials/to modify the nanoparticles with hydrophilic groups and to incorporate them into the polymer membranes
- To characterize the prepared/modified nanoparticles by X-ray Diffraction (XRD), Fourier Transform Infrared Spectroscopy (FTIR), Scanning Electron Microscope (SEM) and Transmission Electron Microscope (TEM)
- To incorporate the commercially available nanoparticles into the polymer membranes in order to enhance the properties of the membranes
- To study the morphology of the prepared nanocomposite membranes by SEM
- To investigate the hydrophilicity of the prepared membranes by contact angle measurement and performance by permeation, solution rejection and antifouling nature of the nanocomposite membranes
- To carry out heavy metal ion rejection and dye rejection/removal for selective membranes

CHAPTER 2

PREPARATION AND ANTIFOULING PROPERTIES OF POLYVINYLIDENE FLUORIDE (PVDF) ULTRAFILTRATION MEMBRANES WITH POLYANILINE (PANI) NANOFIBRE AND HYDROLYSED PSMA (H-PSMA) AS ADDITIVES

Abstract

This chapter deals with the preparation of PVDF ultrafiltration membranes with additives such as polyaniline (PANI) nanofibers and hydrolyzed-Polystyrene-co-maleic anhydride (H-PSMA). The variation in properties of the PVDF membranes with the addition of PANI nanofibers is presented. The PVDF membrane containing 1.0 wt. % of PANI nanofibers showed a maximum rejection of 98.52% and 97.38% for Pb^{2+} and Cd^{2+} ions respectively during Polymer Enhanced Ultrafiltration Process (PUEF).

2.1 INTRODUCTION

Ultrafiltration (UF) membranes have been widely used in various separation processes, generally in water treatment (Yan et al. 2005). The properties of a membrane such as its hydrophilicity, high permeability, high surface porosity, good pore structure, and antifouling nature are very crucial and have great influence on membrane performance (Nair et al. 2013, Yan et al. 2006). These properties are usually observed in asymmetric membranes. Among the various polymer materials, polyvinylidene fluoride (PVDF) is one of the outstanding materials that can form asymmetric membranes (Rahimpour et al. 2012, Yan et al. 2005). This homopolymer contains alternating CH_2 and CF_2 groups along the polymer chain making it a distinctive polymer (Figure 2.1), providing high mechanical strength, good chemical resistance, and thermal stability and it exhibits good membrane forming abilities (Yuliwati et al. 2011).

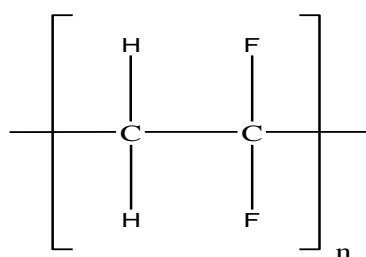


Figure 2.1 Structure of Polyvinylidene fluoride (PVDF)

Most of the polymeric materials applied to water treatment like PVDF are hydrophobic in nature. When a hydrophobic polymer membrane comes in contact with the protein solutions, fouling takes place on the membrane surface. Therefore, use of PVDF often results in intense membrane fouling and tremendous decline of

water flux which limits its use in water treatment (Zhao et al. 2013). Many studies such as physical blending, surface modifications and blending with hydrophilic additives have been performed to improve the hydrophilicity of PVDF membranes. Polystyrene-co-maleic anhydride (PSMA) is a hydrophobic, alternating copolymer having alternating styrene and maleic anhydride units (Figure 2.2). On hydrolysis in alkaline conditions, the anhydride ring of PSMA opens up and gives two carboxylic groups making it hydrophilic and hence can be used as a hydrophilic additive (Martínez et al. 2005). Also in the recent years, modifications on PVDF blends have

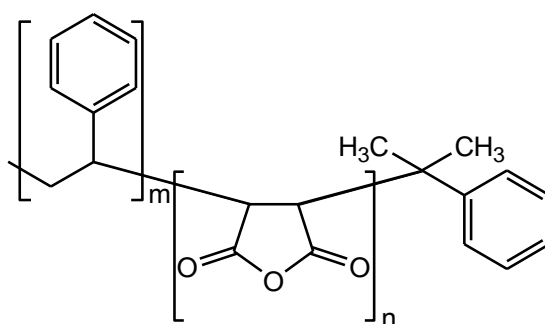


Figure 2.2 Structure of Polystyrene-co-maleic anhydride (PSMA)

been devoted to the blending of polymers with inorganic materials like alumina Al_2O_3 (Yan et al. 2005), silica (SiO_2) (Wu et al. 2013), ZnO (Zhang et al. 2014), and TiO_2 (Shi et al. 2013) nanoparticles. These nanoparticles when used as additives enhance the pore formation and the interconnectivity of pores in the membrane and also improve the membrane hydrophilicity (Razali et al. 2013).

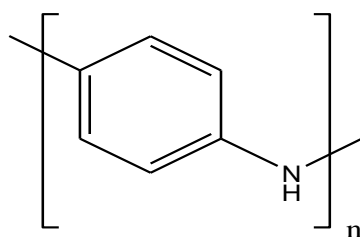


Figure 2.3 Structure of polyaniline

Polyaniline (PANI) is a well-known polymer which has gained importance due to its ease of preparation, high conductivity, chemical stability, and low cost and also exhibits great separation characteristics (Teli et al. 2012). Structure of polyaniline is shown in Figure 2.3. PANI nanofibers possess high surface energy and hydrophilic property because of which they are used to achieve super hydrophilic surfaces (Fan et

al. 2008). PANI has been used to prepare membranes for gas separation, pervaporation and electro dialysis (Teli et al. 2012).

Fan et al. (2008) prepared PSf UF membrane by filtration of PANI nanofibers on the membrane surface, resulting in the formation of layer of PANI nanofibers on the surface of the membrane. The nanocomposite membrane exhibited better permeability, good hydrophilicity due to the presence of PANI nanofibers. The PANI-PSf membranes also showed better antifouling nature because of its hydrophilicity and also because of its steric hindrance effect due to its nanofiber layer.

Zhao et al. (2011) reported polysulfone PSf UF membranes with two different additives such as poly(vinylpyrrolidone) (PVP) and PANI nanofibers and studied their effect on membrane performance. It was observed that at the same content of additive, PSf/PANI membranes exhibited higher protein rejection, antifouling property, higher breaking strength and better additive stability when compared with that of PSf/PVP membranes.

Liao et al. (2013) prepared electroactive switchable UF membrane with single walled carbon tube-PANI (SWCT-PANI) nanofibers as additives. SWCT-PANI nanofibers were prepared by in situ polymerization. These membranes were electrically conductive and exhibited ultrafiltration properties.

Kajekar et al. (2015) prepared PANI nanofibers by interfacial polymerization and used them as additives in PSf hollow fiber membranes along with PVP. The membranes showed maximum rejection of 99.25% for Reactive Red 120 dye. The membrane properties such as PWF, rejection, antifouling nature and thermal resistance increased with the PANI nanofiber content in the membrane. Also the presence of PANI nanofibers resulted in improvement of hydrophilicity of the membranes.

However, the effect of PANI nanofibers on PVDF membranes has not yet been studied by any of the researchers. As PVDF membranes are hydrophobic, an attempt has been made to improve its hydrophilicity by the addition of PANI nanofibers. In the present work, polyaniline (PANI) nanofibers and H-PSMA were used as hydrophilic additives to improve the hydrophilicity of PVDF. Polyaniline nanofibers were added in increasing concentrations into the PVDF-HPSMA

membranes and their effect on membrane performance was studied. To the best of our knowledge it is the first time polyaniline (PANI) nanofibers and H-PSMA were being used as additives in PVDF membranes for increasing the performance.

2.2 EXPERIMENTAL

2.2.1 Materials

PVDF ($M_w \sim 1,80,000$), Poly(styrene-co-maleic anhydride), cumene terminated (PSMA) ($M_n \sim 1600$) and aniline (99.5%) were purchased from Sigma-Aldrich Co., Bangalore, India. Ammonium peroxydisulfate (APS) and Bovine Serum Albumin (BSA) ($M_w \sim 69$ kDa) were purchased from Central Drug House (CDH), New Delhi, India. Hydrochloric acid (HCl) and N-methyl-2-pyrrolidone (NMP) were purchased from Merck India, Ltd. Polyethyleneimine (PEI) ($M_n \sim 60,000$), 50 wt.% aq. solution (branched), was purchased from Acros Organics, USA. Cadmium nitrate tetrahydrate and lead (II) nitrate were purchased from Sigma-Aldrich Co., Bangalore, India.

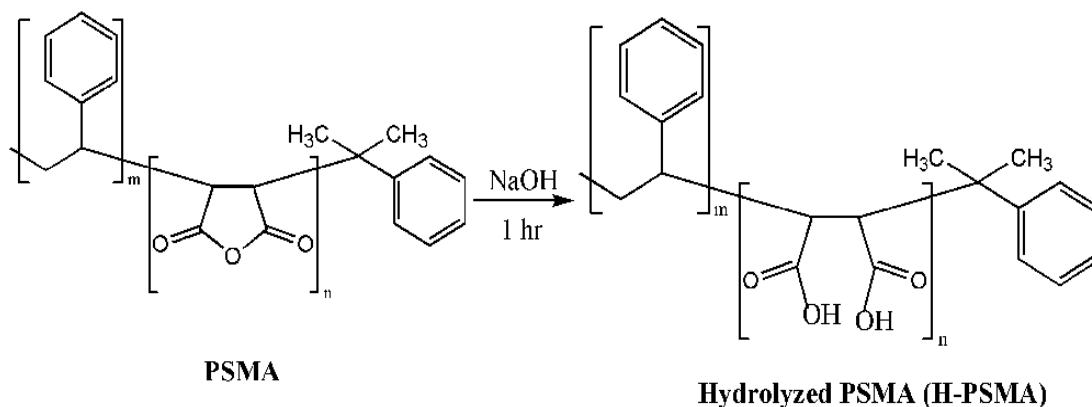
2.2.2 Preparation of PANI nanofibers

PANI nanofibers were prepared by rapidly mixing reactions, a facile one step method using APS as oxidant, following the procedure reported in the literature (Huang and Kaner 2004). First an aqueous solution of 3 mL of aniline in 100 mL of 1M HCl and solution of 1.82 g of APS (0.8 mmol) in 100 mL of 1M HCl were prepared. In the typical reaction, the two solutions were rapidly mixed under stirring at 1000 rpm, to ensure sufficient mixing, at 0°C, using an ice bath. The stirring was stopped when the polymerization was observed where the aqueous dispersion turned to characteristic green color of polyaniline. The product formed was isolated from the dispersion by centrifugation, purified by washing with HCl 3-4 times and then with water until the suspension reached a neutral pH and then dried in oven at 40°C for 24 h, which yielded PANI nanofibers of nearly 2 g.

2.2.3 Hydrolysis of Polystyrene-co-maleic anhydride (PSMA)

PSMA was subjected to hydrolysis in aqueous solution under alkaline conditions (Scheme 2.1). PSMA (2 g) was added to 100 mL of 1 N NaOH solution and stirred for 1 h until complete dissolution took place. The hydrolyzed-PSMA (H-

PSMA) was precipitated by adding 1 N HCl drop wise until white precipitate was obtained. The hydrolyzed product was washed with water to neutralize the acid and kept for drying in oven for 24 h.



Scheme 2.1 Hydrolysis of PSMA

2.2.4 Preparation of PVDF–H-PSMA–PANI membrane

PVDF–H-PSMA–PANI membranes were prepared by immersion precipitation method (Padaki et al. 2011) as follows. At first 2 wt.% of H-PSMA was dissolved in NMP under stirring. Then the synthesized PANI nanofibers were added to the solution. The solution containing PANI nanofibers was sonicated using sonicator at a frequency of 40 KHz at 25°C for 30 min for their uniform dispersion and then kept under stirring. Then 20 wt.% PVDF was added to the same dispersion and stirred for 15 h at 70°C. After the complete dissolution of PVDF, the casting solution was sonicated for 35°C at a frequency of 40 KHz for 15 min and left still for 30 min to remove any trapped air bubbles. The solution was then casted on to the glass plate and dipped in the water coagulation bath for 24 h for the phase inversion to occur. The PVDF and H-PSMA concentration in the casting solution was fixed at 20 and 2 wt.% respectively for all the membranes, whereas the concentration of PANI nanofibers was varied as 0, 0.1, 0.5, 1.0, and 1.5 wt.% and accordingly the membranes were labeled as M0, M1, M2, M3, and M4. The concentration of H-PSMA was fixed at 2 wt.% for all the membranes in order to evaluate the effect of addition of PANI nanofibers in the membrane with increasing concentration. Figure 2.4 shows the images of the prepared membranes. As the content of PANI nanofibers increased in

the membranes, the membranes became uniformly white to blue, blue to green in color, showing the uniform dispersion of PANI nanofibers in the membranes.

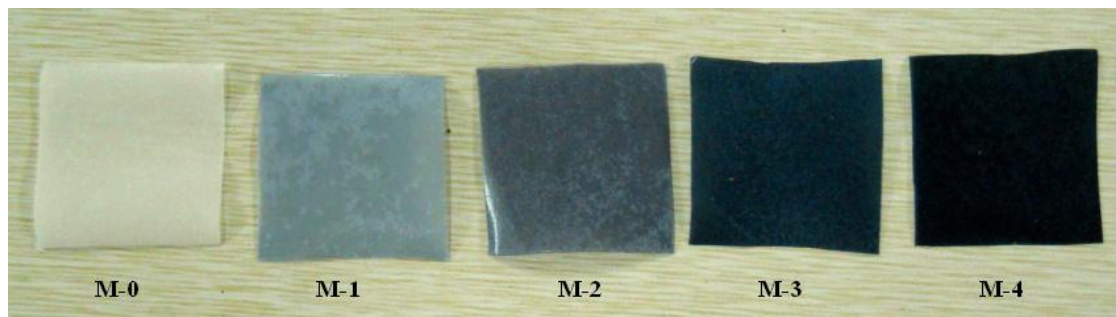


Figure 2.4 Images of the prepared membranes

2.3 CHARACTERIZATION

2.3.1 Characterization of PANI nanofibers

FTIR spectrum and X-ray Diffraction (XRD) pattern were obtained to confirm the formation of PANI nanofibers. An ATR-FTIR spectrophotometer (JASCO 4200) was used to obtain the IR spectrum. XRD pattern was obtained from Rigaku Miniflex 600 with Cu K α radiation. Scanning electron microscope (JEOL JSM-6380LA) and transmission electron microscope (JEOL JEM-2100) were used to observe the morphology of the PANI nanofibers.

2.3.2 Characterization of PSMA and H-PSMA

ATR-FTIR spectrophotometer (JASCO 4200) was used to record the IR spectra of the PSMA and H-PSMA in the range of 4000–650 cm⁻¹.

2.3.3 Characterization of membranes

2.3.3.1 Membrane morphology

The morphology of the prepared membranes was analyzed by taking the cross sectional images of the membranes using scanning electron microscope (SEM). The membrane samples were frozen in liquid nitrogen and broken and then sputtered with gold for electron conductivity before they were observed under scanning electron microscope (JEOL JSM-6380LA).

2.3.3.2 Contact angle measurement

The contact angle of the membranes was measured using FTA-200 dynamic contact angle analyzer by sessile droplet method (Padaki et al. 2011). In order to minimize the experimental error, for each sample, the contact angle was measured at three different locations on the membranes and the average value was reported (Kumar et al. 2013).

2.3.3.3 Water uptake measurements

Membrane samples were cut into 1 cm² size and immersed in distilled water for 24 h and weighed immediately after removing the surface water. The wet membranes were dried in a vacuum oven for 3 h at 45°C, and then the dry membrane samples were weighed (Arthanareeswaran et al. 2008). From the dry and wet weights of the samples, the water uptake was calculated using the following equation

$$\% \text{ water uptake} = \left(\frac{W_w - W_d}{W_w} \right) \times 100 \dots \dots \text{eqn 2.1}$$

where, W_w and W_d are weights of the wet and dry membrane samples respectively.

2.3.3.4 Water flux study

The pure water flux (PWF) of the membranes was tested using dead end filtration cell (Figure 2.5). An effective membrane area of 5 cm² was used for the permeation studies. The membranes were kept immersed in water for 24 h before carrying out the permeation experiments. Initially the membranes were subjected to compaction at 0.4 MPa transmembrane pressure (TMP) for 30 min. Then time dependent pure water flux of the different membranes was measured at 0.2 MPa TMP at 25°C for every 1 min time interval (Nair et al. 2013). The PWF of the membranes was calculated using the following equation.

$$J_w = \frac{Q}{A \Delta t} \dots \dots \dots \text{eqn 2.2}$$

where, J_w is the pure water flux expressed in L/m²h and Q is the amount of pure water collected in liters (L) for time Δt (h) using effective membrane area of A (m²).

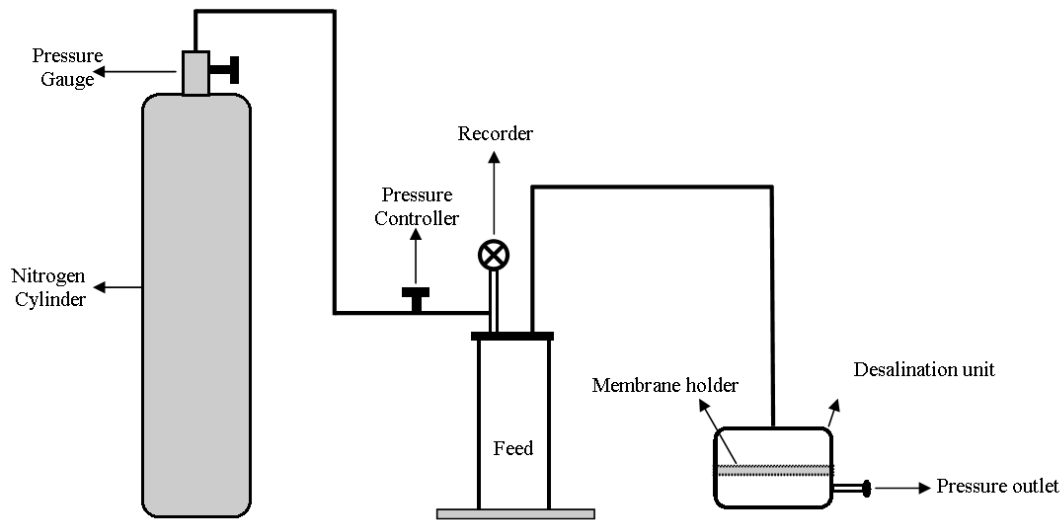


Figure 2.5 Schematic representation of lab scale dead end filtration cell set up

2.3.3.5 Antifouling study

The antifouling property of the membranes was studied as follows (Kumar et al. 2013, Nair et al. 2013). First the pure water flux J_{w1} (L/m^2h) of the membranes was measured at 0.2 MPa TMP. In order to study the antifouling property of membranes, BSA was taken as the model protein. An aqueous solution of BSA with concentration of 0.8 g/L was prepared and was fed into the filtration cell and was filtered through the membranes for 30 min. After the BSA filtration, the membranes were flushed with pure water for 20 min and then the water flux J_{w2} (L/m^2h) was measured again. In order to evaluate the antifouling property of the membranes, the flux recovery ratio (FRR) was calculated by the equation

$$FRR (\%) = \frac{J_{w2}}{J_{w1}} \times 100 \dots \dots \dots eqn 2.3$$

The concentration of BSA in the feed and the permeate was measured using UV-spectrophotometer at a wavelength of 280 nm (Kumar et al. 2013). The BSA rejection % of the membranes was calculated using the following equation

$$\%R = \left(1 - \frac{C_p}{C_f} \right) \times 100 \dots \dots \dots eqn 2.4$$

where, C_p (mg/ml) and C_f (mg/ml) are concentrations of BSA in permeate and feed respectively.

2.3.3.6 Heavy metal ion rejection

The heavy metal ion rejection study by the membranes was performed as per the literature (Nagendran et al. 2008). Here Polyethyleneimine (PEI) was used as a complexing agent, to complex with the metal ions (Figure 2.6). Briefly, aqueous solution of Pb^{2+} and Cd^{2+} was prepared in PEI solution at a concentration of 1000 ppm. PEI solution was prepared by dissolving 1 wt.% of PEI in deionized water. Then the pH of the solution was adjusted to 6.25 using 0.1 N HCl and NaOH. The solutions containing PEI and metal ions were thoroughly mixed individually and left for 5 days for the complete binding between PEI and the metal ions. Then metal ion complexed PEI solution was fed into the filtration set and was filtered through the membranes. Permeate was collected in order to study the rejection of the metal ions by membranes. Concentration of the metal ions in the feed and permeate was evaluated using Atomic Absorption Spectrophotometer (GBC 932 Plus). Metal ion rejection percentage by the membranes was calculated using the formula

$$\%R = \left(1 - \frac{C_p}{C_f}\right) \times 100 \dots \dots \dots eqn 2.5$$

where C_p (mg/mL) and C_f (mg/mL) are concentrations of metal ions in the permeate and the feed respectively.

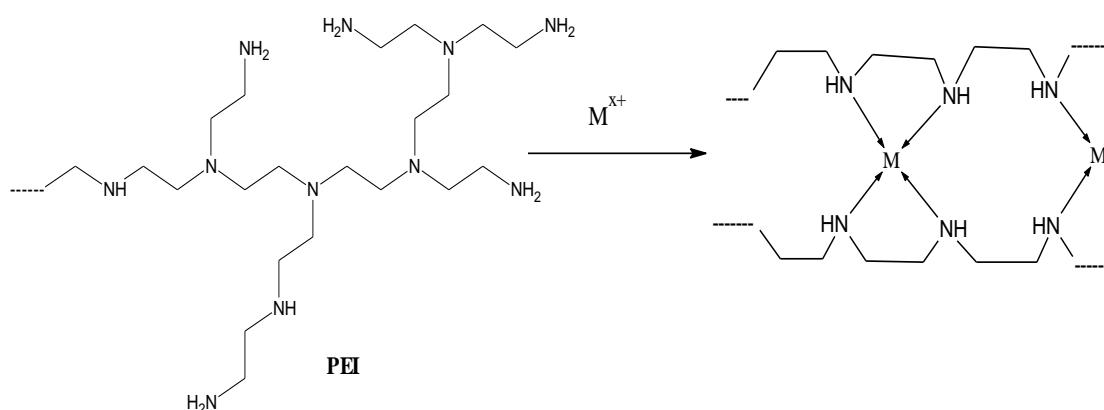


Figure 2.6 Metal ion complexation by PEI

2.4 RESULTS AND DISCUSSIONS

2.4.1 Characterization of PANI nanofibers

The FTIR spectrum of PANI nanofibers is shown in Figure. 2.7. The spectrum contains all the characteristic peaks of PANI. The peaks at 1570 and 1490cm^{-1} correspond to the C=N and C=C stretching vibrations of quinoid and benzenoid rings of PANI. Peaks at 1299 and 1244 cm^{-1} are due to the stretching mode for the benzenoid ring and the peak at 828 cm^{-1} can be ascribed to out of plane bending of C-H.

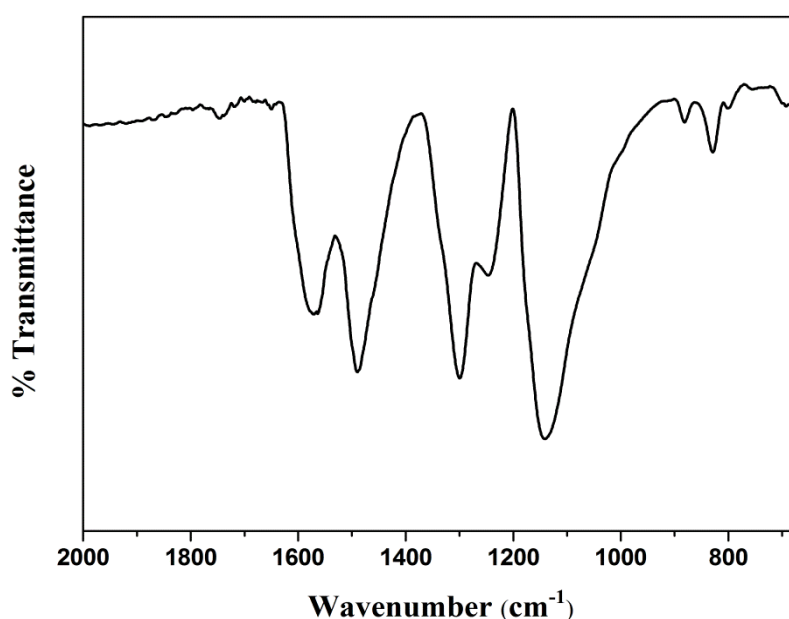


Figure 2.7 FTIR spectrum of PANI nanofibers

X-ray Diffraction (XRD) pattern of PANI nanofibers is shown in Figure 2.8. Two broad peaks at $2\theta=17^\circ$ and 23° with respect to (111) and (110) planes appear in the pattern, which also indicates amorphous nature of PANI (Bhaiswar et al. 2013).

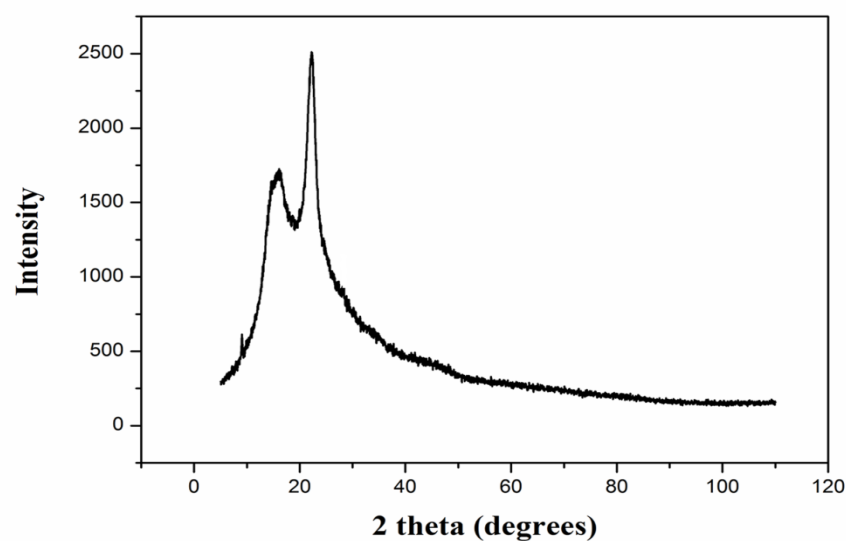


Figure 2.8 X-ray Diffraction pattern of PANI

Figure 2.9 shows the SEM image of synthesized PANI nanofibers. From SEM, it was found that, prepared nanofibers had uniform diameter of 96.3 nm. Figure 2.10 shows the TEM image of the PANI nanofibers.

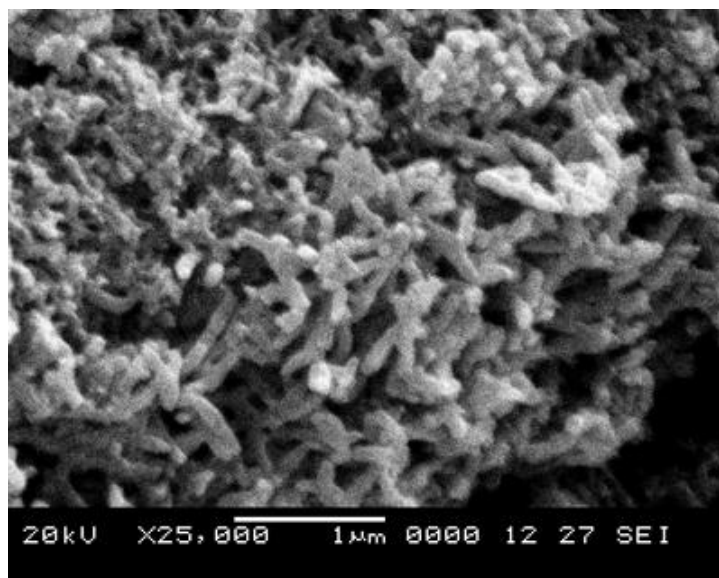


Figure 2.9 SEM image of PANI nanofibers

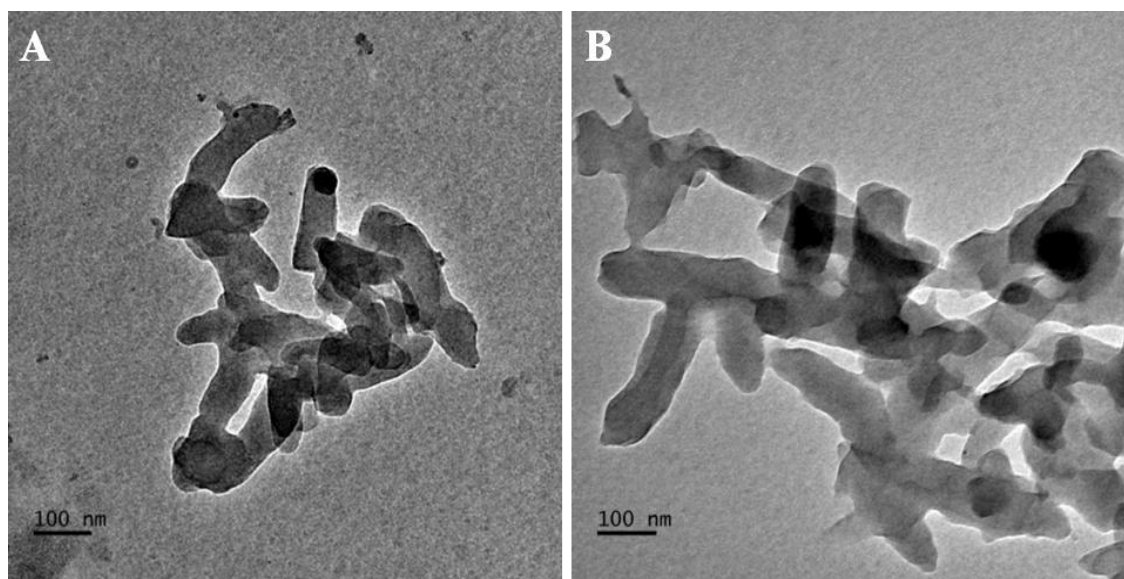


Figure 2.10 TEM images of the PANI nanofibers (A and B)

2.4.2 FTIR analysis of PSMA and H-PSMA

The FTIR spectra of PSMA and H-PSMA are shown in Figure 2.11. The IR spectrum of PSMA shows two bands at 1853 and 1774 cm^{-1} which can be attributed to the five ring cyclic anhydride which correspond to the maleic anhydride groups in PSMA (Haddadine-rahmoun et al. 2008). The IR spectra of H-PSMA show the absence of these two bands and show a new peak at 1701 cm^{-1} which corresponds to the carbonyl stretching frequency of the carboxylic acids present in H-PSMA. Also a broad band appears at around 3397 cm^{-1} which is due to the -OH stretching of carboxylic groups in H-PSMA.

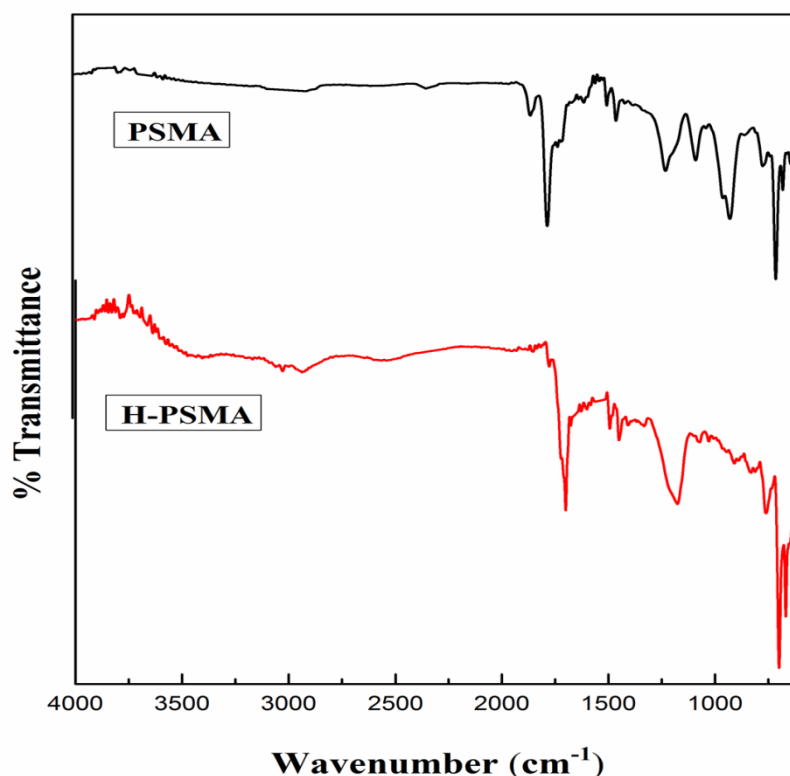


Figure 2.11 FTIR Spectra of PSMA and H-PSMA

2.4.3 Membrane characterization

2.4.3.1 Membrane morphology

The SEM cross-sectional images of membranes with different contents of PANI nanofibers are shown in Figure 2.12. All the membranes exhibit typical asymmetric structure with dense top layer, porous sublayer and fully developed macropores at the bottom (Teli et al. 2013). The pristine PVDF–HPSMA membrane showed macrovoids in the sublayer, whereas the macrovoids in the PANI nanofiber incorporated membranes were suppressed. Also long finger like projections were observed in the PANI incorporated PVDF–HPSMA membranes. It was observed that the finger like projections in the membranes increased with increasing length as the concentration of PANI nanofibers increased. The change in morphology of the membranes with PANI nanofibers can be attributed to the phase inversion process taking place during the membrane formation (Zhao et al. 2012). The addition of PANI nanofibers reduces the miscibility of the casting solution with water which accelerates

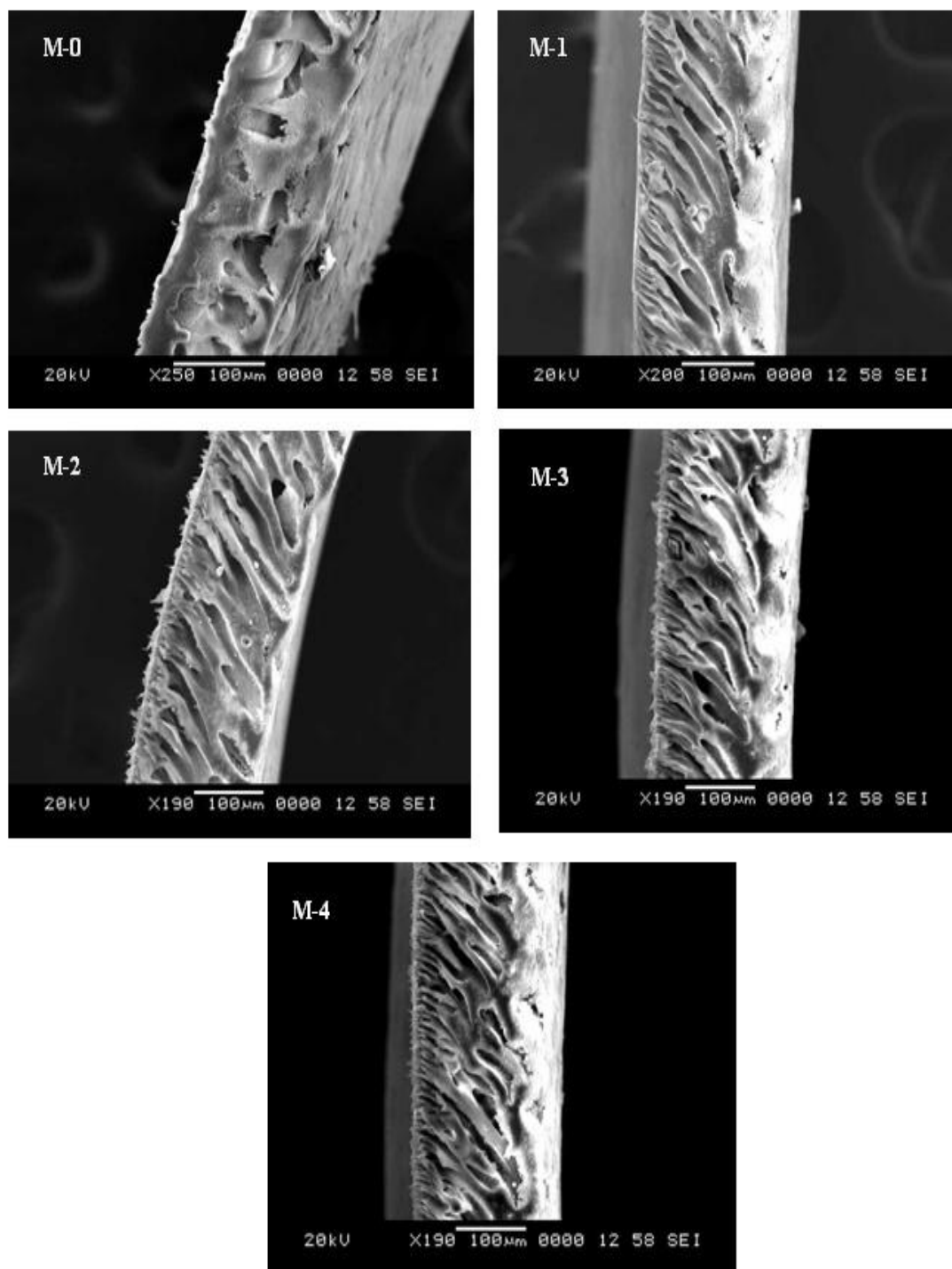


Figure 2.12 SEM cross-sectional images of membranes

the phase inversion process. Also some amount of the additive, H-PSMA may diffuse into the coagulation bath during the phase inversion. Thus the PANI nanofibers and

H-PSMA act as the hydrophilic and pore forming agents respectively during the phase inversion process. The presence of PANI nanofibers in the casting solution resulted in the good interconnection between the pores due to the migration of PANI nanofibers and also the pores become run through giving the long finger like projections during the membrane formation (Zhao et al. 2011, 2012). Thus PVDF–H-PSMA–PANI membranes had long finger like projections than the pristine PVDF–H-PSMA membrane.

2.4.3.2 Contact angle

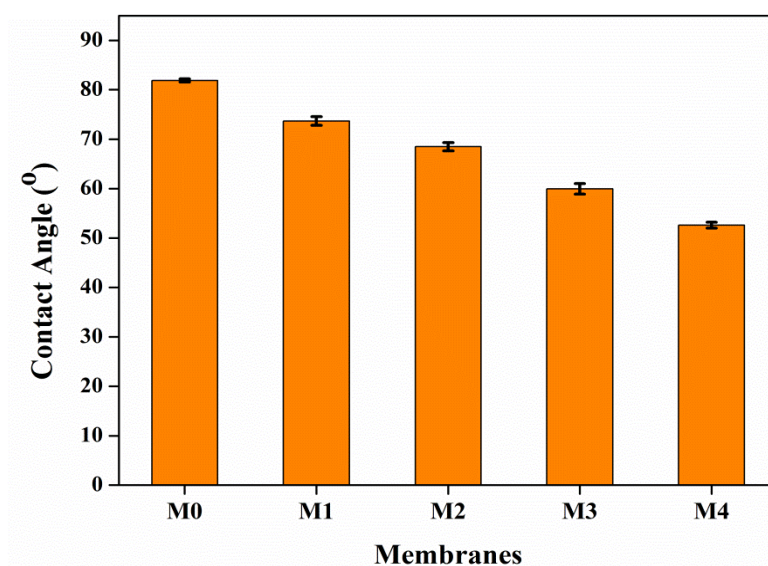


Figure 2.13 Contact angle of membranes

The surface hydrophilicity of the membranes was determined by using contact angle instrument. Lower the contact angle, more hydrophilic is the membrane. Among the prepared membranes, M0 membrane which did not contain any PANI nanofibers showed the highest contact angle of 81.6°, whereas M4 membrane with highest PANI content showed the lowest contact angle of 52.2°. The contact angle of the prepared membranes decreased gradually in the order M0>M1>M2>M3>M4 as shown in Figure 2.13, indicating that the membrane hydrophilicity increases with the increase in concentration of PANI nanofibers. The increase in hydrophilicity with PANI nanofibers can be assigned to the porous nature of PANI (Teli et al. 2013).

2.4.3.3 Water uptake measurement

Water uptake by the property depends on the porosity of the membranes. The water uptake by the membranes increased in the order $M_0 < M_1 < M_2 < M_3$ as the PANI content increased, after which the water uptake decreased for M_4 membrane (Figure 2.14). The increase in water uptake is due to the increase in internal porosity of the membranes with the increase in PANI content. The decrease in water uptake for M_4 can be explained by the higher concentration of PANI. When the concentration of PANI is more than 1.0 wt.%, PANI nanofibers may agglomerate and block the membrane pores resulting in reduced water uptake.

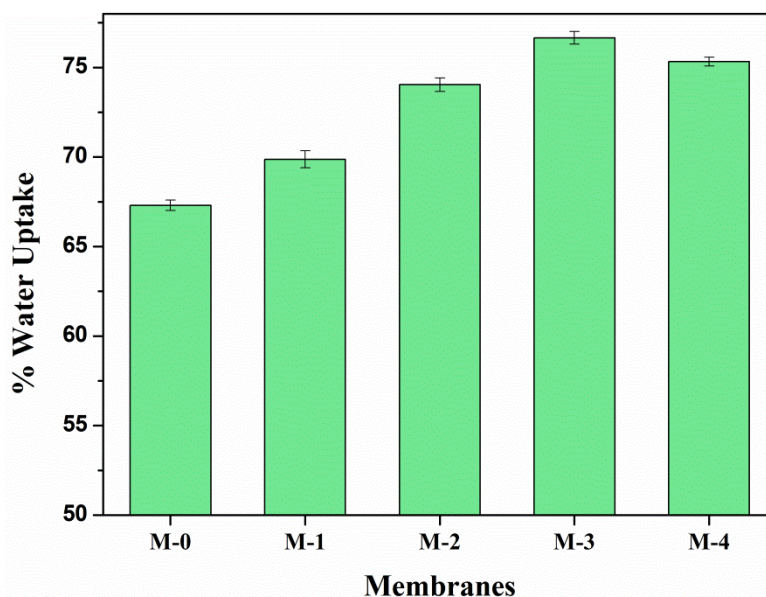


Figure 2.14 Water uptake of membranes

2.4.3.4 Water flux study

Figure 2.15 shows the pure water flux of the membranes. From the figure it is evident that, PANI nanofiber incorporated membranes showed higher flux than the pristine PVDF–H-PSMA membrane. The increase in flux of the membranes with PANI content may be due to the more hydrophilic surface, greater porosity, better interconnected pores and longer pore length. Also the number of pores in the skin layer increased with the content of PANI (Figure 2.12). These factors lowered the resistance of water permeability through the membranes, and forced the water through the membranes which improved the membrane permeability (Teli et al. 2013).

However the decrease in flux was observed for M4 membrane with highest content of PANI. Similar results were observed during the membrane permeation studies in PANI incorporated membranes (Zhao et al. 2011, Zhao et al. 2012). The decrease in water flux by the membrane at 1.5 wt.% of PANI may be the result of agglomeration of PANI nanofibers which occurs at higher loading of PANI. This results in blocking of membrane pores causing improper distribution of nanofibers in the membrane, in turn decreasing the membrane permeability. The stability of hydrophilic additive in the membrane also affects the membrane performance. The M4 membrane, with 1.5 wt.% PANI, showed leaching of PANI during the phase inversion process to some extent. The loss of PANI might have been responsible for the decreased permeability (Zhao et al. 2012). However the water flux of all the membranes including the membrane M4 with 1.5 wt.% of PANI was much higher than the pristine PVDF–H-PSMA membrane.

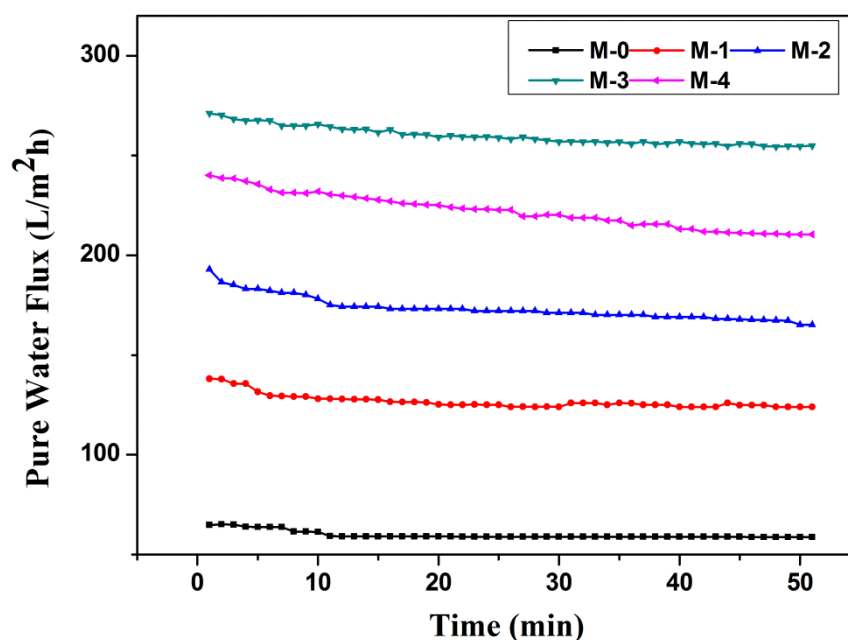


Figure 2.15 Pure water flux of the membranes

2.4.3.5 Antifouling study

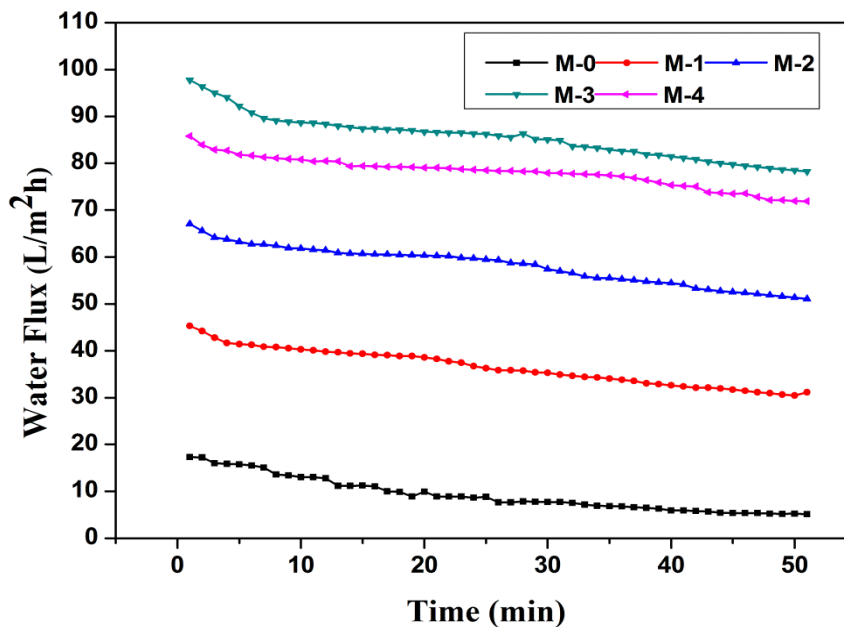


Figure 2.16 Flux of membranes during BSA filtration

The water flux of the membranes during BSA filtration is shown in Figure 2.16. The water flux of all the membranes during BSA filtration was observed to be lesser than the pure water flux of the membranes which may be attributed to the adsorption of BSA on the membrane surface and pores. Among the prepared membranes, PANI–PVDF–H–PSMA membranes showed higher flux than PVDF–H–PSMA membrane during BSA filtration which indicated that the BSA molecules were less deposited on the PANI incorporated membranes. BSA molecules get adsorbed more easily on the hydrophobic surface than the hydrophilic surface. Thus the adsorption of BSA was not favored in the presence of PANI nanofibers, which make the membranes hydrophilic. The FRR values of all the membranes are higher than the pristine PVDF–H–PSMA membrane (Figure 2.17). The higher the FRR value, the better is the antifouling nature of the membranes. It can be noted that the FRR values of the membranes increased with PANI nanofibers. The membrane M0, without any PANI nanofibers, showed least FRR value due to the hydrophobic interaction between PVDF and protein molecules. Nevertheless better fouling resistance by membranes

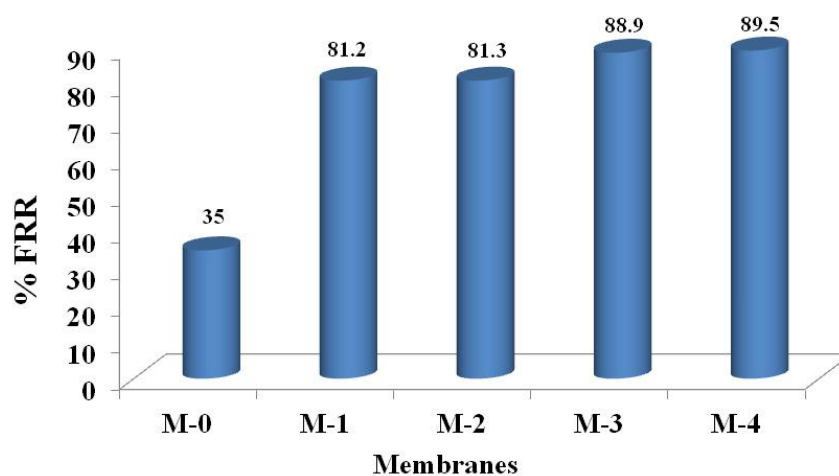


Figure 2.17 Flux recovery ratio of the membranes

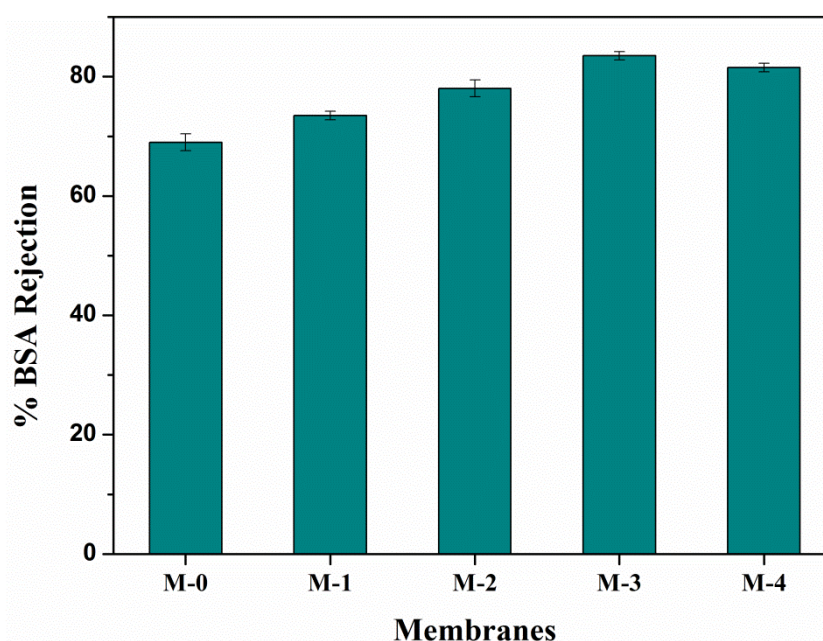


Figure 2.18 % BSA rejection % by the membranes

with PANI nanofibers indicated that the protein molecules adsorbed on the membrane surface and pores (reversible membrane adsorption) during BSA filtration were easily removed when the membranes were flushed with water. Thus from the FRR values and water flux measurement, it was evident that membranes with PANI had better antifouling nature than the pristine membranes. Higher antifouling ability of the

membranes is due to the higher hydrophilicity of membranes due to PANI. The presence of PANI can prevent the adsorption of protein on the surface due to the existence of hydrophilic functional group. The BSA rejection % of the membranes is in the range of 68–83% as shown in Figure 2.18

2.4.3.6 Heavy metal ion rejection

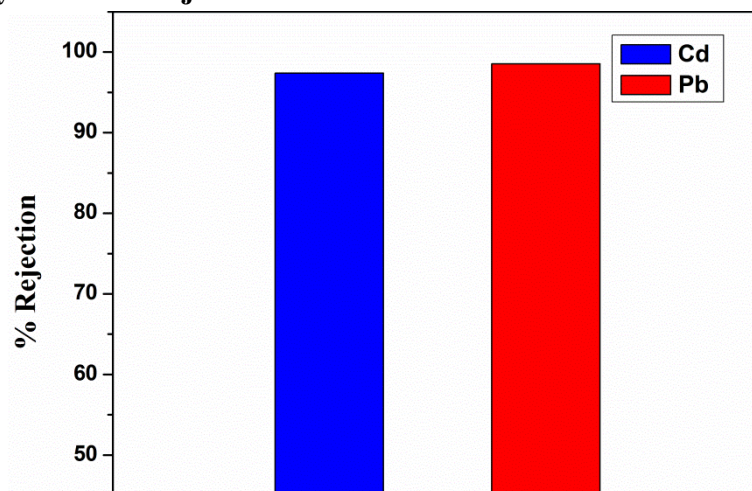


Figure 2.19 Heavy metal ion rejection

Polymer enhanced ultrafiltration process has been used for the removal of metal ions from solutions by ultrafiltration membranes. The pore size of UF membranes is not ideal for the rejection of metal ions from aqueous solution (Maheswari et al. 2013). Hence metal ions are first complexed with polymer PEI, to form macromolecular complex. Thus the metal ions are effectively removed by the polymer–metal complex. In the present work, the well performed membrane among all the prepared membranes, M3 with 1 wt.% PANI, was used for heavy metal ion rejection studies. The % rejection of Pb^{2+} and Cd^{2+} by the membrane is shown in Figure 2.19. The membrane showed 98.52 % rejection for Pb^{2+} and 97.39 % rejection for Cd^{2+} ions. Good rejection by the membranes can be attributed to the larger size of Pb^{2+} –PEI complex and Cd^{2+} –PEI complex than the membrane pore size. Also the hydrated metal ions are highly rejected because of the surrounding water molecules. The % rejection of Pb^{2+} was found to be slightly higher than that of Cd^{2+} . As reported by Liang et al. (2012), H-PSMA can also have strong co-ordination ability towards Pb^{2+} and can selectively adsorb Pb^{2+} through its carboxylate ion to form Pb –PSMA

complex which might have resulted in the high rejection of Pb^{2+} ions. Also the smaller size of Cd^{2+} than the Pb^{2+} ions might have resulted in the more number of Cd^{2+} ions than Pb^{2+} ions in the permeate solution.

2.5 CONCLUSIONS

PANI nanofibers were synthesized by facile rapidly mixed reaction method, which acted as a hydrophilic agent for PVDF UF membranes. A novel additive, hydrolyzed PSMA (H-PSMA) was used as a dispersant and pore forming agent. It was found that, the hydrophilicity of the membranes increased with the addition of PANI nanofibers. PANI nanofiber incorporated membranes showed enhancement in the membrane properties such as better permeability, water uptake and contact angle values. The pristine membrane PVDF–HPSMA fouled easily, whereas membrane with PANI nanofibers showed better antifouling nature. The morphology of the membranes also improved with better pores, as the content of PANI nanofibers in the membranes increased. However from water uptake, pure water flux (PWF) and BSA filtration experiments, it was found that membrane performance increased with the increase in concentration of PANI nanofibers till 1.0 wt.%, beyond which the performance of the membranes decreased. Thus it can be concluded that 1.0 wt.% of PANI nanofibers in the membranes is the threshold content for the prepared membranes, above which the membranes show a decrease in the performance. From the heavy metal ion rejection studies it can be concluded that the well performed membrane (1.0 wt.% of PANI nanofibers) has good potential for rejection of heavy metal ions such as Pb^{2+} and Cd^{2+} , which exhibits a % rejection of 98.52% and 97.38% for metal ions Pb^{2+} and Cd^{2+} respectively.

CHAPTER 3

PREPARATION, CHARACTERIZATION AND THE EFFECT OF POLYANILINE (PANI) COATED TiO₂ NANOCOMPOSITES ON THE PERFORMANCE OF POLYSULFONE ULTRAFILTRATION MEMBRANES

Abstract

This chapter details the preparation of polysulfone (PSf) membranes with PANI-TiO₂ nanotubes as additives. Here PANI-TiO₂ nanotubes were prepared by coating PANI over TiO₂ nanotubes and were dispersed in PSf membranes. Polyethylene Glycol (PEG-1000) was used as a pore former. The effect of addition of PANI-TiO₂ nanocomposites on the membrane performance was evaluated. The membrane containing 1.0 wt.% of PANI-TiO₂ exhibited a rejection of 83.75% and 73.41% during the Polymer Enhanced Ultrafiltration Process.

3.1 INTRODUCTION

Ultrafiltration is an important membrane separation process which is used for the purification of water, (Yi et al. 2013) for concentration of solutes and wastewater treatment. Polysulfone is one of the widely used materials for the preparation of ultrafiltration membranes, (Song et al. 2014) because of its excellent mechanical strength, chemical resistance, thermal stability and good film forming ability (Kumar et al. 2013). Structure of polysulfone is given in Figure 3.1. However polysulfone membranes being hydrophobic in nature are susceptible to fouling. Thus the modification of polysulfone membranes is inevitable. In the recent years, researches have been focused on incorporation of nanomaterials into the membranes to improve the separation performance and fouling resistance (Moghimifar et al. 2014). Among these inorganic nanoparticles, TiO₂ has received much attention and is one of the mostly used nanoparticles, due to its stability, availability, antibacterial nature and hydrophilicity (Zhang et al. 2013).

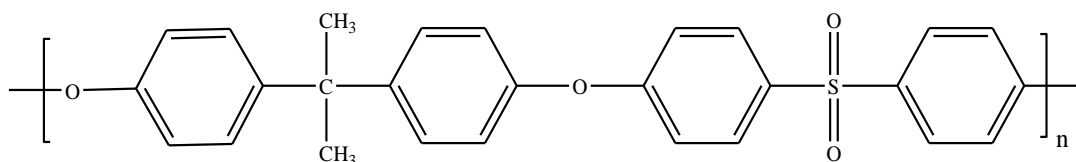


Figure 3.1 Structure of polysulfone

In the recent years, nanohybrid materials with at least two different nanomaterials are gaining interest where the benefits of two different particles could be combined to have improvement in properties (Wu et al. 2014). Polyaniline (PANI) based nanocomposites have been extensively studied due to its facile preparation and

environmental stability (Wang et al. 2013). A large number of studies have been focused on preparation of PANI-TiO₂ composites (Han et al. 2009). TiO₂ is considered as the best material to prepare hybrid material with PANI (Li et al. 2013). Ti of TiO₂ has tendency to form co-ordinate bond with 'N' atom of PANI (Teli et al. 2013). PANI-TiO₂ nanocomposites have applications in photocatalysis, charge storage and gas sensors (Han et al. 2009, Li et al. 2013, Pang et al. 2014). Also polymer/PANI and PANI/inorganic materials have shown improvement in performance of membranes due to the hydrophilicity of PANI.

Aminabhavi et al. (2010) prepared PANI-coated TiO₂-PVA membranes and TiO₂-PVA membranes for dehydration of 1,4-dioxane/THF aqueous solution by pervaporation. The addition of nanofillers resulted an increase in membrane selectivity to water. It was also found that the PANI modified TiO₂ membranes had higher flux than TiO₂-PVA membranes which is due to the higher hydrophilicity of PANI than TiO₂.

Daraei et al. (2012) prepared mixed matrix polyethersulfone membranes with PANI coated Fe₃O₄ nanoparticles as additives having affinity for copper ions. The core shell PANI-Fe₃O₄ nanoparticles were synthesized by chemical oxidative polymerization with iron oxide as core. Different concentrations of additives were used to determine the optimum value. The membrane containing 0.1 wt.% of nanoparticles exhibited highest Cu(II) removal.

Liu et al. (2014) synthesized polyaniline coated TiO₂/SiO₂ (TS) nanofiber membranes. TiO₂/SiO₂ (TS) nanofibers were prepared by electro spinning and calcinations, which were used as templates for in situ polymerization of aniline. The results indicated that PANI was uniformly coated on TS nanofibers. The nanocomposite membranes showed photocatalytic degradation of methyl orange under visible light which is reasoned due to the synergistic effect of PANI and TiO₂.

TiO₂ nanotubes, can act as excellent support materials for PANI, due to their high surface area (Xie et al. 2014). On the other hand, TiO₂ nanomaterials are known to undergo agglomeration in order to reduce their surface energy (Katoch et al. 2012). The presence of PANI on TiO₂ can prevent the agglomeration, increasing the stability of TiO₂ nanomaterials and facilitate uniform dispersion in the polymer matrix. Our

previous study indicated that, addition of TiO₂ nanotube has significantly improved the membrane performance (Kumar et al. 2013). The synthesized PANI-TiO₂ nanocomposite could combine the merit of both TiO₂ and PANI and have synergistic effect (Katoch et al. 2012, Radoičić et al. 2015). Also PANI-TiO₂ having strong interaction between PANI and TiO₂ is known to have well dispersible nature in solvents such as NMP (N-Methyl-2-pyrrolidone). These merits of PANI-TiO₂ are beneficial to the improvement of properties of membrane and hence enhancement in the performance of the membrane is expected.

In view of these observations, PANI-TiO₂ nanocomposites with average diameter of 50 nm were synthesized by coating PANI over TiO₂ nanotubes. The synthesized PANI-TiO₂ nanocomposites were stable and were dispersed in polysulfone membranes with increasing concentration. Polyethylene glycol 1000 (PEG 1000) was added as a pore former. The effect of addition of PANI-TiO₂ nanocomposite on the membrane performance, such as permeability, hydrophilicity, porosity and antifouling properties was studied. To the best of our knowledge, it is the first time TiO₂ nanotubes coated with PANI have been used as hydrophilic additives for the performance improvement of polysulfone membranes.

3.2 EXPERIMENTAL

3.2.1 Materials

Polysulfone (PSf) with molecular weight 35,000 Da, aniline (99.5%) and TiO₂ nanoparticles were purchased from Sigma Aldrich Co. Bangalore, India. Polyethylene glycol 1000 (PEG 1000) was purchased from Himedia Laboratories Pvt. Ltd., India. Ammonium peroxydisulfate (APS) and Bovine Serum Albumin (BSA) was purchased from Central Drug House (CDH), New Delhi. Hydrochloric acid (HCl), sodium hydroxide (NaOH) and N-Methyl-2-pyrrolidone (NMP) was purchased from Merck India, Ltd. Polyethyleneimine (PEI) (Mn~60,000) 50 wt% aq. solution, branched was purchased from Acros Organics, USA. Lead (II) nitrate and Cadmium nitrate tetrahydrate and were purchased from Sigma-Aldrich Co, Bangalore, India.

3.2.2 Preparation of PANI coated TiO₂ nanotubes

Preparation of TiO₂ nanotubes from TiO₂ nanoparticles was done as per the literature (Kumar et al. 2013). 50 mL of 10 M NaOH solution was taken in a 100 mL round bottom flask attached to a condenser with chilling. The solution was first heated to 120°C followed by the addition of 2 g of TiO₂ nanoparticles. The solution was then refluxed at the same temperature for 48 h under stirring. Then the mixture was cooled to room temperature and poured into de-ionised water. After the nanotubes were settled at the bottom, the supernatant solution was decanted and was washed repeatedly with water. 150 mL of 0.1 M HCl was then added to the solution and was stirred for 12 h at 60°C. Then the nanotubes were again washed with de-ionized water until the neutral pH was obtained. The solution was centrifuged and the obtained nanotubes were calcined at 450°C for 4 h.

Surface modification of the TiO₂ nanotubes by PANI was carried out by chemical oxidative polymerization as follows (Lokesh et al. 2008). 1 mL of aniline was added to 100 mL of 2 M HCl solution. 1 g of TiO₂ nanotubes were added to 5 mL of water and sonicated at 40 KHz for a few minutes in order to prevent the agglomeration of the TiO₂ nanotubes. This solution was then added to the solution containing aniline and stirred for two hours. The polymerization of aniline was carried out by the addition 2.4 g of ammonium persulfate solution with an equal molar ratio to aniline to the above suspension at room temperature. The product formed was isolated from the dispersion by centrifugation, washed with dil. HCl and water and dried at 80°C for 24 h.

3.2.3 Preparation of membranes

The nanocomposite membranes were prepared by the phase inversion method. Firstly, PANI coated TiO₂ nanotubes were dispersed in NMP and sonicated for 10 minutes for well dispersion. 5 wt.% of PEG 1000 was dissolved in NMP and was added as a pore former for all the membranes. 2 g of PSf was added to the same dispersion, and was kept for stirring at 60°C for 6 h. After the complete dissolution of Polysulfone, the casting solution was sonicated for 15 min at 40 KHz to remove any trapped air bubbles and left still under heating without stirring for 30 min to remove any trapped air bubbles. Then the homogenous solution was casted onto the glass

plate. After casting, the glass plate was immersed in a coagulation bath (water) for the phase inversion. The obtained membranes were washed thoroughly with water and dried. The composition of the prepared membranes is given in Table 3.1

Table 3.1 Composition of the membranes

Membranes	Psf (wt.%)	PEG (wt.%)	PANI-TiO ₂ (wt %)	NMP (wt.%)
P-0	20	5	0	75
P-0.05	20	5	0.05	74.95
P-0.5	20	5	0.5	74.5
P-1.0	20	5	1.0	74
P-1.5	20	5	1.5	73.5

3.3 CHARACTERIZATION

3.3.1 Characterization of PANI coated TiO₂ nanotubes

PANI coated TiO₂ nanotubes were characterized by Fourier Transform Infrared (FTIR) spectroscopy, X-ray Diffraction (XRD) and Transmission Electron Microscope (TEM). FTIR spectra were recorded from SHIMADZU ATR-FTIR spectrophotometer. XRD measurements were obtained from Rigaku Miniflex 600 with Cu K α radiation. Transmission Electron Microscope (JEOL JEM-2100) was used to analyze the morphology of PANI coated TiO₂ nanotubes.

3.3.2 Membrane Characterization

3.3.2.1 Morphology of membranes

The morphology of the prepared membranes was examined using Scanning Electron Microscope (JEOL JSM-6380LA). Before the Scanning Electron Microscope (SEM) analysis, the membranes were dipped and broken in liquid nitrogen and sputtered with gold for conductivity.

3.3.2.2 Atomic Force Microscopy (AFM) measurements

The AFM measurements were carried out using Innova SPM Atomic Force Microscope. The measurements were done on dry membrane samples. The membrane surfaces were imaged in tapping mode. Antimony doped silicon cantilever having

force constant in the range of 20-80 N/m was used to analyze the membrane surface topography. The surface roughness of the membranes, expressed in terms of average roughness (R_a) and root mean square roughness (R_q) was measured.

3.3.2.3 Porosity and pore size

The porosity (ε) of the membranes was obtained by gravimetric method (Kumar et al. 2013).

$$\varepsilon = \frac{w_1 - w_2}{A \times l \times d_w} \dots \dots \dots \text{eqn 3.1}$$

where w_1 and w_2 is the weight of the wet and dry membranes respectively. 'A' is the effective membrane area (m^2), 'l' is the thickness of the membrane (m) and ' d_w ' is the density of water.

Surface pore size of the membranes in terms of mean pore radius was analyzed using Guerout–Elford–Ferry equation, (Kumar et al. 2013) taking into account porosity and water flux of the membranes

$$r_m = \sqrt{\frac{(2.9 - 1.75\varepsilon) \times 8\eta l Q}{\varepsilon \times A \times \Delta P}} \dots \dots \dots \text{eqn 3.2}$$

where ' ε ' is the porosity, ' η ' is the viscosity of water (8.9×10^{-4} Pa s), 'l' is the thickness of the membrane (m), 'Q' is the volume of pure water permeated through membrane per unit time (m^3/s), 'A' is the effective membrane area (m^2) and ΔP is the operating pressure (0.2 MPa).

3.3.2.4 Water Uptake and contact angle measurement

The water uptake ability and hydrophilicity of the membranes was analyzed using water uptake studies and contact angle analysis. These studies were done following the methods mentioned in section 2.3.3.3 and section 2.3.3.2 of CHAPTER 2.

3.3.2.5 Permeation studies

The performance of the prepared membranes was evaluated by measuring pure water flux, determining antifouling ability along with % FRR using BSA as a foulant. These studies were performed according to the procedure explained earlier in CHAPTER 2 (section 2.3.3.4 and section 2.3.3.5 respectively).

3.3.2.6 Heavy metal ion rejection

Heavy metal ion rejection by the membranes was carried out by polymer enhanced ultrafiltration (PEUF) and ultrafiltration (UF) process. For PEUF process, aqueous solutions of Pb^{2+} and Cd^{2+} were prepared at an initial concentration of 1000 ppm in 1 wt.% of the PEI aqueous solution. The pH of the solutions was adjusted to 6.25 by adding small amounts of either 0.1 M HCl or 0.1 M NaOH. Solutions containing the metal ions and PEI were mixed thoroughly and left standing for 5 days for completion of binding between metal ions and PEI. PEI complexed metal ion solutions were filtered through the membranes and the permeate was collected. In UF process, feed solutions containing 1000 ppm of Pb^{2+} and Cd^{2+} were filtered individually through the membranes and the permeate was collected. The % rejection by the membranes for the metal ions, during the filtration was determined by analyzing the concentration of feed and permeate solution using Atomic Absorption Spectrophotometer (GBC 932 Plus). Heavy metal ion rejection percentage by the membranes was calculated using the formula

$$\%R = \left(1 - \frac{C_p}{C_f}\right) \times 100 \dots \dots \dots \text{eqn 3.3}$$

where, C_p (mg/mL) and C_f (mg/mL) are concentration of metal ions in the permeate and the feed respectively.

3.4 RESULTS AND DISCUSSION

3.4.1 PANI coated TiO_2 nanotubes characteristics

PANI coated TiO_2 nanotubes were prepared via chemical oxidative polymerization. First the synthesised TiO_2 nanotubes were dispersed in HCl solution containing aniline. In the presence of HCl, aniline gets transformed to anilinium cation. Under acidic conditions, the anilinium ions adsorb on the surface of TiO_2 nanotubes and then undergo oxidative polymerization in the presence of ammonium persulfate $(\text{NH}_4)_2\text{S}_2\text{O}_8$, leading to the formation of PANI coating on TiO_2 (Katoch et al. 2012).

FTIR spectra of pure TiO_2 , pure PANI and PANI- TiO_2 nanocomposite were obtained in the range of 500-3700 cm^{-1} . Figure 3.2 shows FTIR spectra. Pure TiO_2 shows broad peak around 3400 cm^{-1} and small peak at 1638 cm^{-1} which is due to the

stretching vibration of hydroxyl group (-OH) and adsorbed water present on TiO₂ (Cheng et al. 2014). Broad peak at 600 cm⁻¹ ranging from 1000 to 550cm⁻¹ is due to the Ti-O-Ti bonds. FTIR spectrum of PANI shows peak at 1567 cm⁻¹ and 1487 cm⁻¹ which is due to the C=N and C=C stretching vibrations of quinoid and benzenoid

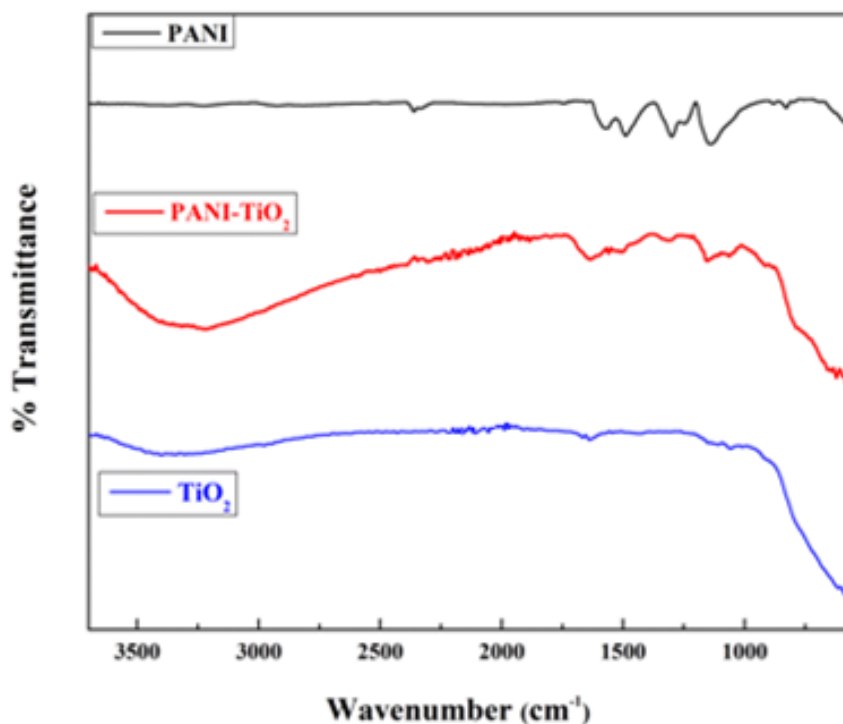


Figure 3.2 FTIR spectra of PANI, PANI-TiO₂ nanocomposite and TiO₂

rings of PANI respectively. Further peaks at 1298 cm⁻¹ and 1246 cm⁻¹ can be ascribed to the C-N stretching mode of benzenoid ring. Peaks at 1141 cm⁻¹ and 812 cm⁻¹ correspond to the C-H in plane and out of plane bending vibrations respectively (Pereira et al. 2014). All these peaks of PANI were observed in the IR spectrum of PANI-TiO₂ nanocomposite along with the broad -OH peak at 3400 cm⁻¹ which is observed to surface hydroxyl group of TiO₂. Also the broad peak ranging from 1000 to 550 cm⁻¹ due to Ti-O-Ti vibrations was observed in PANI-TiO₂ nanocomposite, indicating the presence of PANI on TiO₂.

X-Ray Diffraction patterns of PANI-TiO₂ nanocomposite, compared with pure PANI and pure TiO₂ are shown in Figure 3.3. Pure PANI shows two broad peaks at $2\theta=17^\circ$ and 23° which can be ascribed to the (111) and (110) planes. The XRD pattern of pure TiO₂ shows sharp peaks at 25.3° , 37.8° , 48.1° , 54.6° and 62.6° with respect to

(101), (103), (200), (105) and (213) planes respectively of anatase phase of TiO_2 (Li et al. 2013, Nasirian and Milani Moghaddam 2014). The PANI- TiO_2 nanocomposite showed two broad peaks at $2\theta=17^\circ$ and 23° and also all sharp peaks of TiO_2 which confirmed the presence of PANI coating on TiO_2 nanotubes.

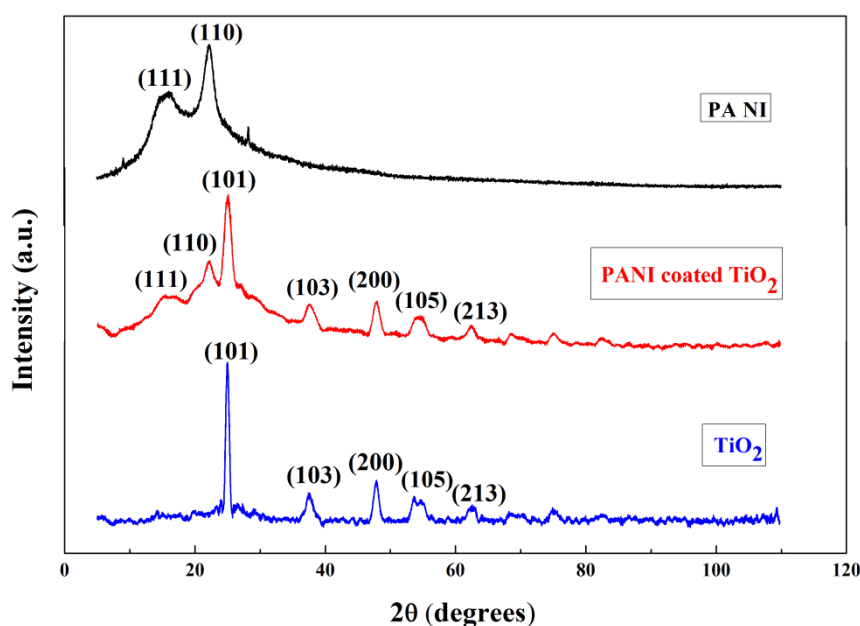


Figure 3.3 X-Ray Diffraction patterns of pure PANI, PANI- TiO_2 nanocomposite and pure TiO_2

TEM was carried out to observe the shape and size of PANI-coated TiO_2 nanotubes. TEM images of PANI-coated TiO_2 nanotubes are shown in Figure 3.4. PANI-coated TiO_2 nanotubes had a diameter in the range of 40-50 nm.

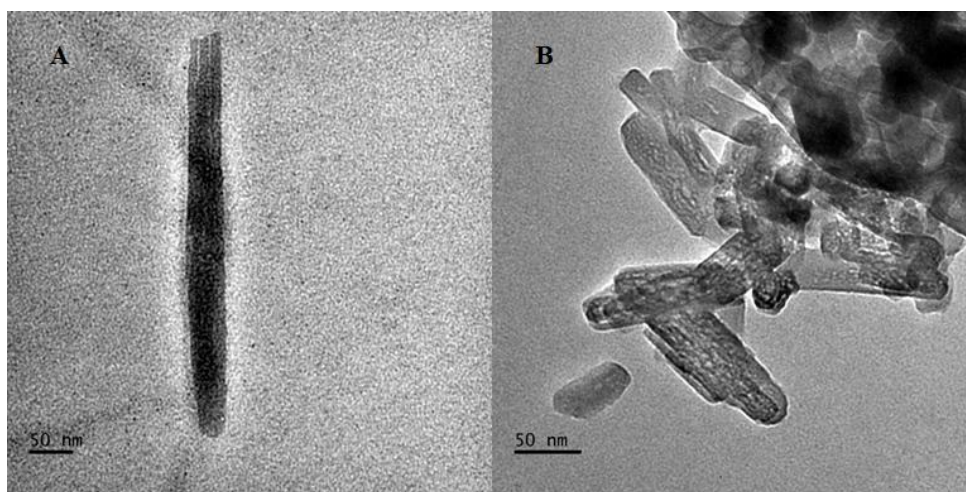


Figure 3.4 TEM images of PANI coated TiO_2 nanotubes (A and B)

3.4.2 Membrane characterization

3.4.2.1 Membrane morphology

The internal structure and the pore morphology of all the membranes was studied using SEM. Figure 3.5 displays the cross-sectional morphologies of the prepared membranes. The cross sectional images show that all the membranes exhibited typical asymmetric structure with dense top layer and porous sub layer. The nanocomposite membranes had well interconnected finger like pores from membrane top layer to sub layer. The addition of PANI- TiO_2 to the membranes brings about change in membrane structure. The finger like pore walls were linked with each other by sponge wall, which allow the finger like pores to communicate with each other. This is due to the well distribution of PANI- TiO_2 nanocomposite in the membranes (Teli et al. 2013). The SEM images showed that membrane porosity increased along with pore length as the PANI- TiO_2 content in the membranes increased. Also the skin layer becomes thin and more porous with PANI- TiO_2 content. This is due to the migration behavior of PANI i.e. during membrane formation, the hydrophilic additive would migrate near the membrane water interface in order to minimize the interfacial energy, thus acting as hydrophilic modifying agent (Zhao et al. 2012). As a pore former, the addition of PEG would also favor the pore formation. However the effect of PEG on the membrane morphology would be same for all membranes as same amount PEG was added to all the membranes.

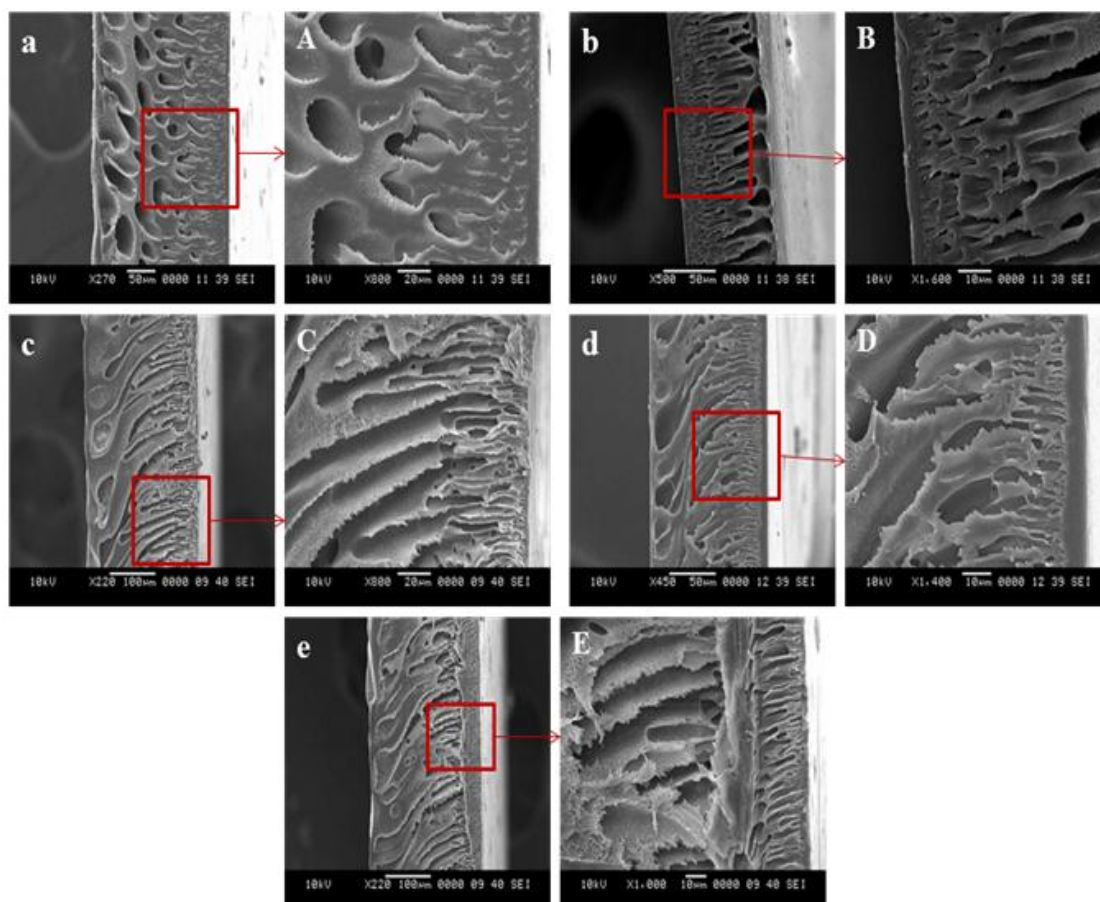


Figure 3.5 SEM cross sectional images of (a) P-0 (b) P-0.05 (c) P-0.5 (d) P-1.0 and (e) P-1.5 membranes (A, B, C, D and E are the enlarged images of a, b, c, d and e respectively)

3.4.2.2 Surface topography of membranes

The surface roughness of the membranes was studied using AFM under tapping mode. Figure 3.6 shows two-dimensional and three-dimensional scans of P-0, P-0.5 and P-1.0 membranes. From the images, it can be seen that the surface of the membrane P-0 was very rough and the surface roughness reduced for membranes P-0.5 and P-1.0, containing PANI-TiO₂ nanocomposite. The decrease in membrane surface roughness may be due to the uniform dispersion of PANI-TiO₂ in the polymer matrix (Daraei et al. 2012, Zhang et al. 2012). The decrease in surface roughness of the membranes was confirmed by the surface roughness parameters obtained for P-0, P-0.5 and P-1.0 membranes (Table 3.2). The mean roughness (R_a) and root mean

square roughness (R_q) was 334 and 402 nm for P-0, 54.2 and 67 nm for P-0.5 and 41.6 and 51.8 nm for P-1.0 membrane respectively.

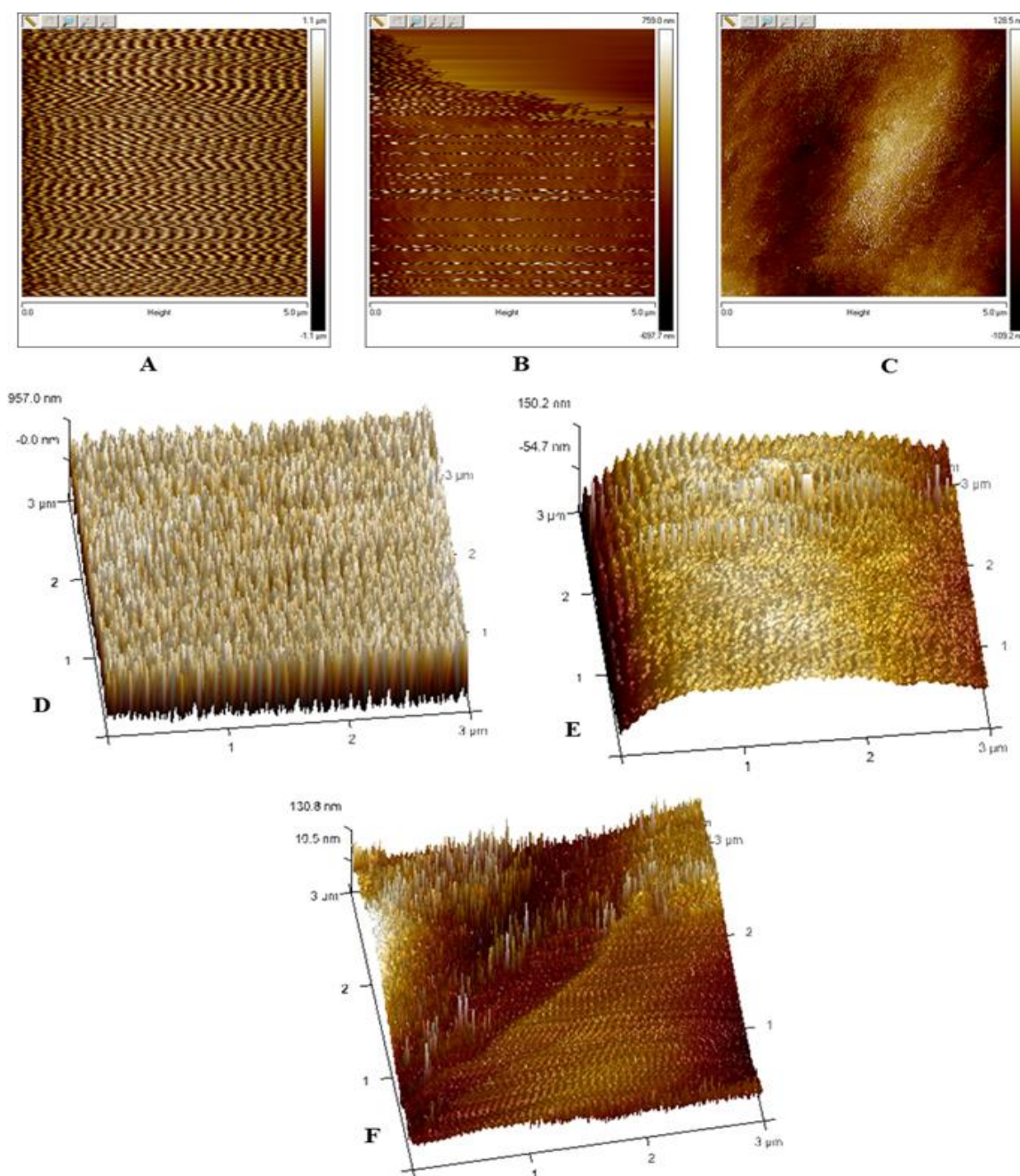


Figure 3.6 Two-dimensional scans of (A) P-0, (B) P-0.5 and (C) P-1.0 membranes and three-dimensional scans of (D) P-0, (E) P-0.5 and (F) P-1.0 membranes

Table 3.2 Surface roughness parameters of membranes

Membranes	Roughness Parameters	
	R _a (nm)	R _q (nm)
P-0	334	402
P-0.5	54.2	67
P-1.0	41.6	51.8

3.4.2.3 Porosity and pore size of membranes

The surface pore radius and porosity of the membranes are presented in Table 3.3. The addition of PANI-TiO₂ nanocomposite to the membranes increases the pore size of the membranes except for P-0.5. The higher hydrophilicity of PANI coated TiO₂ nanotubes at higher content would cause an increase of pore size. It is observed that with the initial addition of PANI-TiO₂, the membranes showed a sudden increase in pore size for P-0.05 with 0.05 wt.% of PANI-TiO₂ content. The initial increase in pore size may be due to the reason that the addition of nanocomposites to the casting solution increases the thermodynamic instability of the solution, causing rapid demixing, resulting in large pore formation at lower concentration. The low pore radius for P-0.5 membrane is due to the reason that as the addition of PANI-TiO₂ is increased from 0.05 wt.% to 0.5 wt.%, the viscosity of the casting solution is increased. This delays the exchange of solvent and nonsolvent which results in the suppression of the pore size (Vatanpour et al. 2012, Zhao et al. 2012). The membrane with highest PANI-TiO₂ content showed slight reduction in pore size, which might be due to the clogging of pores by the nanocomposite. The clogging of pores at higher concentration of PANI nanocomposite has also been observed in literature (Teli et al. 2013). The porosity measurements indicate that the nanocomposite membranes have higher porosity than the pristine membrane. Thus the addition of PANI-TiO₂ has led to the increase in porosity of membranes which is evident from SEM images (Figure 3.5).

Table 3.3 Mean pore radii and porosity of membranes

Membranes	Mean pore radius (nm)	Porosity (%)
P-0	8.25	53.36
P-0.05	14.21	69.60
P-0.5	7.02	76.09
P-1.0	10.72	72.34
P-1.5	8.52	82.60

3.4.2.4 Water Uptake

Figure 3.7 shows the water uptake by the membranes. The least water uptake is shown by membrane P-0 whereas the water uptake of nanocomposite membranes is higher and increases with the increase in PANI-TiO₂ nanocomposite. Water uptake property of the membranes depends on the porosity of the membranes. As the porosity of P-0 membrane is least among all the membranes (Table 3.3), membrane P-0 showed least water uptake. The increase in water uptake by PANI-TiO₂ nanocomposite membranes with PANI-TiO₂ is due the increasing porosity of the membranes. A slight decrease in water uptake shown by P-1.0 membrane may be due to the less porosity observed for the membrane.

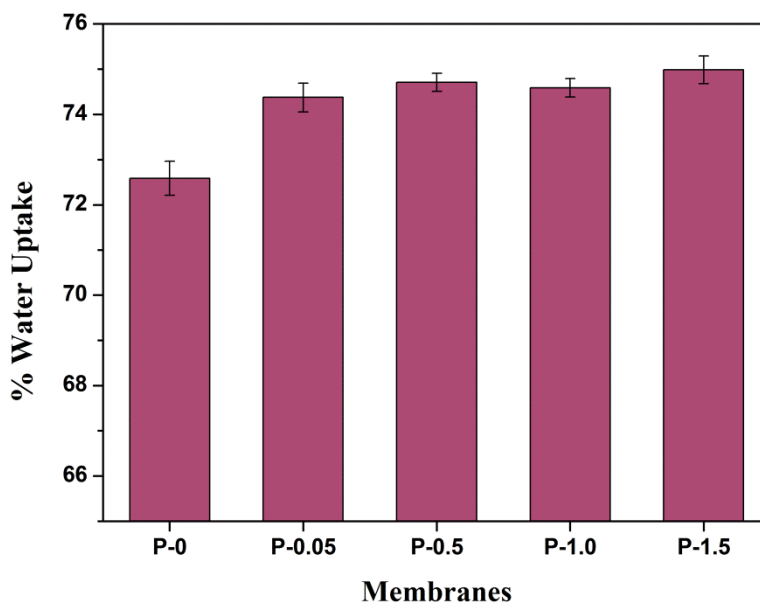


Figure 3.7 Water uptake by the membranes

3.4.2.5 Contact Angle of membrane surfaces

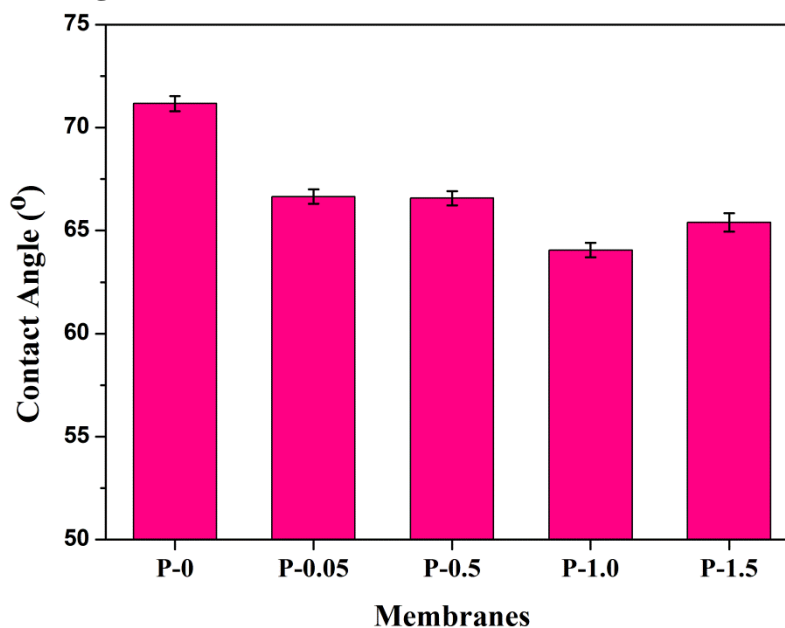


Figure 3.8 Contact angle of the membranes

The contact angle of membranes represents the hydrophilicity and wettability of membranes. Figure 3.8 shows the contact angle of the membranes. Membrane P-0, showed highest contact angle indicating its hydrophobic nature. Membrane P-0 did not contain any PANI-TiO₂ nanocomposite and having high contact angle is supposed to be due to the hydrophobic nature of polysulfone. The contact angle of PANI-TiO₂ nanocomposite membranes were in the range of 66-64°. Also the contact angle decreased with the increase of PANI-TiO₂ content in the membranes. The membrane with 1.0 wt.% PANI-TiO₂ content showed least contact angle. The decrease in contact angle with the increasing concentration of PANI-TiO₂ in membranes indicated that PANI-TiO₂ nanocomposite enhanced the hydrophilicity of the membranes. Figure 3.9 shows the images of contact angle measured on the membranes.

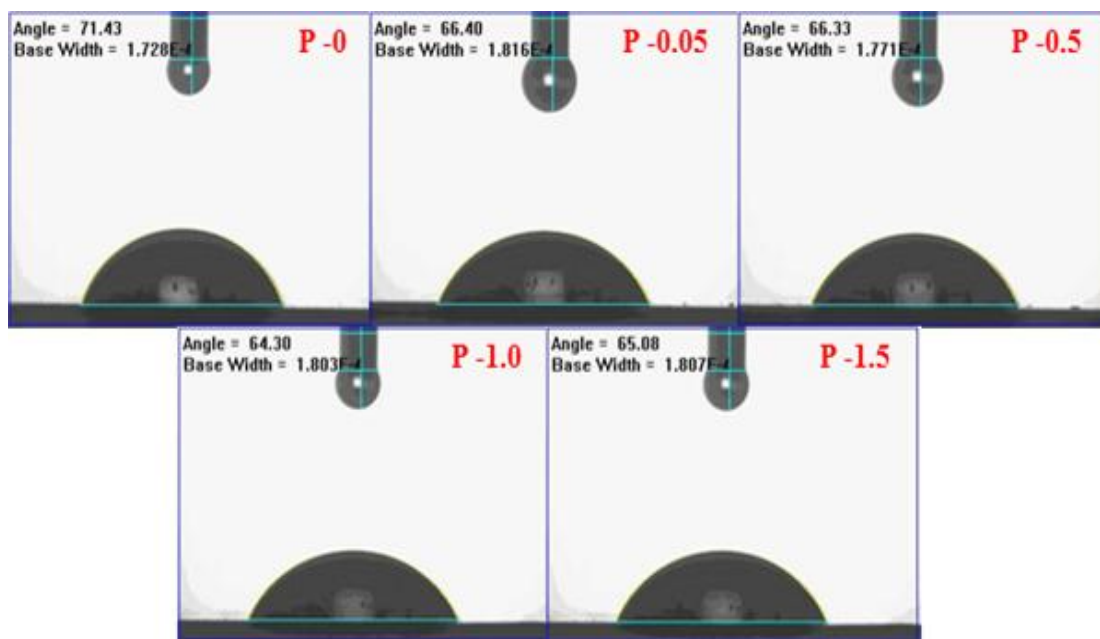


Figure 3.9 Images of contact angle measured on the membrane surfaces

3.4.2.6 Permeation properties

Permeation properties of the membranes were studied by permeating pure water through the membranes using dead end filtration cell at 0.2 MPa, TMP. The pure water flux of the membranes is shown in Figure 3.10. All the nanocomposite membranes showed higher permeate flux than the polysulfone membrane. The nanocomposite membranes possessed higher hydrophilicity, higher porosity and better vertically interconnected pores than the polysulfone membrane which led to the water permeability of the membranes. The pure water flux of the membranes is in the order $P-0 < P-0.5 < P-1.5 < P-0.05 < P-1.0$. The membranes P-0.05 and P-1.0 showed higher water flux among the synthesized membranes. This is due to the higher pore sizes of these membranes when compared to the other membranes (Table 3.3). Among P-0.05 and P-1.0 membranes, though the pore radius of P-1.0 was lower than that of P-0.05 membrane, the higher PWF is due to the higher hydrophilic nature of P-1.0 membrane than P-0.05 membrane. The contact angle measurements showed that, membrane P-1.0 possessed highest hydrophilicity. Higher PANI-TiO₂ content, higher would be the hydrophilic nature of PANI and TiO₂ which would attract water molecules easily into the membrane matrix thereby increasing the permeability

(Zhang et al. 2013). Among P-0, P-0.5 and P-1.5 membranes, P-0 showed least PWF due to the reason that membrane P-0 is hydrophobic in nature and did not contain any PANI-TiO₂ nanocomposite. Though the pore radius of P-0.5 was lesser than that of P-0 membrane, the PWF is higher because of the presence of hydrophilic PANI-TiO₂ and higher porosity of the membrane.

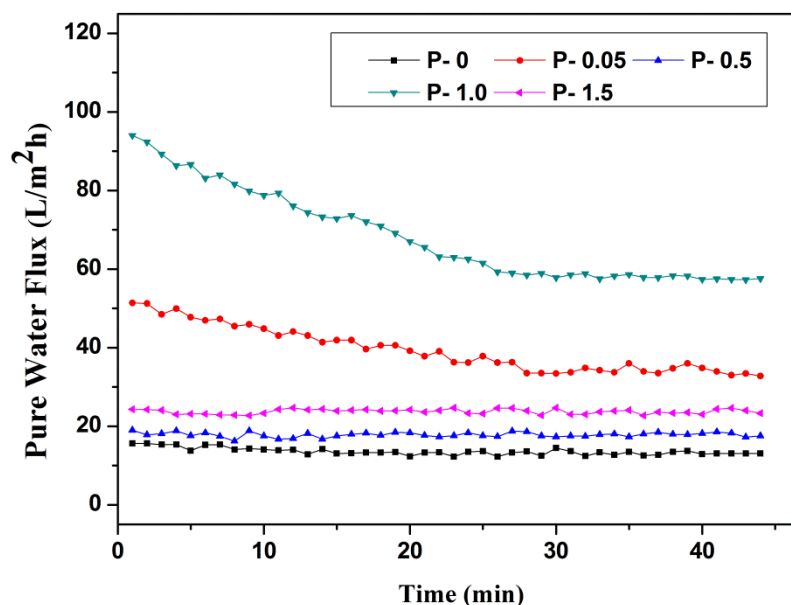


Figure 3.10 Pure water flux of the membranes

Membrane P-1.5 had higher PWF than P-0 and P-0.5 membranes, because its pore size was higher than that of both P-0 and P-0.5 membrane. However the PWF of P-1.5 membrane was lower than that of P-0.05 and P-1.0 membranes, because the presence of excessive PANI-TiO₂ content led to the clogging of pores which in turn decreased the permeability of the membrane. Similar results showing decrease in flux with the increase in concentration of PANI and PANI based nanocomposites in the membranes has been found in literature (Pereira et al. 2014, Zhao et al. 2012).

3.4.2.7 Antifouling properties

The fouling nature of the membranes was investigated through protein filtration, using BSA as a model protein. The flux of the membranes during BSA filtration is shown in Figure 3.11. The figure shows decline in flux of membranes for initial few minutes. This initial decline of flux is due to the adsorption of BSA molecules onto the surface of the membranes (Zhao et al. 2011). All the membranes

showed higher flux than P-0 membrane. Since the nanocomposite membranes had higher hydrophilicity, protein molecules could not be easily adsorbed on the membrane surface indicating antifouling nature of membranes (Zhao et al. 2012). The % FRR values of the membranes are shown in Figure 3.12. Higher the FRR value better is the antifouling nature of the membranes. Membrane P-0 had least FRR value among all the membranes. The membranes showed increase in FRR value with PANI-TiO₂ content, indicating that addition of PANI-TiO₂ enhance the fouling resistance of membranes.

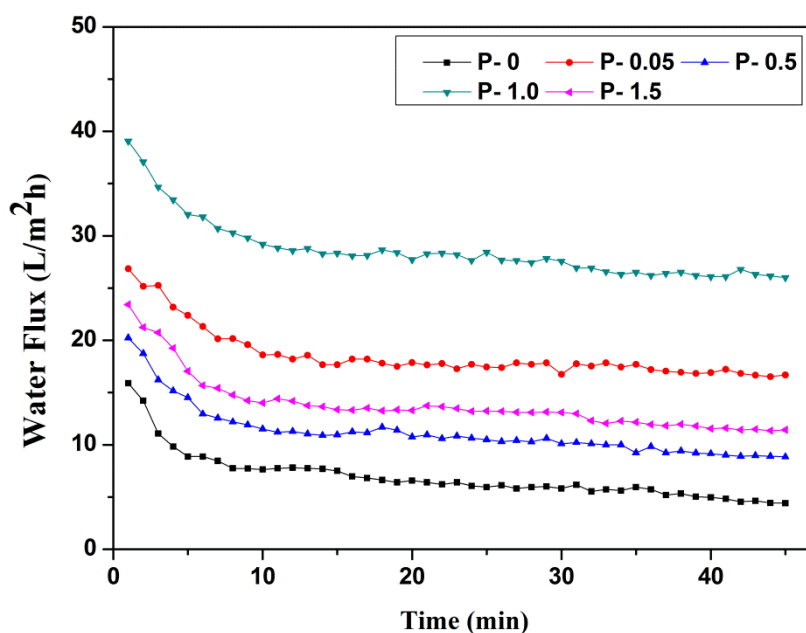


Figure 3.11 Flux of the membranes during BSA filtration

As the hydrophilicity of the membranes increased with PANI-TiO₂ content, it weakened the interaction between membrane surface and the protein molecules. Thus the adsorbed BSA molecules on the membrane surface were easily removed by simple washing resulting in high flux recovery ratio. The membrane P-1.5 showed little decrease in FRR value. This may be due to the decrease in hydrophilicity as observed by contact angle measurement.

The AFM results further confirmed that, addition of PANI-TiO₂ nanocomposite into the membranes improved the antifouling nature of membranes. It is well known that, lower the surface roughness of the membranes, better is the

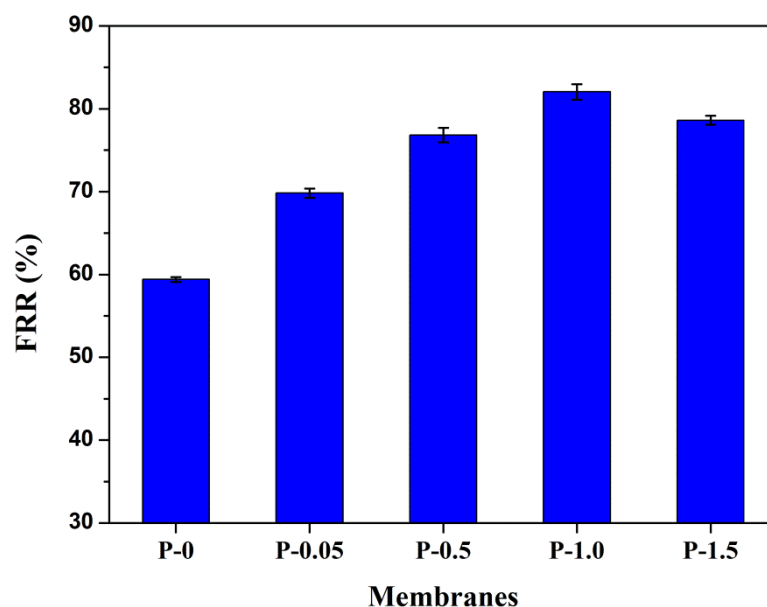


Figure 3.12 % FRR values of the membranes

antifouling ability. From Figure 3.6 and Table 3.2 it can be seen that membrane P-0 with no PANI-TiO₂ content was rough and surface roughness was reduced for P-0.5 and P-1.0 membranes. This decrease in surface roughness increased the antifouling nature of the membranes since the foulants are more likely to adsorb on coarse surfaces than smooth surface (Razmjou et al. 2011).

3.4.2.8 Heavy Metal Ion Rejection

The heavy metal ion rejection by the membrane for metal ions Pb²⁺ and Cd²⁺ was studied by UF and PEUF process. Among the prepared membranes, the well performed membrane M-1.0 which possessed highest hydrophilicity, better permeability, highest FRR value was selected for the heavy metal ion rejection studies. Figure 3.13 displays the % Rejection by the membrane during PEUF and UF process for heavy metal ions Pb²⁺ and Cd²⁺ respectively. The membrane exhibited 83.75% rejection for Pb²⁺ ions and 73.41% rejection for Cd²⁺ ions during PEUF. The % Rejection was higher for Pb than Cd this is because Pb²⁺-PEI complex was larger in size than Cd²⁺-PEI complex. The % rejection for Pb²⁺ and Cd²⁺ during UF was 68% and 53.78% respectively. The rejection of metal ions during UF process is due to the adsorption of metal ions the membrane surface. Figure 3.14 shows the elemental mapping of Pb and Cd adsorbed on the membranes. The main adsorption sites for

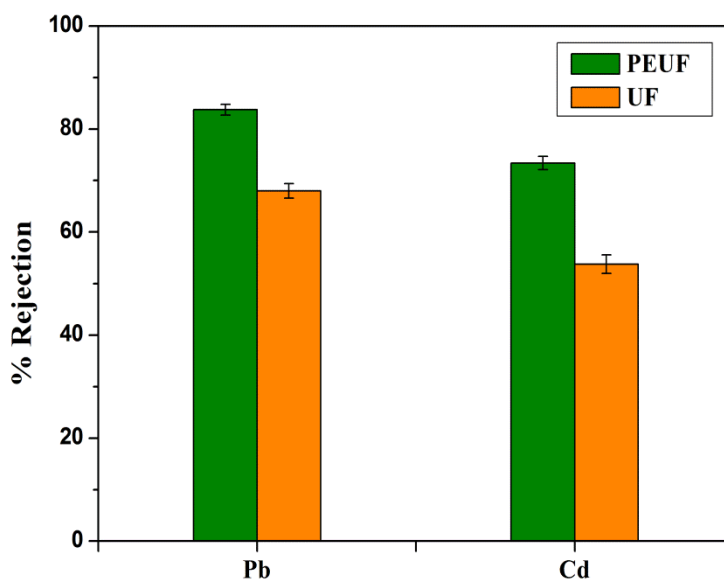


Figure 3.13 Heavy metal ion rejection by the membranes

metal ions were the nitrogen atoms of PANI of PANITiO₂ nanocomposite (Eisazadeh et al. 2013). The unpaired electrons of the amine group of PANI can create coordinate bond with metal ions resulting in the adsorption of metal ions on the membrane surface (Min et al. 2012). The membranes showed higher % of rejection during PEUF process than UF process. This is because the metal ion-PEI complex has greater size than the membrane pore size. Hence the complexed metal ions are retained in the feed solution. During the UF process, most of the metal ions would easily pass through the membrane, as the pore size of the membrane is much higher than that of the metal ions. Only the metal ions adsorbed on to the membrane surface would contribute to the % rejection.

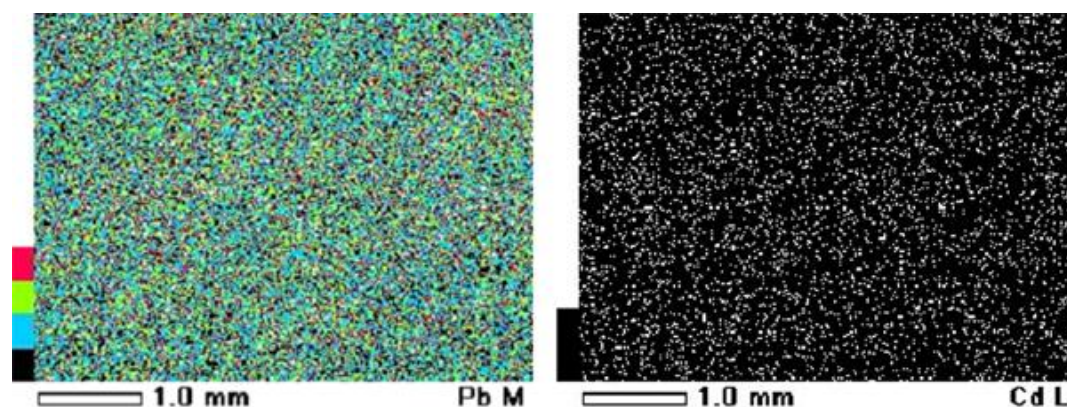


Figure 3.14 Adsorption of Pb and Cd on the membranes

3.5 CONCLUSIONS

The performance of the polysulfone membranes can be improved by using PANI-TiO₂ nanocomposite as a hydrophilic additive. The properties of the membranes such as hydrophilicity, permeability, water uptake, porosity, antifouling nature enhance with the addition of PANI-TiO₂ nanocomposite. The nanocomposite membranes also showed good rejection for Pb²⁺ and Cd²⁺ ions by PEUF process. Taking into account the contact angle, PWF, % FRR value, it is found that the properties of the membranes improved when the addition of PANI-TiO₂ nanocomposite was increased up to 1.0 wt. %. When the concentration of the PANI-TiO₂ nanocomposite in the membranes was further increased to 1.5 wt.%, the membranes showed slight decrease in performance. The decrease in performance by the membranes may be due to the agglomeration of the nanocomposite at higher concentration leading to clogging to pores. Overall the PANI-TiO₂ nanocomposite membranes can be used for water purification namely heavy metal ion removal with minimum fouling.

CHAPTER 4

PREPARATION AND PERFORMANCE STUDIES OF POLYSULFONE-SULFATED NANO-TITANIA (S-TiO₂) NANOFILTRATION MEMBRANES FOR DYE REMOVAL

Abstract

This chapter gives insight into the modification of TiO₂ nanoparticles with sulfate groups. The modified TiO₂ nanoparticles were then used as additives in the polysulfone membranes and the properties of the nanocomposite membranes were studied. This chapter explores the use of sulfated TiO₂ (S-TiO₂) for dye removal from aqueous solutions and the optimum conditions required. A maximum of 90.4% rejection was obtained for Methylene Blue (MB) for the membrane having 2.0 wt% of S-TiO₂ under UV light radiation.

4.1 INTRODUCTION

Membrane technology has been an important tool in water treatment because of its selective and efficient separation, stability, ease in operation, flexible to be integrated with other separation processes (Aluigi et al. 2014, Cheng et al. 2015, Mahlambi et al. 2014, Zhao et al. 2015). Blending membranes with inorganic materials such as nanoparticles is of interest because of facile preparation, good dispersion, effective hydrophilicity (Qin et al. 2015, Zhao et al. 2013). TiO₂ is one of the extensively used nanomaterial in preparing nanocomposite membranes (Emadzadeh et al. 2014). This is because, TiO₂ nanoparticles provide hydrophilicity, have stability and can also act as photocatalyst in hybrid photocatalyst-membrane based waste water treatment (Hamid et al. 2011, Rajesh et al. 2013). TiO₂ is known to have photocatalytic activity. Focus has been laid on improving its photocatalytic efficiency. One among the efforts is sulfation of TiO₂, where the presence of SO₄²⁻ increases the light absorption and the photocatalytic activity. SO₄²⁻-TiO₂ has also been used as photocatalyst for the degradation of dyes.

Synthetic dyes have been extensively used in industries such as textile, rubber, paper, plastic, leather etc. It has been estimated that nearly 10,000 types of commercial dyes are available and more than 7×10⁵ tons of dyes are produced annually worldwide. The synthesis and usage of dyes can cause serious environmental problems (Wei et al. 2013). Dyeing and finishing processes in textile industries produce large quantities of wastewater streams containing nearly 50-200 mg/L of unfixed dyes (Mondal and De 2016). Various techniques like adsorption, membrane filtration are being used to remove the dyes from effluents of textile industry (Salem

et al. 2009). Removal of dyes by adsorption is a slow and equilibrium governed process. Also powder form of adsorbents are difficult to remove from the filtrate, in addition to their high operating and disposal cost (Mondal and De 2016). Therefore membrane based separation process offer an attractive alternative. The advantages include physical separation, low energy, high scalability (Mondal and De 2016).

Methylene Blue (MB) is a cationic heterocyclic aromatic dye which has wide applications in textile industry, for coloring paper, dyeing cotton, wool, as hair colorant etc (Huang et al. 2010). Structure of Methylene Blue is shown in Figure 4.1. However, acute exposure to MB can cause health hazards such as increased heart rate, vomiting, cyanosis, tissue necrosis (Mohapatra and Parida 2006). Also effluents containing dye such as MB is a major toxic industrial waste (Shao et al. 2013, Zeng et al. 2011). MB containing waste water stream are highly colored, cause water pollution and are also hazardous to aquatic organisms (Fradj et al. 2014, Zeng et al. 2011). MB is nonbiodegradable, exhibits high stability, difficult to degrade by traditional methods. Hence the colored water needs to be treated and removed before its disposal (Fradj et al. 2014).

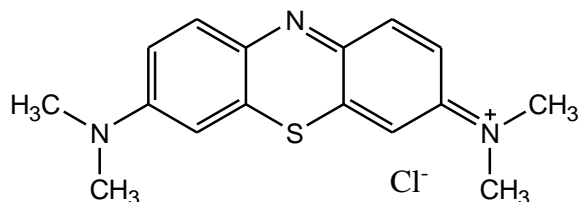


Figure 4.1 Structure of Methylene Blue

Mohamed and Al-Esaimi (2006) prepared sulfated TiO_2 and non-sulfate TiO_2 modified by NH_4VO_3 . Degradation of MB was tested for the sample effectiveness. The results indicated that MB degradation was improved with V supported $\text{TiO}_2\text{-SO}_4^{2-}$, showing 98% after UV irradiation, exceeding that of SO_4^{2-} free TiO_2 which showed degradation of 78% under same conditions. This is due to high surface area, small crystallite size, decreased band-gap and acidity gained after sulfation.

Zou et al. (2009) synthesized sulfated TiO_2 and sensitized using hydrogen peroxide and used as a photocatalyst under visible light. Results showed that TiO_2 with strong surface acidity was obtained with sulfate groups anchoring on TiO_2 surface. It was found that the degradation of methyl orange dye by sulfated TiO_2 was

significantly faster when compared with that of commercially available Degussa P25 TiO₂.

Ghambire et al. (2011) prepared transition metal loaded SO₄²⁻/TiO₂ powders. It was reported that the sulfation process stabilizes TiO₂ catalyst, increases the surface area of SO₄²⁻/TiO₂ when compared with pure TiO₂. It was found that maximum photocatalytic decomposition of Methylene Blue was obtained using sulfated TiO₂. SO₄²⁻/TiO₂ enhanced the photocatalytic activity due to increased surface area, high surface acidity.

Zhang and Liu (2015) prepared polysulfone membranes through phase inversion process by doping with sulfated TiO₂ deposited on SiO₂ nanotubes (STSNs). The STSNs were first prepared and then added through micro-reaction locations inside channels and on the surface of the membranes. The properties of the polysulfone membranes such as hydrophilicity, antifouling and anticompression enhanced on addition of STSNs.

In our present approach, sulfated TiO₂ nanoparticles (S-TiO₂) were synthesized and were used as additives into PSf membranes. S-TiO₂ was added in increasing concentrations into the PSf membranes. The effect of addition of S-TiO₂ on the performance of PSf membranes was analyzed. The membranes containing sulfated nano TiO₂ were used for the removal of MB dye. The MB dye removal with respect to the concentration of S-TiO₂ in the membranes, with and without UV radiation was investigated.

4.2 EXPERIMENTAL

4.2.1 Materials

Polysulfone (PSf) having molecular weight of 35,000 Da and TiO₂ nanoparticles were purchased from Sigma Aldrich Co. Bangalore, India. Bovine Serum Albumin (BSA) was obtained from Central Drug House (CDH), New Delhi. Isopropanol and N-methyl-2-pyrrolidone (NMP) was purchased from Merck India, Ltd. Sulphuric acid (H₂SO₄) was purchased from Nice Chemicals Pvt. Ltd., India. Methylene Blue (MB) was purchased from Sigma Aldrich Co. Bangalore, India.

4.2.2 Preparation of sulfated TiO₂

Sulfated-TiO₂ was synthesized as per the reported literature (Krishnakumar and Swaminathan 2011). TiO₂ nanopowder was dispersed in 50 mL of isopropanol. 2 mL of 1M H₂SO₄ was added to the solution drop wise under stirring. The solution was kept under stirring for about 4 h. The resulting suspension was centrifuged, washed and dried in oven at 100°C for 24 h. The dry sample was calcined for 5 h at 500°C.

4.2.3 Preparation of membranes

Membranes were prepared by phase inversion technique. 20 wt. % of Psf was dissolved in NMP by stirring at 60°C for 24 h to get a homogenous mixture. S-TiO₂ was added to the solution and sonicated for 5 minutes to avoid agglomeration. The solution was further stirred for 1 h. Then the solution was sonicated for 15 min for degassing i.e. to remove any trapped air bubbles. The solution was then left still under heating for 30 min. Finally the solution was casted on the glass plate using Doctor's blade and immersed in distilled water for 24 h for phase inversion. The prepared membranes were then washed thoroughly and air dried. Membranes were prepared with different concentrations of S-TiO₂, whereas the concentration of PSf was fixed to 20 wt. % for all the membranes. The concentration of S-TiO₂ in the membranes was varied as 0 wt. %, 0.05 wt. %, 0.5 wt. %, 1.0 wt. %, 1.5 wt. % and 2.0 wt. % and the membranes were labeled S-0, S-0.05, S-0.5, S-1.0, S-1.5 and S-2.0 accordingly.

4.3 CHARACTERIZATION

4.3.1 Characterization of S-TiO₂

Fourier Transform Infrared FTIR spectrometer (SHIMADZU) was used to obtain the IR spectra of TiO₂ and S-TiO₂. Elemental analysis of sulfated samples was carried out with the help of Energy Dispersive Spectrophotometer (EDS)-(JEOL JSM-6380LA). Transmission electron microscope (TEM)-(JEOL JEM-2100) was used to observe the morphology of sulfated TiO₂.

4.3.2 Characterization of membranes

4.3.2.1 Morphology of membranes

The morphology of the synthesized membranes was studied by using the cross sectional images of the membranes. The images were taken through Scanning Electron Microscope (SEM) (JEOL JSM-6380LA).

4.3.2.2 Porosity and water uptake of membranes

The porosity (ε) of the membranes was determined by gravimetric method, (Kumar et al. 2013) which gives the equation

$$\varepsilon = \frac{w_1 - w_2}{A \times l \times d_w} \dots \dots \dots \text{eqn 4.1}$$

where w_1 and w_2 are the weights of the wet and dry membrane samples respectively. 'A' is the effective membrane area (m^2), 'l' is the membrane thickness (m), d_w is the water density.

The water uptake study of membranes was done following the procedure mentioned in section 2.3.3.3 of CHAPTER 2 and percent water uptake was calculated using equation 2.1.

4.3.2.3 Mechanical property of membranes

The mechanical properties of the membranes were tested using tensile tester (Model: LRX 2.5KN, LLYOD) at room temperature (Zheng et al. 2009). Rectangular specimens of length 3 cm and width 1 cm were analyzed with gauge length of 30 mm. The testing was done at strain rate of 10 mm/min. Triplicate measurements of the samples were taken and the average values were reported (Vilakati et al. 2014).

4.3.2.4 AFM analysis

The AFM analysis of the membranes was performed using Innova SPM Atomic Force Microscope. The membrane surfaces were imaged as per the details given in section 3.3.2.2 of CHAPTER 3.

4.3.2.5 Contact angle of membranes

The contact angle of membranes was measured by sessile droplet method as explained in section 2.3.3.2 of CHAPTER 2.

4.3.2.6 Water Permeability

Water permeability of the membranes was analyzed by measuring the pure water flux (PWF) using dead end filtration cell. The PWF of membranes was measured as per the method explained in section 2.3.3.4 of CHAPTER 2, except that the membranes were initially compacted for 1 h at 0.8 MPa and the PWF was measured at 0.6 MPa TMP (Transmembrane Pressure) at intervals of 5 min for each of the membrane.

The pure water flux was also measured by varying the pressure from 0.6 to 1.0 MPa for a fixed interval of time for each membrane.

4.3.2.7 Antifouling ability of membranes

Antifouling nature of membranes was evaluated by choosing BSA as a model protein. The BSA flux was measured by following the procedure described in section 2.3.3.5 of CHAPTER 2 and the flux was measured at 0.6 MPa TMP.

4.3.2.8 Dye Removal by membranes

The dye removal efficiency of membranes was evaluated using Methylene Blue (MB) dye. Aqueous solutions of MB at a concentration of 10 ppm and 20 ppm were prepared. 0.1 g of each of the membrane was weighed and then cut into smaller pieces and were transferred into 6 different conical flasks containing 25 mL of 10 ppm aqueous MB solution. The solutions were shaken continuously at 120 rpm inside an orbital shaker (ORBITEK LT) for 15 h under closed/dark conditions. After 15 hrs, aliquots of the suspensions were taken and the concentration of MB dye in the aqueous solutions was analyzed using UV/Vis Spectrophotometer (SPECORD S 600). The experiments were repeated in a similar manner for MB solutions at 20 ppm concentration.

To study the degradation of MB using UV light, a UV source-UV tube (UV-C) of 11W (PHILIPS) was placed 15 cm above the solutions inside the orbital shaker. The experiments were carried out under UV light, in a similar manner as mentioned above, for 15 h, for 10 ppm and 20 ppm concentration of MB solutions for each of the membrane samples. The dye removal by the membranes was evaluated in terms of % rejection, which was calculated using the formula

$$\% \text{ Rejection} = \left(1 - \frac{C_p}{C_f} \right) \times 100 \dots \dots \dots \text{eqn 4.2}$$

where, C_i (mg/mL) and C_f (mg/mL) are the initial and final concentrations of MB in the aqueous solutions.

4.4 RESULTS AND DISCUSSIONS

4.4.1 Characterization of S-TiO₂ nanoparticles

The FTIR spectra of S-TiO₂ and TiO₂ are shown in Figure 4.2. Broad peak around 3200 cm⁻¹ and peak at 1642 cm⁻¹ is due to the stretching vibrations of surface hydroxyl group and adsorbed water (Pereira et al. 2015). The peak at 1399 cm⁻¹ is due to the stretching frequency of S=O bond and two peaks at 1130 cm⁻¹ and 1045 cm⁻¹ correspond to the characteristic frequencies of SO₄²⁻ (Gambhire et al. 2011, Krishnakumar and Swaminathan 2011). These peaks are not found in TiO₂. Bands in the lower wavelength region ranging from 600-1000cm⁻¹ can be ascribed to the Ti-O-Ti vibration (Gambhire et al. 2011).

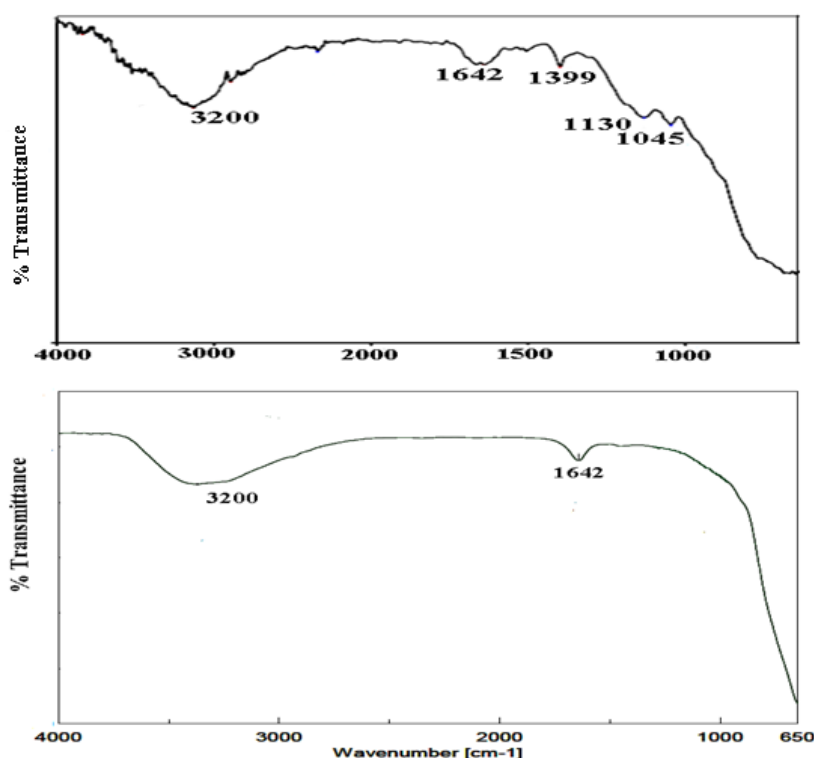


Figure 4.2 FTIR spectra of S-TiO₂ and TiO₂

The EDX spectrum of S-TiO₂ is given in Figure 4.3 which shows the presence of sulfur in the sample (Krishnakumar and Swaminathan 2011). The presence of sulfur in S-TiO₂ was also analysed by elemental mapping of S-TiO₂ (Figure 4.4).

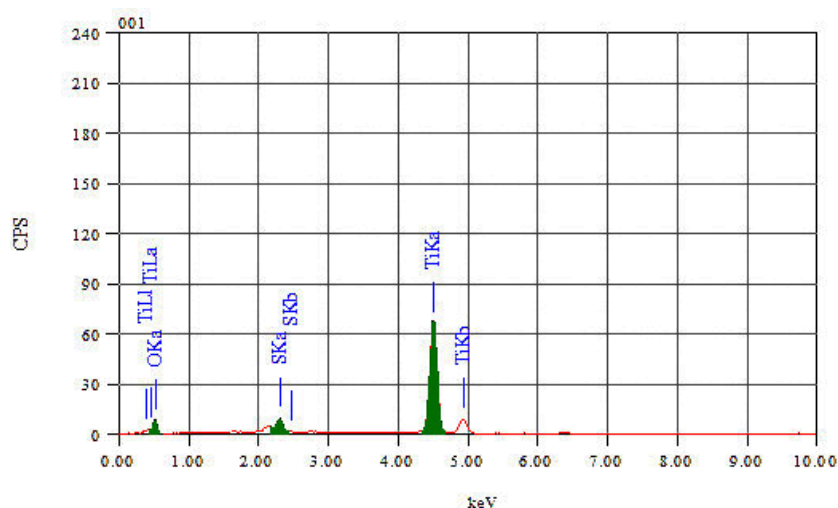


Figure 4.3 EDX spectrum of S-TiO₂

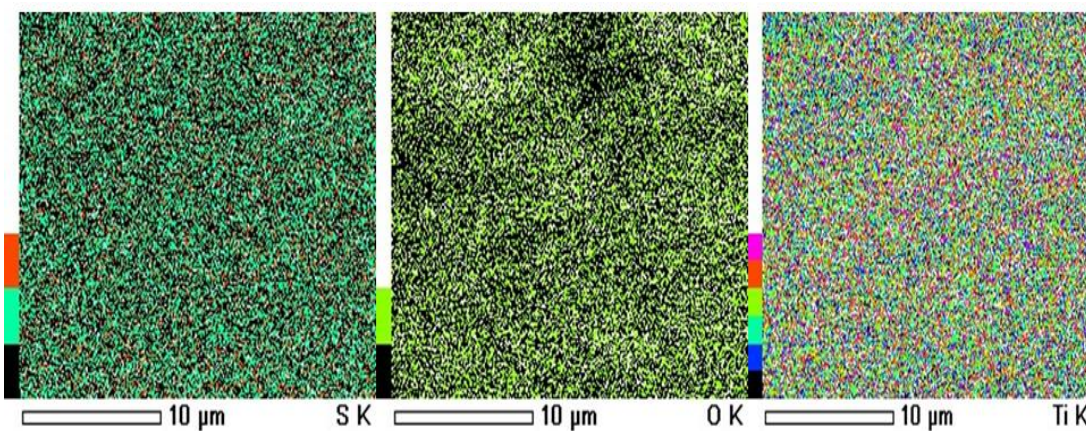


Figure 4.4 Elemental mapping of S-TiO₂ showing the presence of Sulfur (S), Oxygen (O) and Titanium (Ti) in the sample

Figure 4.5 shows the TEM images of TiO₂ and S-TiO₂ nanoparticles. The nanoparticle diameters were found to range from 20 to 30 nm. The morphology of the TiO₂ nanoparticles which is spherical in shape (Figure 4.5 A) turned to somewhat oval shape after sulfation (Figure 4.5 B), which may be due to the result of action of sulfuric acid treatment during sulfation (Krishnakumar and Swaminathan 2011).

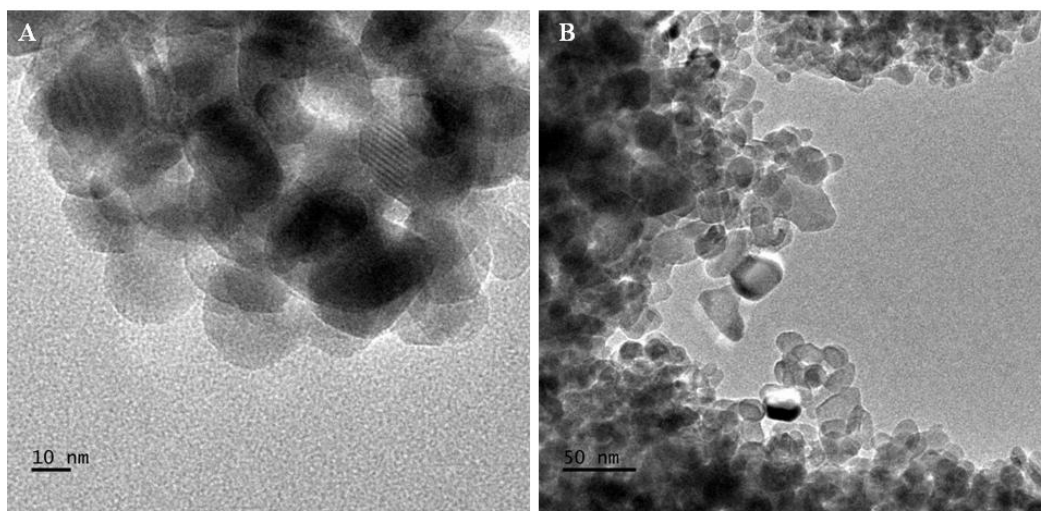


Figure 4.5 TEM Images of A) TiO₂ and B) S-TiO₂

4.4.2 Membrane characteristics

4.4.2.1 Membrane morphology

The cross sectional images of the membranes are shown in Figure 4.6 and Figure 4.7. The SEM images display the typical asymmetric structure of membranes having dense top layer, porous sublayer and macrovoids at the bottom. With the addition of S-TiO₂ to the membranes, change in morphology of the membranes is observed.

The porous nature of the membranes was found to increase with the addition of S-TiO₂ and was maximum for S-2.0 membrane whereas, the pristine membrane S-0, which did not contain any S-TiO₂ had very less pores in it. Except for the membranes S-0, S-0.05, the porous nature was also observed in the skin layer of the membranes. The addition of S-TiO₂ has resulted in imparting significant change to the morphology of the membranes. The addition of S-TiO₂ decreases the thermodynamic stability of the system. This leads to the rapid demixing between the solvent and non solvent which results in enhanced porosity of the membranes (Rabiee et al. 2014, Zhang et al. 2013). It can also be noted that, the macrovoids which were prominent in the pristine, S-0 and S-0.05 membranes, were suppressed and were almost disappearing in the S-1.5, S-2.0 membranes, where the concentration of S-TiO₂ was higher. Similar results were also observed, when TiO₂ was added to the polysulfone membranes (Yang et al. 2007).

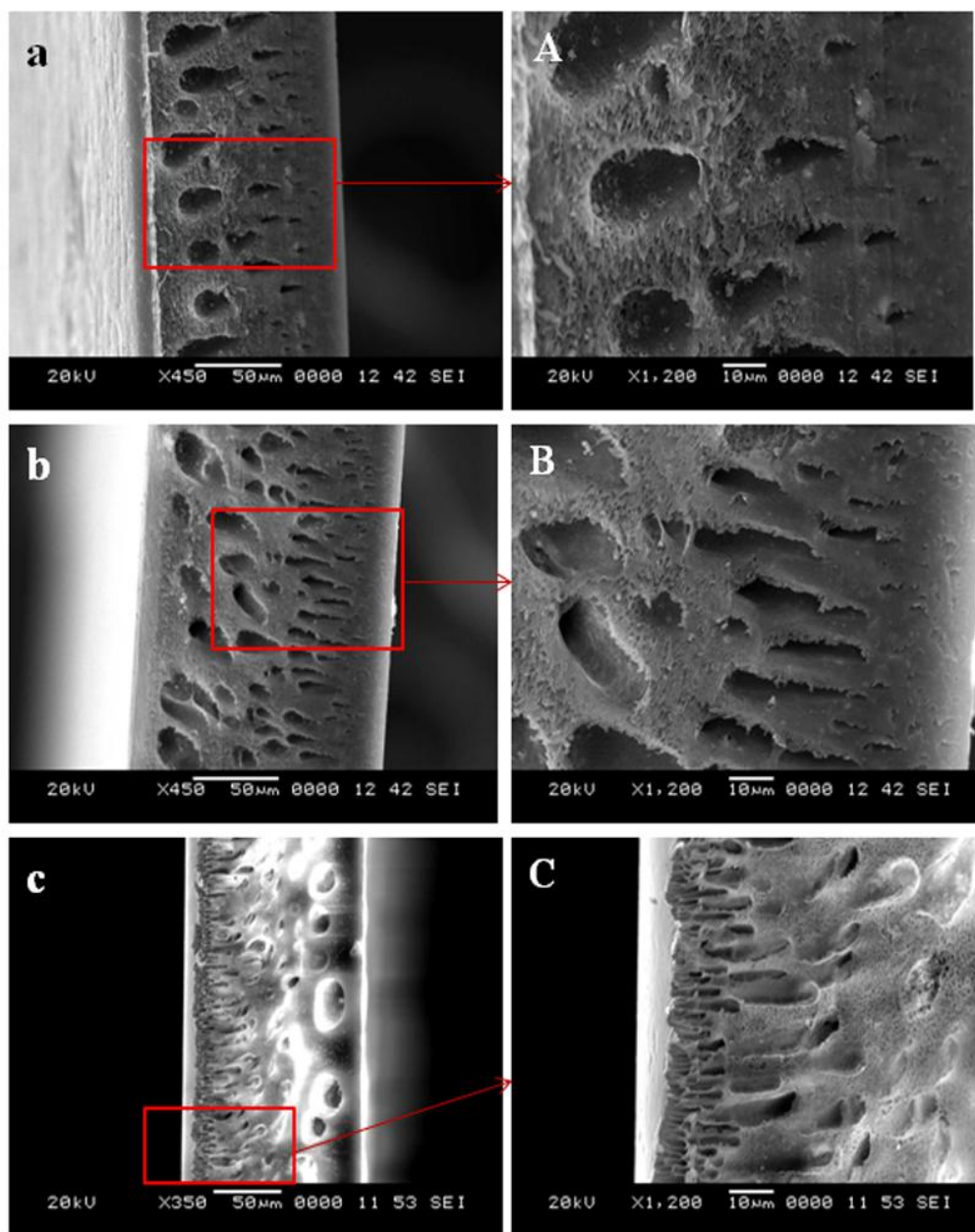


Figure 4.6 SEM cross sectional images of membranes a) S-0 b) S-0.05 c) S-0.5
(A, B, C are magnified images of a, b, c respectively)

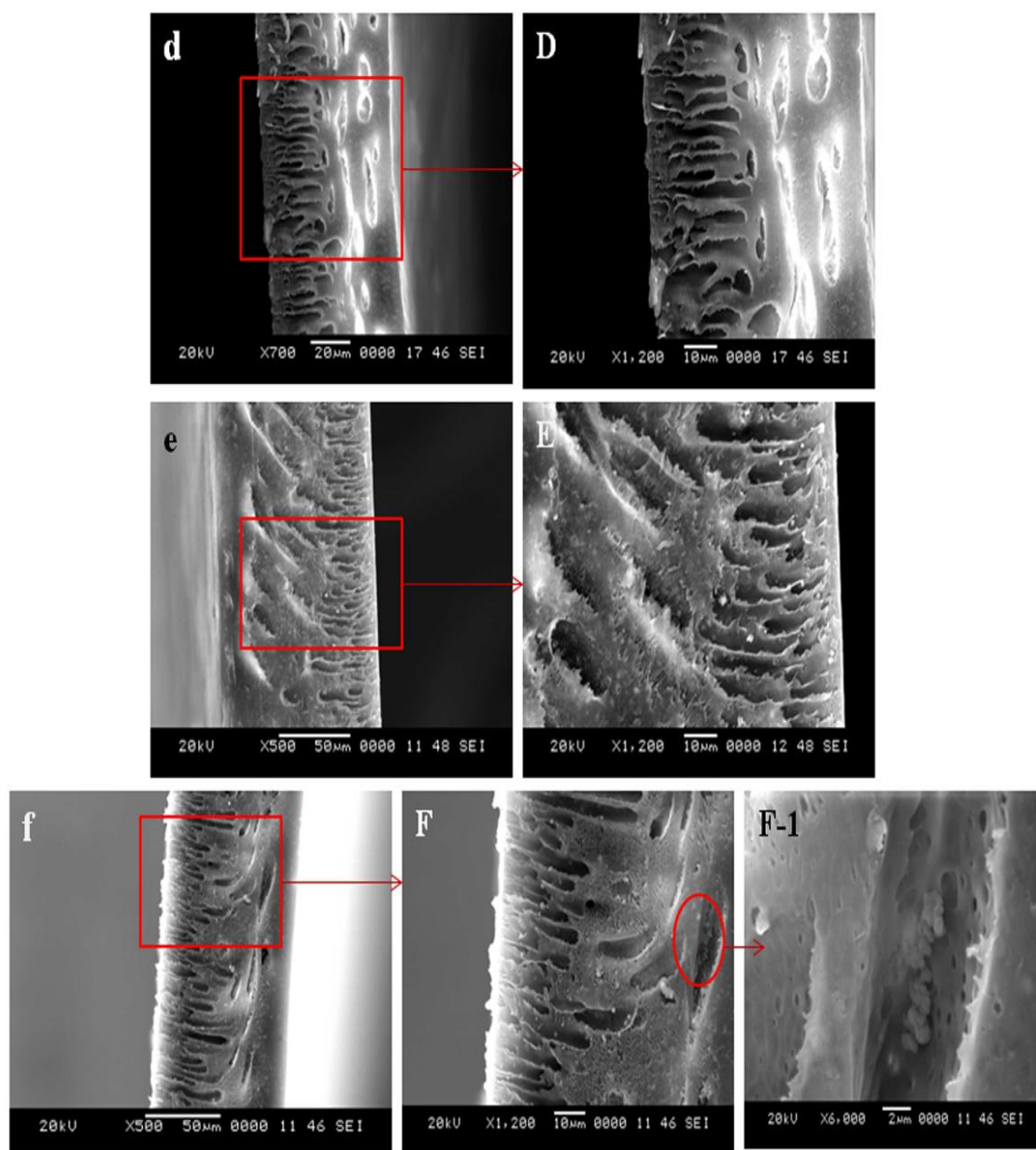


Figure 4.7 SEM cross sectional images of membranes d) S-1.0 e) S-1.5 f) S-2.0 (D, E, F are the magnified images of d, e, f respectively)

As observed in SEM images (Figure 4.7 E, F), the membranes at higher concentrations, which contained 1.5 and 2.0 wt. % of S-TiO₂, showed the presence of S-TiO₂ in the membrane pores. Also some of the S-TiO₂ nanoparticles at 2.0 wt. %, were found to form large aggregates and hence blocking the pores, as displayed in the magnified image (Figure 4.7 F-1) of S-2.0 membrane.

4.4.2.2 Porosity and Water Uptake of membranes

The porosity and water uptake of the membranes is given in Table 4.1. It is observed that, the porosity of the membranes increases with the addition of S-TiO₂. The presence of hydrophilic S-TiO₂ would facilitate the formation of pores. Hence as the concentration of S-TiO₂ in the membranes increases, more number of pores would be formed, resulting in higher porosity of the membranes.

The water uptake of the membranes was in the order S-0<S-0.05<S-0.5<S-1.0<S-1.5<S-2.0 (Table 4.1) i.e., as the concentration of S-TiO₂ in the membranes increased, the water uptake also increased. Water uptake by the membranes depends on membrane porosity. As the porosity of the membranes increases, water uptake ability of the membranes also increases.

Table 4.1 Porosity and Water Uptake of membranes

Membranes	Porosity (%)	Water Uptake (%)
S-0	11.6	23.3
S-0.05	15.3	29.2
S-0.5	23.6	33.9
S-1.0	25.4	36.8
S-1.5	27.9	40.3
S-2.0	31.3	47.2

4.4.2.3 Mechanical strength analysis

Tensile strength and elongation at break are two important criteria which decide the mechanical stability of the membranes (Shi et al. 2012). As seen in Table 4.2, the tensile strength and elongation at break of the membranes increased with the increase in S-TiO₂, from 12.29 MPa (S-0) to 23.59 MPa (S-2.0) and 111.43% (S-0) to 123.63% (S-2.0) respectively. The improvement in mechanical property is be due to TiO₂ which is known to have good mechanical stability and also due to the good dispersion of S-TiO₂ in the membrane matrix, which causes strong interaction between S-TiO₂ and polymer matrix (Abdal-hay et al. 2014). Also the presence of S-

TiO₂ suppresses the formation of macrovoids, thus improving the mechanical properties of the membranes (Shi et al. 2012).

Table 4.2 Mechanical Properties of membranes

Membranes	Tensile Strength (MPa)	Elongation at break (%)
S-0	12.29	111.43
S-0.05	15.59	111.95
S-0.5	19.86	114.55
S-1.0	20.96	121.40
S-1.5	21.38	123.63
S-2.0	23.59	131.40

4.4.2.4 AFM analysis

The two-dimensional and three dimensional AFM images of the selected membranes, S-0, S-1.0 and S-2.0 membranes are shown in Figure 4.8. The addition of S-TiO₂ into the membranes induced changes on the membrane surface. The neat S-0 membrane which did not contain any S-TiO₂ nanoparticles appeared to be rough whereas the surface roughness was found to decrease with the addition of S-TiO₂. This was confirmed by the surface roughness parameters observed for the membranes (Table 4.3) which is expressed in terms of mean roughness (R_a) and root mean square roughness (R_q).

Table 4.3 Surface roughness parameters of membranes

Membranes	Surface roughness parameters	
	R_a (nm)	R_q (nm)
S-0	11.8	16.4
S-1.0	10.6	12.6
S-2.0	8.10	10.5

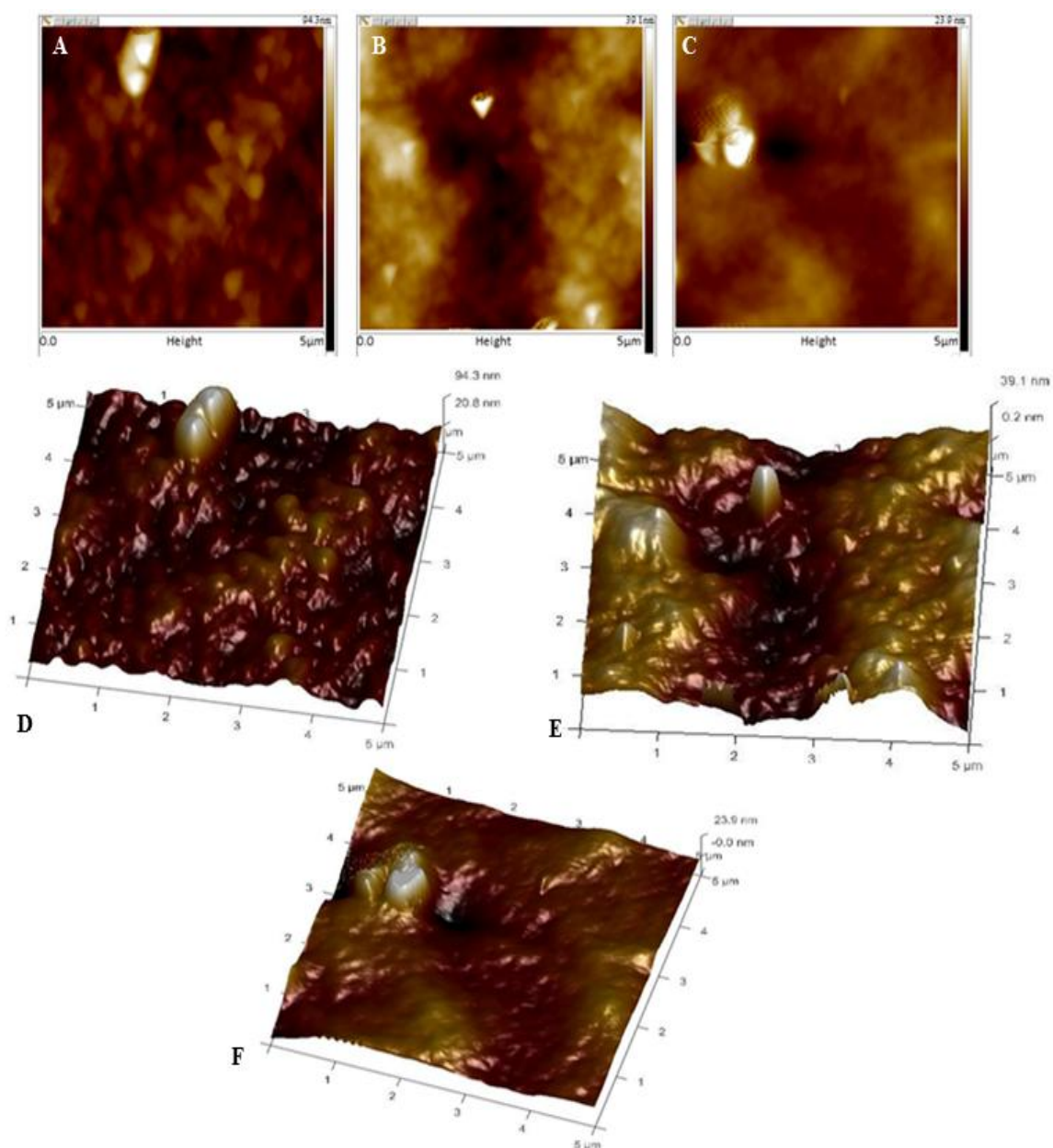


Figure 4.8 Two-dimensional scans of A) S-0, B) S-1.0 and C) S-2.0 membranes and three dimensional scans of D) S-0, E) S-1.0 and F) S-2.0 membranes

4.4.2.5 Contact Angle of membranes

Contact angle is used to determine the hydrophilicity and wetting ability of membrane surface. The contact angle of neat PSf membrane (S-0) was about 70° , whereas S-TiO₂ containing membranes showed lower contact angle. With the addition

of S-TiO₂, the contact angle of the membranes decreased, indicating that the hydrophilicity of the membranes is elevated by the addition of S-TiO₂. The contact angle was least (60°) for S-1.0 membrane with S-TiO₂ content of 1.0 wt. %, and thereafter for S-1.5 and S-2.0 membranes, the contact angle slightly increased. This may be due to the reason that at 1.5 and 2.0 wt. %, the high content of S-TiO₂ would block the membrane pores, resulting in higher contact angle. However S-1.5 and S-2.0 membranes were more hydrophilic than the neat PSf (S-0) membrane as shown in Figure 4.9. Figure 4.10 shows the images of the contact angles measured on the membrane surfaces.

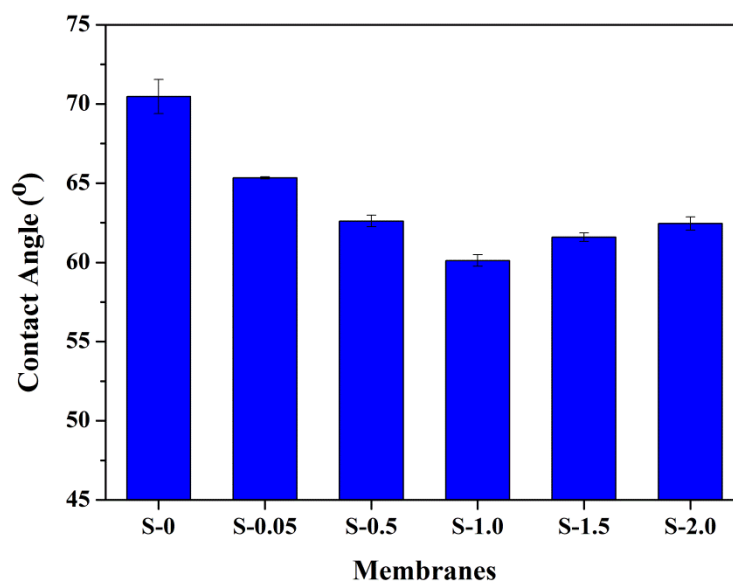


Figure 4.9 Contact Angle of the membranes

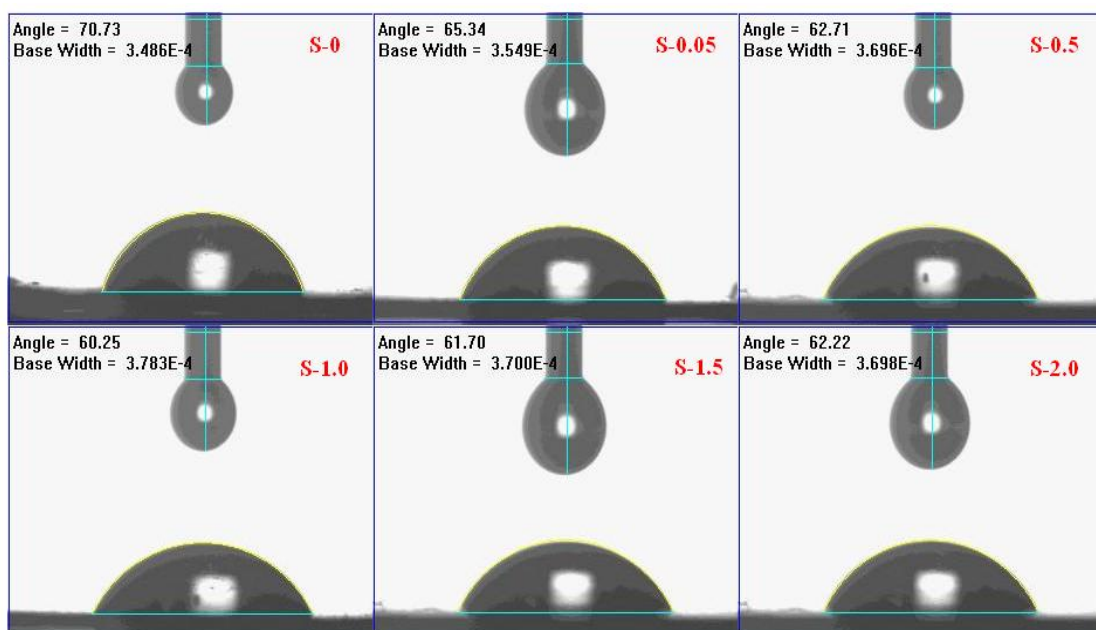


Figure 4.10 Images of contact angles measured on membrane surfaces

4.4.2.6 Water Permeability of membranes

The time dependent pure water flux of the membranes is shown in Figure 4.11. The water permeability of the nanocomposite membranes was superior when compared with the pure PSf membrane. The PWF of the membranes increased with the increase in S-TiO₂ content, especially after 0.05 wt.% of S-TiO₂ content. When the S-TiO₂ content was 2.0 wt.%, the pure water flux reached maximum of about 6.37 L/m²h which is nearly 12 times higher than that of S-0 membrane (Zhang et al. 2012). The increase in flux is due to the lower membrane resistance offered by the thinner skin layer and higher porosity (Peng et al. 2010). The improvement in membrane hydrophilicity with S-TiO₂ will also facilitate the diffusion of water through the membrane (Huang et al. 2013). Water flux of the membranes also depends on the morphology of the membranes. As shown in SEM images of the membranes (Figure 4.6 and 4.7), the internal structure of the membranes changed from closed structure to well interconnected pores, resulting in improving the water flux (Qin et al. 2015).

The PWF of the membranes vs. pressure is shown in Figure 4.12. The pure water flux of all the membranes increased with the increase in applied pressure. This

is because, the driving force for the permeation of pure water through membranes is enhanced by the increase in transmembrane pressure.

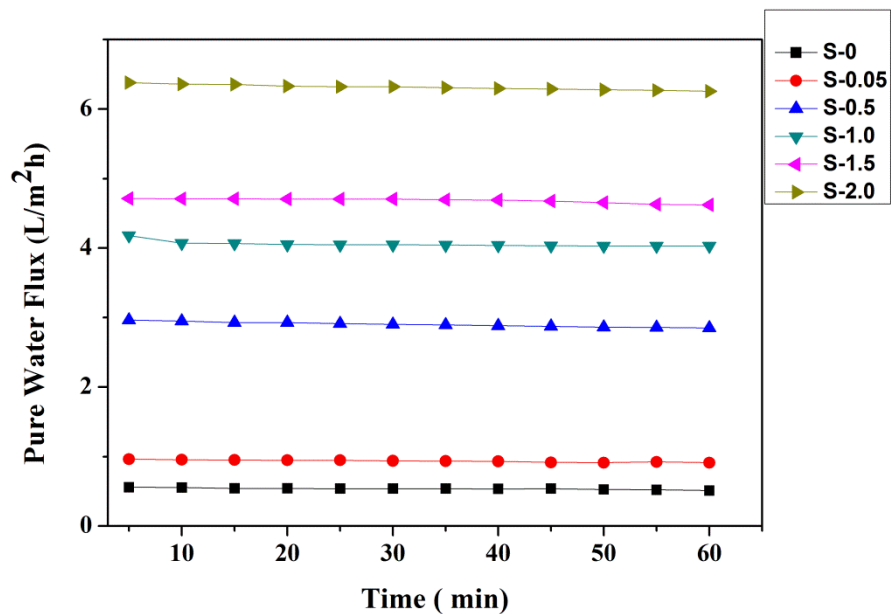


Figure 4.11 Pure water flux of the membranes at 0.6 MPa

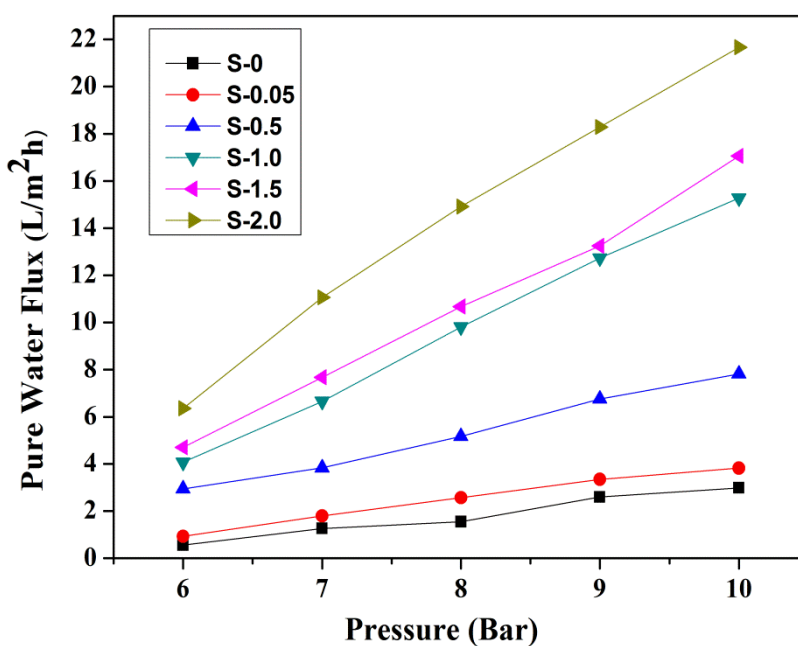


Figure 4.12 Pure water flux vs. pressure

4.4.2.7 Antifouling nature of membranes

Figure 4.13 shows the time dependent flux behavior of the membranes during BSA filtration along with the water flux before and after the BSA filtration. As

observed in Figure 4.13, the initial flux for 30 minutes refers to the pure water flux. For next 30 minutes the flux given is with respect to the BSA filtration. The flux of the membranes during BSA filtration was much lower than that of the pure water flux. This is due to the reason that, the BSA molecules present in the feed solution get adsorbed or deposit on the membrane surface resulting in partial blocking of the pores, thus resulting in lower flux (Kumar et al. 2013, Peng et al. 2010).

After the BSA filtration, the membranes were washed thoroughly and the water flux was measured again (Zhao et al. 2015). Here we observe an increase in flux, which implies that BSA molecules were removed from membrane surface during washing, which results in good flux recovery. Depending on the obtained flux value, FRR value for each of the membranes was calculated in order to evaluate the antifouling ability of the membranes. FRR is the measure of antifouling nature of the membranes. Higher the FRR value, better is the antifouling nature of the membranes.

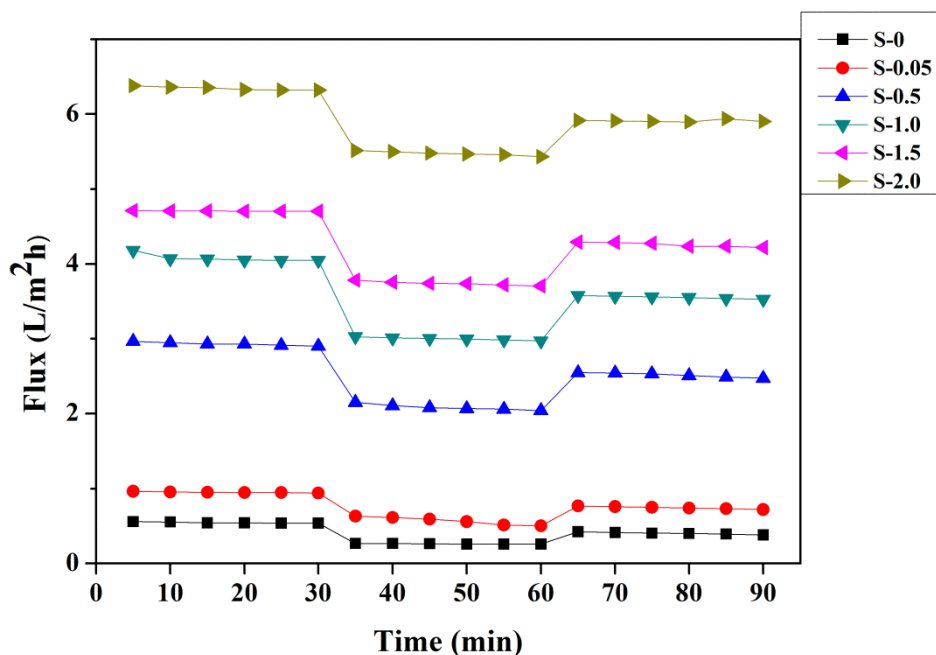


Figure 4.13 Flux of the membranes during BSA filtration

Figure 4.14 shows the FRR values of the membranes. FRR value is least for S-0 membrane which is about 76%, whereas for the nanocomposite membranes, FRR increased with the S-TiO₂ content and reached maximum of 93% for S-2.0 membrane. The presence of sulfated nano TiO₂ weakened the interaction between the membrane

surface and BSA molecules. Also high FRR value indicated that, the adsorbed BSA molecules on the membrane surface were removed during hydraulic cleaning.

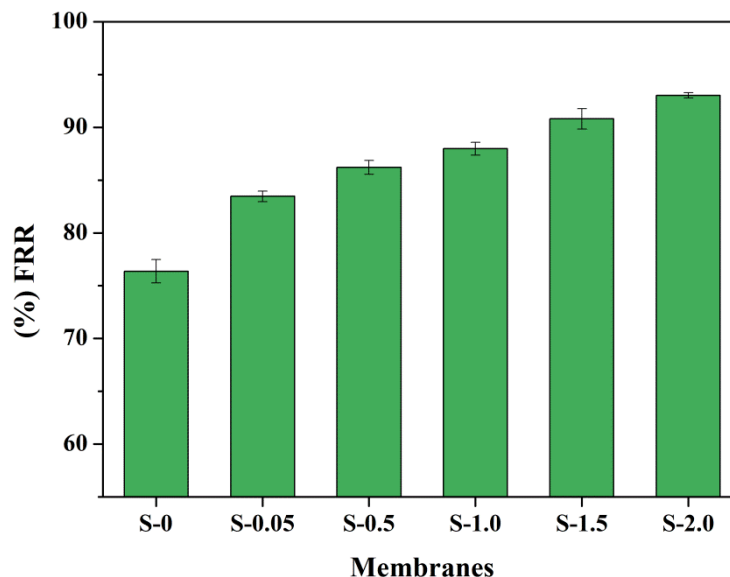


Figure 4.14 Flux Recovery Ratio (FRR) of membranes

The antifouling nature of the membranes was supported by the AFM results. From AFM measurements it was found that the membranes containing S-TiO₂ nanoparticles were smooth (Figure 4.8, Table 4.3). Lower the surface roughness of the membranes, higher would be the antifouling nature of the membranes (Razmjou et al. 2011).

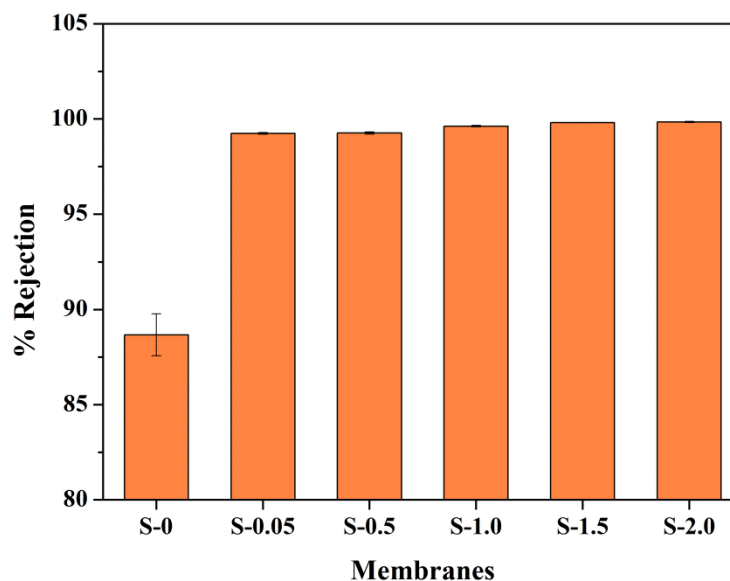


Figure 4.15 BSA Rejection % by the membranes

The BSA rejection % by the membranes is shown in Figure 4.15. The rejection properties of all the nanocomposite membranes except neat PSf membrane were almost same. The rejection % of BSA by the neat PSf membrane (S-0) was 88% and the rejection % of all the nanocomposite membranes was 99%. Since the BSA molecules were larger in size than the pore size of the membranes, almost all the BSA molecules were rejected by the membranes.

4.4.2.8 Dye Removal by membranes

Figure 4.16 and Figure 4.17 shows the MB rejection by the membranes under dark and UV conditions at 10 ppm and 20 ppm MB concentrations respectively. The membranes showed a maximum rejection of 90.4% at 10 ppm concentration of MB under UV radiation, whereas the neat PSf membranes showed lowest rejection of 13.3% at 20 ppm of MB concentration.

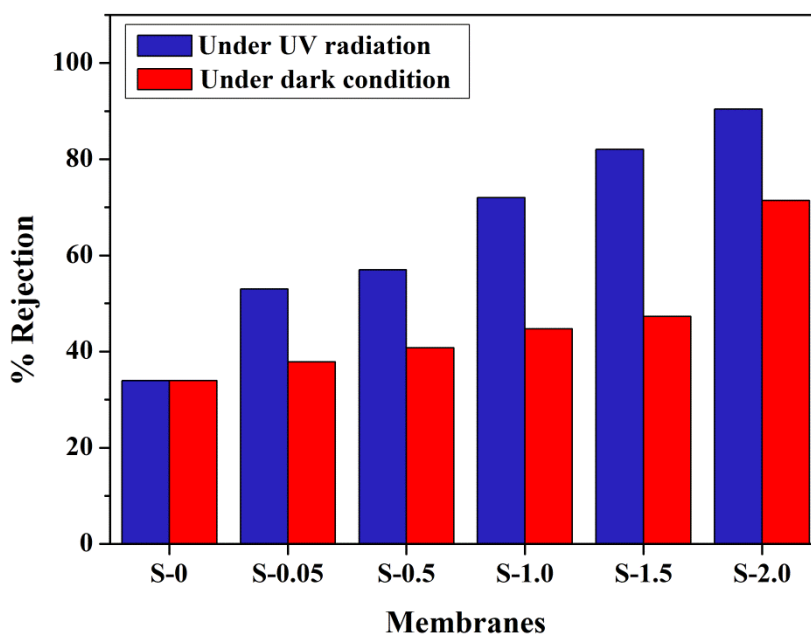


Figure 4.16 MB dye rejection by the membranes at 10 ppm

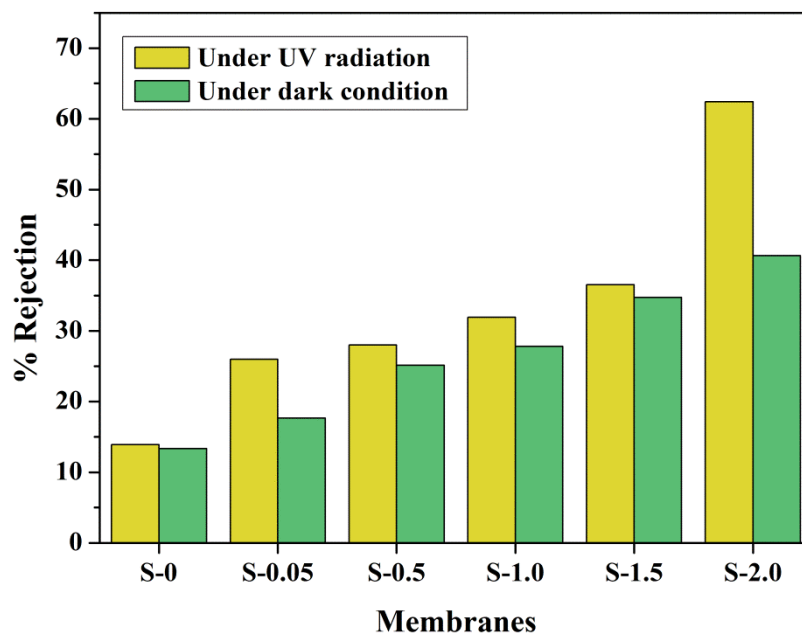


Figure 4.17 MB dye rejection by the membranes at 20 ppm

It can be seen that, the MB rejection increased with the increase in S-TiO₂ content in the membranes and was found to be least for the PSf membranes. The MB dye removal by the membranes takes place by two mechanisms, i.e., by adsorption and photodegradation (Mozia et al. 2007).

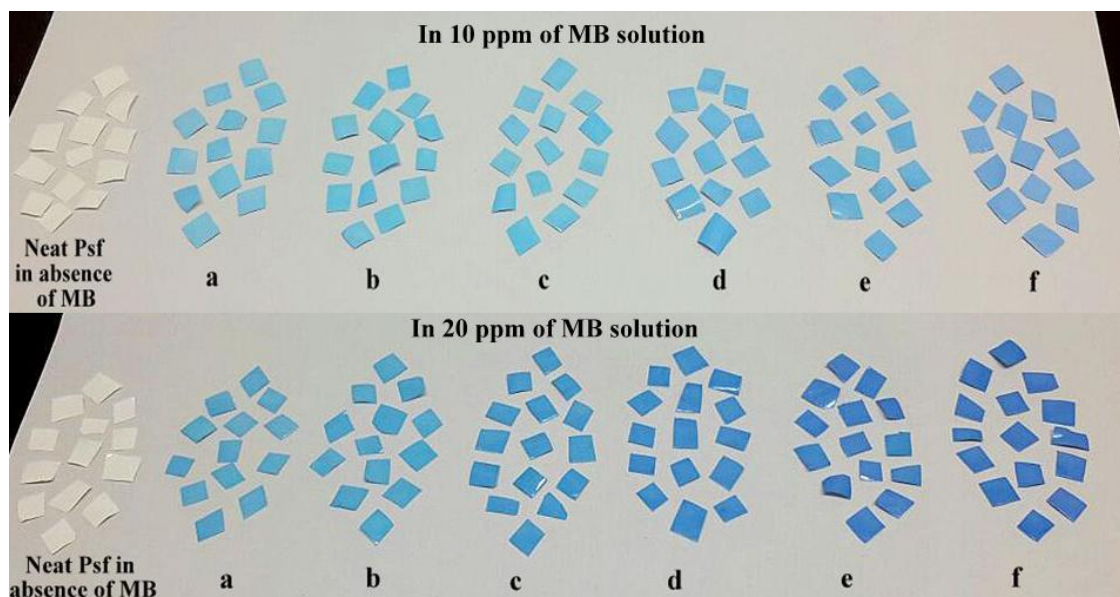


Figure 4.18 Adsorption of MB on the membrane surface under dark conditions (a, b, c, d, e and f are membrane pieces of S-0, S-0.05, S-0.5, S-1.0, S-1.5 and S-2.0 respectively)

The dye removal by adsorption is as follows. Due to the presence of SO_4^{2-} - TiO_2 , the membrane is negatively charged. Since MB is a cationic dye, it can easily get adsorbed on the membrane surface by electrostatic interactions (Li et al. 2011). Hence the retention of MB by the membranes is due to the adsorption of MB on the membrane surface and in the pores (Fradj et al. 2014). The adsorption of MB on the membrane surface is shown in the Figure 4.18 and Figure 4.19. It is seen that, the membranes changed from white to blue when immersed in MB solution and also as the S- TiO_2 content in the membranes increases, the adsorption also increases (Zheng et al. 2009). This is because, more adsorption sites are available at higher content of S- TiO_2 . The adsorption of MB on the membrane surface was confirmed by elemental mapping of Nitrogen (element which is present in MB) as shown in Figure 4.20.

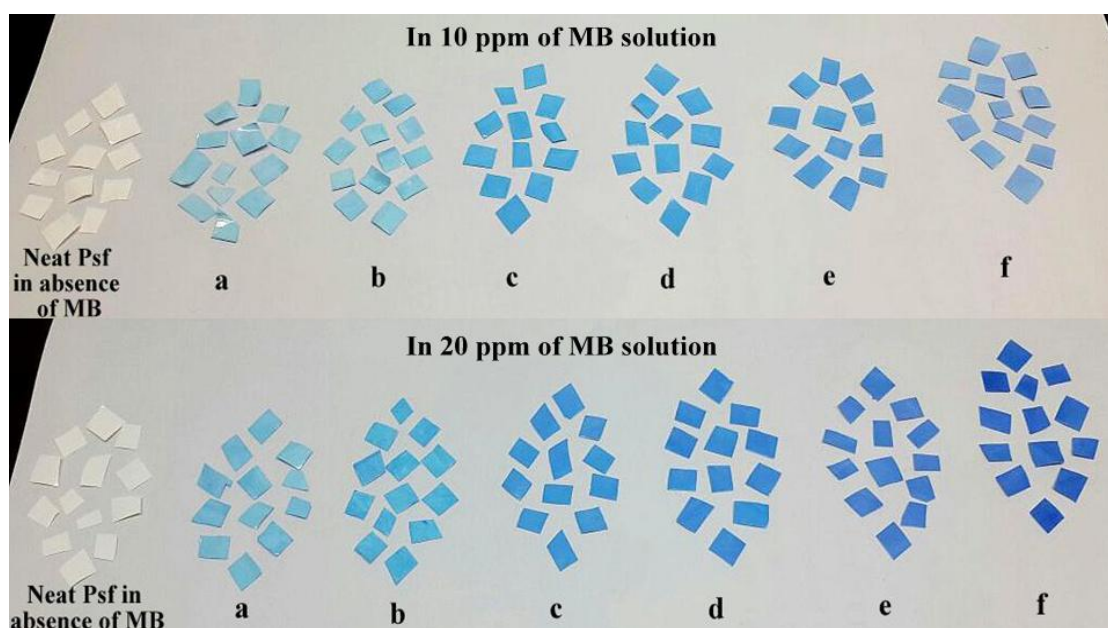


Figure 4.19 Adsorption of MB on the membrane surface under UV (a, b, c, d, e and f are membrane pieces of S-0, S-0.05, S-0.5, S-1.0, S-1.5 and S-2.0 respectively)

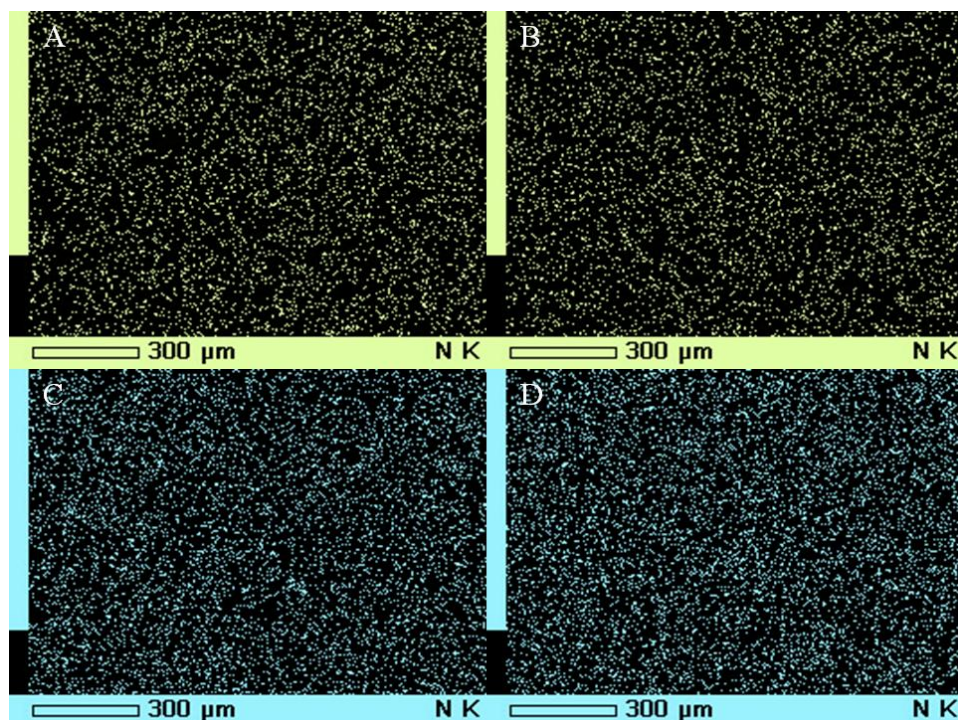


Figure 4.20 Elemental mapping of N for adsorption of MB on the membrane surface (A, B are surfaces of S-0 membrane after adsorption at 10 ppm and C, D are the surfaces of S-2.0 membrane after adsorption at 20 ppm)

Comparing dye rejection in Figure 4.16 and Figure 4.17, it can be noted that the increase in MB concentration from 10 ppm to 20 ppm results in fall of dye rejection by the membranes. MB being a cationic dye, present in the solution get adsorbed on the membrane surface and neutralize the negative charge present on the membrane surface. Hence the available adsorption sites on the membrane surface for MB becomes gradually less and also the electrostatic force of attraction between the membrane surface and MB is gradually weakened (Mozia et al. 2007). Hence the possible interaction between MB and membrane surface is reduced at higher concentration of MB. Therefore the rejection of MB by the membranes was low at higher concentration. Figure 4.21 shows rejection of MB by the membranes with reference to the color of the solutions.

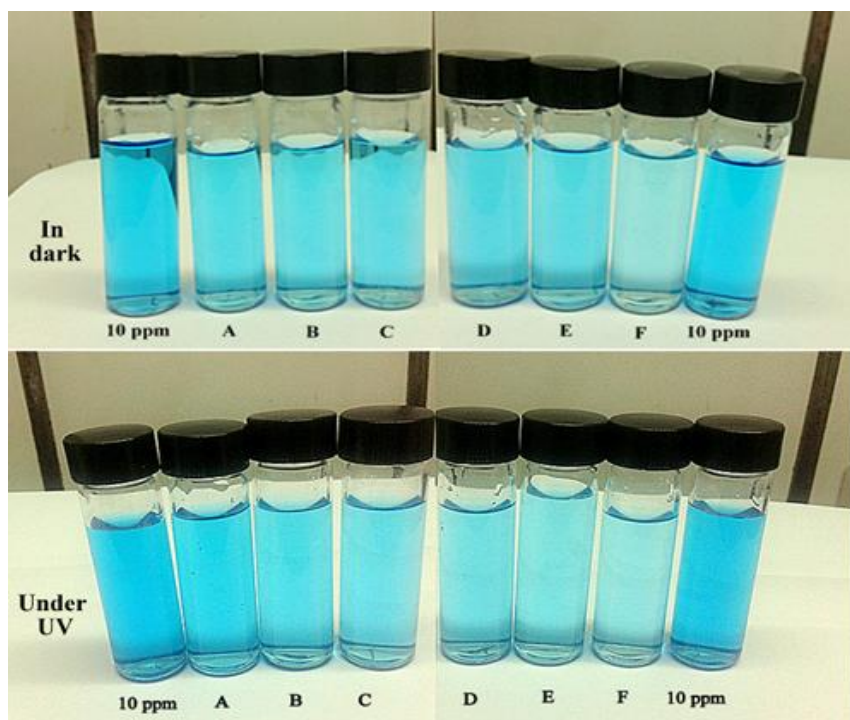


Figure 4.21 Rejection of MB by membranes at 10 ppm (A, B, C, D, E and F are the solutions of MB after the rejection by the membranes S-0, S-0.05, S-0.5, S-1.0, S-1.5 and S-2.0 respectively)

The dye removal by the membranes by photodecomposition takes place as follows. During the photodecomposition, MB degradation occurs mainly due to the hydroxyl radical ($\cdot\text{OH}$). TiO_2 is a photo catalyst, which when photoexcited at a wavelength below 380 nm, the photons excite the electrons (e^-) from valence band to the conduction band, leaving behind the holes (h^+) in the valence band. The holes react with water or hydroxide ions producing hydroxyl radical, which degrade MB (Mohamed and Al-Esaimi 2006). But in TiO_2 , photocatalytic activity is limited due to the recombination of electrons and holes resulting in low photo efficiency (Zhan et al. 2014). In sulfated TiO_2 , the presence of SO_4^{2-} improves the photocatalytic efficiency and hence intern increases the MB degradation. The sulfation of TiO_2 in S- TiO_2 results in strong acidity giving rise to Lewis acid sites or electron deficient sites. They act as electron trap for photogenerated electron, thereby increasing the life time of $\cdot\text{OH}$ radical resulting in enhanced photocatalytic activity (Mohamed and Al-Esaimi 2006, Zhan et al. 2014). Also the acidified surface in S- TiO_2 , on calcination, would

lead to the generation of oxygen deficiency, which again serve as capture centers for photoexcited electrons. This hinders the recombination of electrons and holes, while the surrounding hydroxyl groups react with photoexcited holes to generate $\cdot\text{OH}$ radicals, which are the main oxidants in MB degradation (Gambhire et al. 2011, Zhan et al. 2014).

4.5 CONCLUSIONS

Sulfated-TiO₂ (S-TiO₂) can be used as effective additives to Polysulfone (PSf) membranes to improve the properties of membranes in terms of hydrophilicity, porosity, water uptake and water flux. PSf membranes with S-TiO₂ exhibited good antifouling nature. The improvement in properties of PSf membranes depend on the concentration of S-TiO₂ in the membranes. Higher the S-TiO₂ content, better is the performance of the membranes. However at higher concentration i.e. at 1.5 wt.% and 2.0 wt.% of S-TiO₂, aggregation of nanoparticles in the membranes is observed, which may hinder the performance of the membranes to some extent. The synthesized membranes can be used effectively for the removal of BSA molecules, with rejection of 99%. The PSf-S-TiO₂ membranes are more effective in MB dye removal under UV irradiation. The MB dye removal by the membranes increased with S-TiO₂ content in the membranes and S-2.0 membrane showed highest rejection of 90.4% at 10 ppm concentration of MB under UV radiation. This approach showed that polysulfone-S-TiO₂ membranes displayed good efficiency for dye removal and can be effectively used for the removal of MB dye from aqueous solutions under suitable conditions.

CHAPTER 5

PREPARATION AND CHARACTERIZATION OF POLYSULFONE MEMBRANES CONTAINING TiO₂, SiO₂ 3- AMINOPROPYLTRIETHOXYSILANE (APTES) MODIFIED TiO₂ AND SiO₂ NANOCOMPOSITES

Abstract

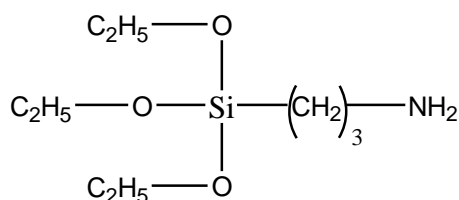
This chapter explores the addition of nano TiO₂ and nano SiO₂ in the PSf membranes. The chapter further presents the modification of these nanomaterials (nano-TiO₂ and nano SiO₂) with –NH₂ groups, which is achieved using 3-Aminopropyltriethoxysilane (APTES). The effect of presence of amine groups in the membranes on the membrane performance in terms of morphology, contact angle, surface topography, permeability and antifouling ability is presented. The membranes were also used for heavy metal ion rejection which showed a maximum rejection of 75.6% for Cd²⁺ metal ions.

5.1 INTRODUCTION

In the recent years, nanocomposites have gained lot of attention from both academics and industries, due to its better mechanical, flow property, alteration in electrical conductivity and thermal properties changing also the physical appearance and minimizing the cost. In order to improve polymer membrane properties, many researches in nanocomposite have been extended into various polymer systems. The enhancement in properties can be due to the nanoscale structure effects and the interaction between the inorganic materials and organic polymers (Lokesh et al. 2008). Many nanoparticles have been introduced to modify organic membranes, such as SiO₂, ZnO, Fe₃O₄, SnO₂ and TiO₂. Addition of inorganic particles into membranes, in relation to modification of polymeric membranes for enhancing its hydrophilic character, has been successfully proved to reduce the membrane fouling. When hydrophilic nanoparticles particles are added in the membrane matrix it increases hydrophilicity of the polymer membrane and enhances the water permeability while mitigating the membrane fouling simultaneously (Martín et al. 2015).

Titanium dioxide (TiO₂) is a very important nanomaterial used in industry. It has been extensively used in paints, cosmetics, photocatalysis and photocatalyst supports (Cheng et al. 2014). Surface modification of SiO₂ or TiO₂ nanoparticles can be achieved by chemical or physical methods. When chemical processes are applied, various organic or inorganic compounds of low molecular weight are preferred. The most common modifying agents are silane promoters terminated with functional groups. The –OH group present on the surface of SiO₂/TiO₂ allow to bond covalently

with different trialkoxyorganosilanes which are functionalized with amine ($-\text{NH}_2$) groups. The amine surface modification results in high yield and uniform distribution of nanoparticles (Gradzik et al. 2011).



3-Aminopropyltriethoxysilane (APTES)

Figure 5.1 Structure of 3-Aminopropyltriethoxysilane (APTES)

3-Aminopropyltriethoxysilane (APTES) has terminal amine group on the propyl chain (Figure 5.1). It is widely used as a coupling agent for attaching the organic molecules on to hydroxylated SiO_2 or TiO_2 (Cheng et al. 2014). The APTES-modified TiO_2 and SiO_2 nanoparticles can be synthesized in a simple method at a low reaction temperature.

Gradzik et al. (2011) modified TiO_2 and SiO_2 nanoparticles using different molecules, where APTES was one among them, in order to reduce the agglomeration of nanoparticles. The modification was confirmed by FTIR and UV-Vis spectroscopy. The best results were obtained when APTES in methylizobutylketone was used as the modifying agent.

Cheng et al. (2014) modified commercially available TiO_2 nanoparticles with APTES and then deposited them on to the surface of paper sample by dip coating method in water. The presence of terminal $-\text{NH}_2$ groups in APTES modified TiO_2 contributed to the attachment of TiO_2 onto the surfaces of fibers of paper samples. Thus the APTES modified TiO_2 coated paper exhibited high stability towards UV-illumination.

Martin et al. (2015) synthesized SiO_2 nanoparticles and functionalized them with amine and carboxylic groups. The amine fictionalization was done using APTES. The functionalized SiO_2 were in corporate into PES membranes. Membrane functions such as water permeability and antifouling property enhanced in the presence of amine and carboxylic groups.

In the present research work, commercially available TiO_2 and SiO_2 nanoparticles were modified using silane coupling agent, in order to have amine groups on TiO_2 and SiO_2 . The effect of addition of TiO_2 and SiO_2 and their aminated forms on the membrane performance was analyzed. The synthesized nanocomposite membranes were also used for the rejection of Cadmium metal ions.

5.2 EXPERIMENTAL

5.2.1 Materials

Polysulfone (PSf) having molecular weight of 35,000 Da, TiO_2 and SiO_2 nanoparticles was purchased from Sigma Aldrich Co., Bangalore, India. Bovine Serum Albumin (BSA) was obtained from Central Drug House (CDH), New Delhi. N-methyl-2- pyrrolidone (NMP) was purchased from Merck India, Ltd. 3- Aminopropyl Triethoxy Silane (APTES), ($\text{C}_9\text{H}_{23}\text{NO}_3\text{Si}$) was purchased from Spectrochem Pvt. Ltd. Mumbai (India). Cadmium nitrate tetrahydrate was purchased from Sigma-Aldrich Co., Bangalore, India.

5.2.2 Modification of TiO_2 and SiO_2 nanoparticles

The modification of TiO_2 and SiO_2 nanoparticles were carried out following a reported literature (Razmjou et al. 2011). 1 g of TiO_2 was dispersed in 50 mL of ethanol under N_2 atmosphere. The solution was sonicated for 30 min at a frequency of 40 kHz for uniform dispersion. Then the silane coupling agent, APTES (3 mL) was added drop wise to the mixture under N_2 atmosphere. The solution was stirred for 2 h at 65°C . The modified TiO_2 nanoparticles were separated from the solution using centrifuge. The aminated TiO_2 (A- TiO_2) nanoparticles were washed several times using ethanol and were dried in oven at 80°C for 24 h yielding 0.9 g of APTES modified TiO_2 (A- TiO_2).

The modification of SiO_2 using APTES, was carried out in a similar manner, where instead of TiO_2 , SiO_2 nanoparticles were used.

5.2.3 Preparation of membranes

The membranes were prepared by phase inversion method. For neat PSf membrane, 20 wt.% of PSf was dissolved in NMP under stirring. For the nanocomposite membranes, the nanoparticles were first added to NMP. The solution

containing nanoparticles was sonicated for 15 min for their uniform dispersion and then kept under stirring. Then 20 wt.% PSf was added to the same dispersion and stirred for 6 h at 70°C. After the complete dissolution of PSf, the casting solution was sonicated for 15 min and left still for 30 min to remove any trapped air bubbles. The solution was then casted on to the glass plate and dipped in the water coagulation bath for 24 h for the phase inversion to occur. The concentration of nanoparticles was fixed to 1.0 wt.% for all the membranes. The composition of the membranes is given in Table 5.1.

Table 5.1 Composition of the membranes

Membrane Codes	PSf (wt. %)	Nanoparticles added	Wt. % of nanoparticles added	NMP (wt. %)
P	20	-	-	80
P-T	20	TiO ₂	1.0	79
P-AT	20	Aminated TiO ₂ (A- TiO ₂)	1.0	79
P-S	20	SiO ₂	1.0	79
P-AS	20	Aminated SiO ₂ (A- SiO ₂)	1.0	79

5.3 CHARACTERIZATION

5.3.1 Characterization of aminated TiO₂ and aminated SiO₂

The modification on TiO₂ and SiO₂ by APTES was confirmed by FTIR. FTIR spectra were recorded from SHIMADZU ATR-FTIR spectrophotometer in the range of 4000-600 cm⁻¹.

5.3.2 Characterization of membranes

The cross sectional morphology of the membranes was studied using SEM. The samples for SEM were prepared as explained earlier in section 2.3.3.1 of CHAPTER 2.

The surface hydrophilicity and water uptake capacity of the membranes was evaluated following the procedures mentioned in sections 2.3.3.2 and 2.3.3.3 of CHAPTER 2.

The permeation properties and antifouling ability of the synthesized membranes were tested by calculating the PWF and FRR values as described in sections 2.3.3.4 and 2.3.3.5 of CHAPTER 2.

The surface topography of the membranes was analyzed using AFM. The samples were imaged in tapping mode following similar methods mentioned in section 3.3.2.2 of CHAPTER 3. The PWF and BSA flux was measured at 0.6 MPa TMP.

The heavy metal ion rejection by the membranes for the metal ion Cd^{2+} was evaluated. The heavy metal ion feed solutions of Cd^{2+} was prepared at a concentration of 1000 ppm. These solutions were filtered individually through the membranes at 0.6 MPa TMP and the permeate was collected. The % rejection for Cd^{2+} by the membranes was calculated using the equation 2.5 of section 2.3.3.6 in CHAPTER 2. The concentration of metal ions in the feed and permeate solution was analyzed using Atomic Absorption Spectrophotometer (GBC 932 Plus).

5.4 RESULTS AND DISCUSSIONS

5.4.1 FTIR analysis

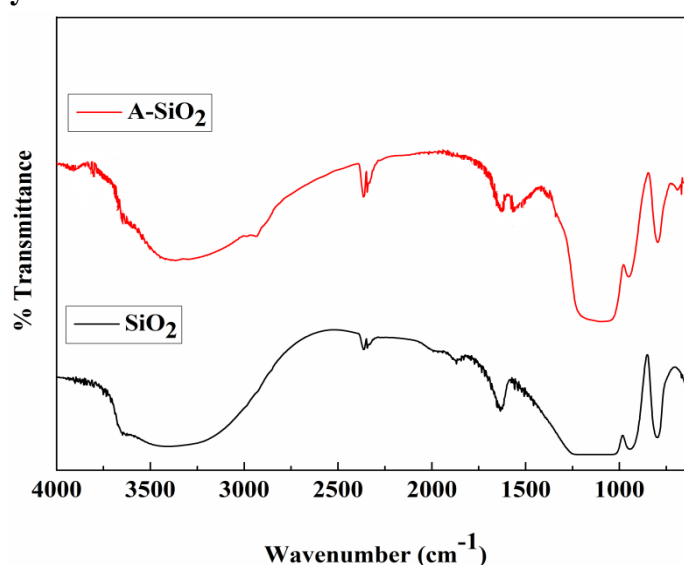


Figure 5.2 FTIR spectra of SiO₂ and A-SiO₂

The FTIR spectra of SiO_2 and aminated SiO_2 (A- SiO_2) is shown in Figure 5.2. In IR spectrum of SiO_2 a broad band appeared between 3000 and 3600 cm^{-1} , which is due to the $-\text{OH}$ stretching of silanol groups (Arantes et al. 2012). Peak at 1640 cm^{-1} is due to the presence of adsorbed water molecules on silica. The characteristic intense band of SiO_2 appeared from 1200 - 1000 cm^{-1} which can be ascribed to the asymmetric stretching vibrations of siloxane (Si-O-Si) (Kim et al. 2012). Peak at 950 cm^{-1} and in the range of 800 - 700 cm^{-1} can be assigned to the Si-OH stretching and symmetric stretching vibrations of siloxane (Si-O-Si) of SiO_2 respectively (Kim et al. 2012, Tsai et al. 2011).

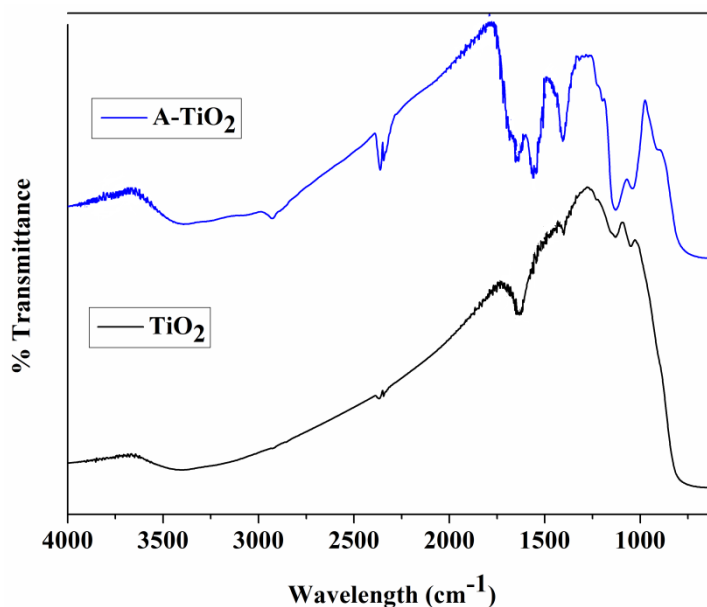


Figure 5.3 FT-IR spectra of TiO_2 and A- TiO_2

Figure 5.3 displays the FTIR spectra of TiO_2 and aminated TiO_2 . In IR spectrum of TiO_2 , intense peak between 3500 and 3000 cm^{-1} appeared due to the surface hydroxyl group and small peak at 1640 cm^{-1} is due to the adsorbed water on TiO_2 (Gradzik et al. 2011). Band from 600 - 1000 cm^{-1} is ascribed to the Ti-O-Ti vibrations of TiO_2 (Pereira et al. 2015). In A- TiO_2 , apart from the above mentioned peaks, new absorption peaks appeared (Oh et al. 2007). Peak at 2923 cm^{-1} is assigned to the C-H bond stretching of alkyl groups in APTES (Cheng et al. 2014). New band at 1540 cm^{-1} is ascribed to the N-H bending vibration of $-\text{NH}_2$ groups from aminosilane (Gradzik et al. 2011).

5.4.2 Characterization of membranes

5.4.2.1 Morphology of membranes

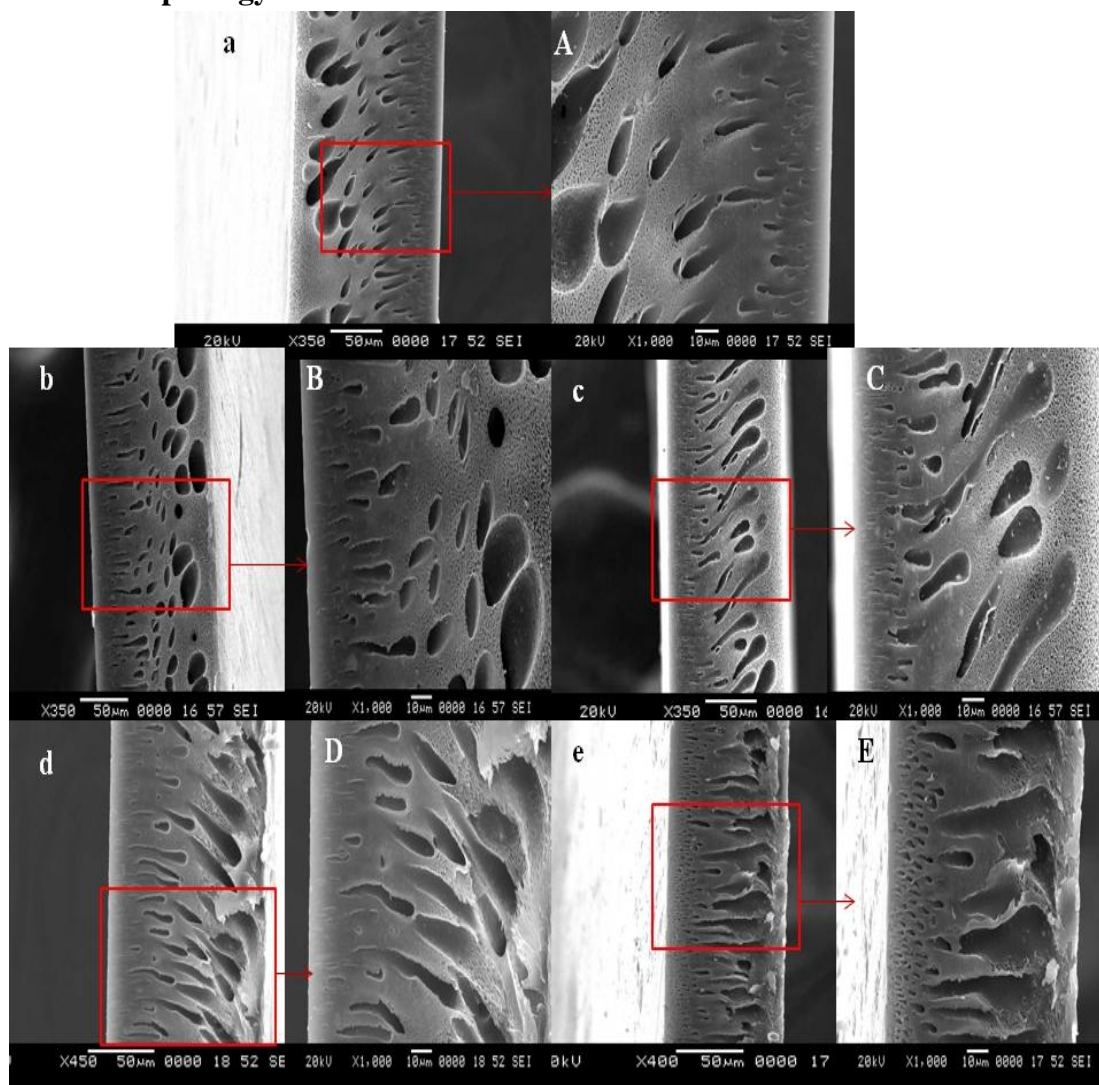


Figure 5.4 SEM cross sectional morphology of the membranes a) P b) P-T c) P-AT d) P-S e) P-AS (A, B, C, D and E are magnified images of a, b, c, d and e)

The SEM cross sectional morphology of the membranes is shown in Figure 5.4. The morphology of the synthesized membranes was studied in order to observe any possible differences in the internal structure of the membranes due to the addition of nanoparticles. All the membranes exhibited typical asymmetric structure with skin layer at the top, dense porous structure and macrovoids at the bottom. However the macrovoids reduced on addition of TiO_2 and SiO_2 in the membranes. On addition of

A-TiO₂ and A-SiO₂ to the membranes, the macrovoids almost disappeared and long finger like projections became more prominent. Also in the case of membranes containing aminated TiO₂ and aminated SiO₂, even the skin layer appeared porous in nature. This contributed to the improved water flux by the membranes as observed in the permeation studies of the membranes.

5.4.2.2 Contact angle and water uptake of membranes

The surface hydrophilicity of the membranes was assessed by contact angle measurement. The neat PSf membrane showed a contact angle of 70.7° due to its hydrophobic nature (Figure 5.5). The hydrophilicity of the membranes increased on addition of nanoparticles, where the membranes P-T and P-S containing nano TiO₂ and nano SiO₂ showed contact angles of 62.4° and 65.08° respectively. The hydrophilicity of the membranes increased even more on amination of TiO₂ and SiO₂. The membranes containing aminated TiO₂ and aminated SiO₂ had lower contact angles than their corresponding amine free nanocomposite membranes. This may be attributed to the presence of hydrophilic –NH₂ groups.

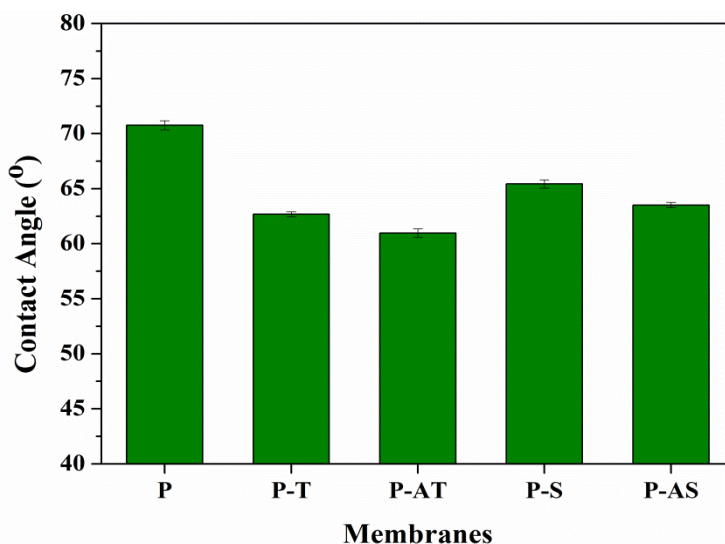


Figure 5.5 Contact angle of membranes

The water uptake of the membranes is given in Figure 5.6. The P-S and P-AS membranes had higher water uptake capacity. This is because water uptake by the membranes depends on the membrane porosity. From SEM images it was clearly seen

that P-S and P-AS membranes exhibited more porous nature than all other membranes.

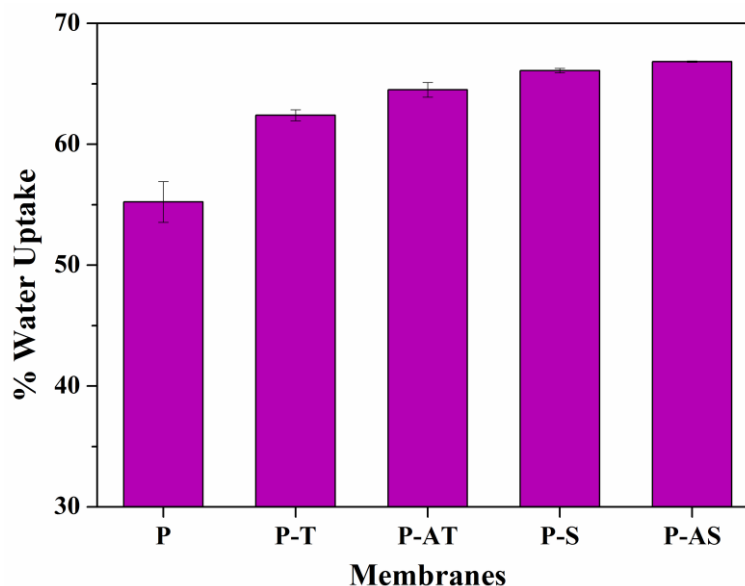


Figure 5.6 Water Uptake by membranes

5.4.2.3 Surface Topography of membranes

The surface topography of membranes was analyzed by AFM studies. The effect of addition of nanoparticles on membrane surface roughness is shown in Figure 5.7 and Figure 5.8. The membrane surface roughness reduced with the addition of nanoparticles. The mean surface roughness (R_a) reduced from 16.1 nm for neat PSf membrane to nearly 7 nm for the nanocomposite membranes (Table 5.2). It is well known that membrane with lower membrane roughness will have better antifouling abilities. This is because the foulants are likely to adsorb on coarse and rough surfaces than smoother surfaces. Therefore the synthesized membranes having lower roughness had higher FRR values as shown in the Figure 5.10.

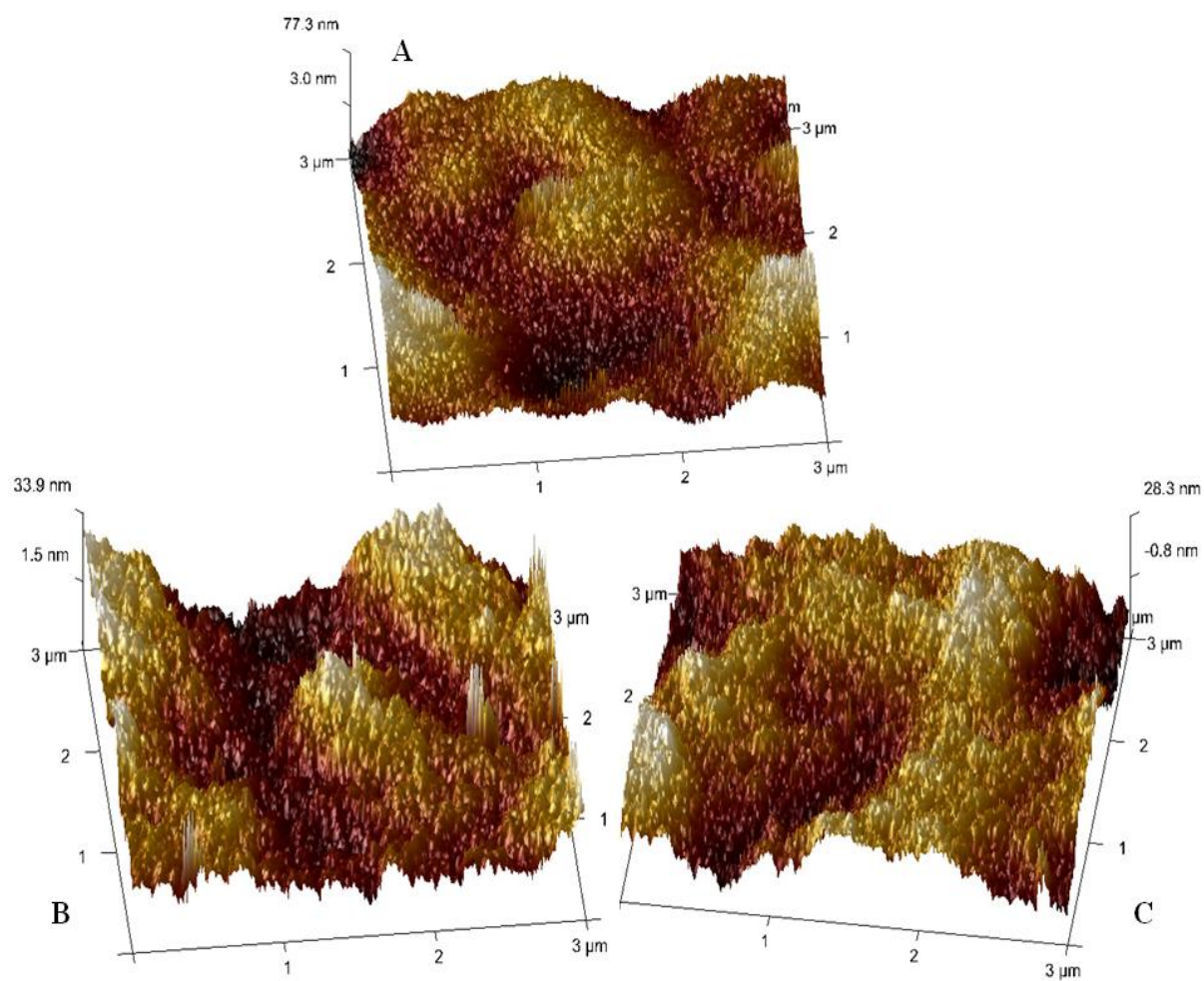


Figure 5.7 Three dimensional AFM images of A) P B) P-T C) P-AT

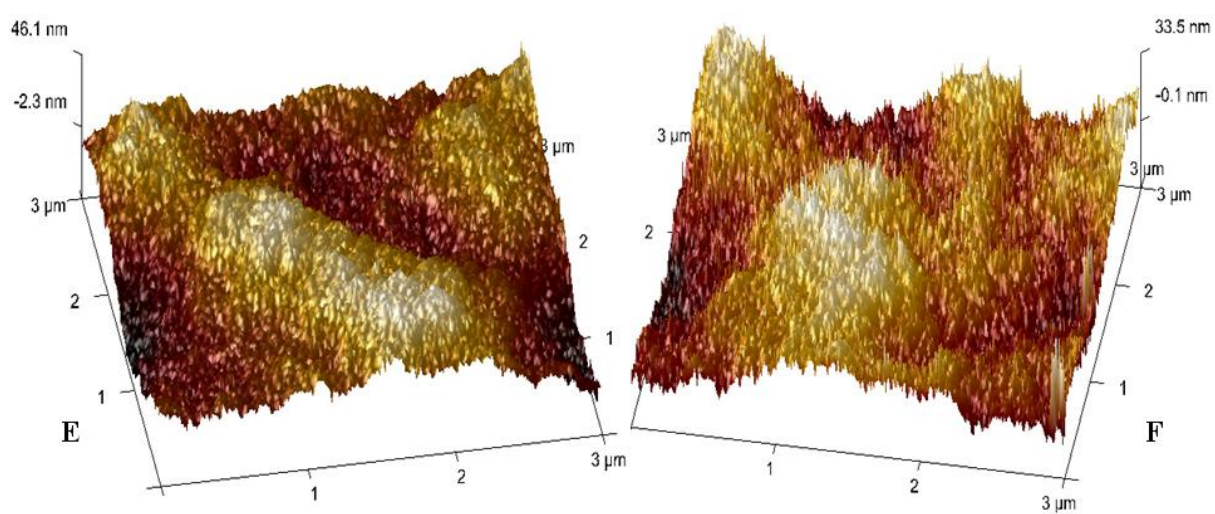


Figure 5.8 Three dimensional AFM images of D) P-S E) P-AS

Table 5.2 Surface roughness of membranes

Membranes	Roughness Parameters	
	R_a (nm)	R_q (nm)
P	16.1	20.4
P-T	8.19	10
P-AT	7.02	8.67
P-S	7.24	9.24
P-AS	7.82	9.79

5.4.2.4 Permeability of membranes

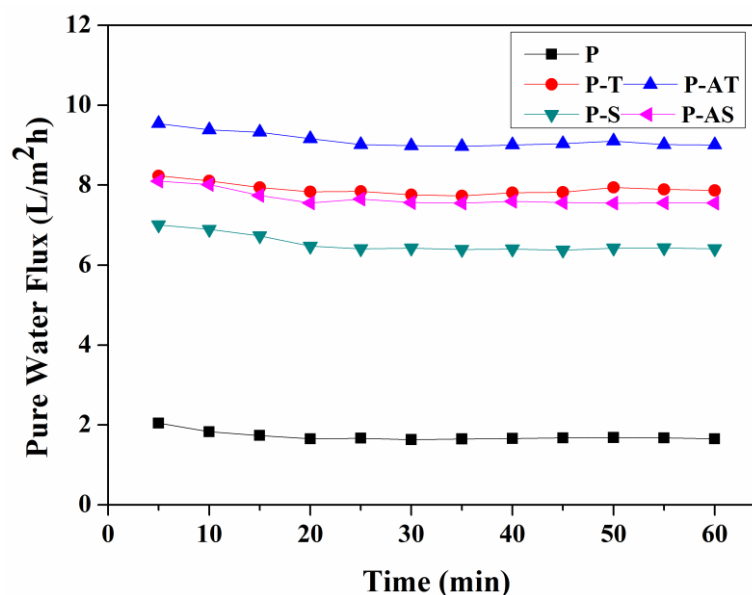


Figure 5.9 Pure Water Flux of the membranes

Figure 5.9 shows the PWF of the membranes. The neat polysulfone membrane showed very low water flux when compared with the nanocomposite membranes. The PWF of the nanocomposite membranes was nearly 4 times more than that of neat PSf membrane. Among the nanocomposite membranes, membranes containing modified nanoparticles, i.e. aminated TiO_2 and aminated SiO_2 showed higher flux values than the membranes containing their amine free forms. This may be due to the presence of more pores in the skin layer of P-AT and P-AS membranes and also due to the elongated pores which facilitate the water permeation through the membranes. Also

the presence of $-OH$ and amine groups on aminated TiO_2 and aminated SiO_2 , would help in improving the water flux, by improving the hydrophilicity of the membranes.

5.4.2.5 Antifouling property of membranes

The flux of the membranes during BSA filtration is shown in Figure 5.10. As expected, the BSA flux of the membranes was lower than that of the corresponding PWF of the membranes. After the BSA flux, membranes were thoroughly washed with water to remove any loosely attached foulants on the membrane surface. To quantify the membrane fouling, FRR of the membranes was calculated. Figure 5.11 shows the FRR values for the membranes. It is seen that nanocomposite membranes had higher FRR values, where the membranes P-AT and P-AS showed maximum FRR of 91% and 88% respectively. This also may be due to the reduced membrane roughness when compared with the pristine membranes (Table 5.2)

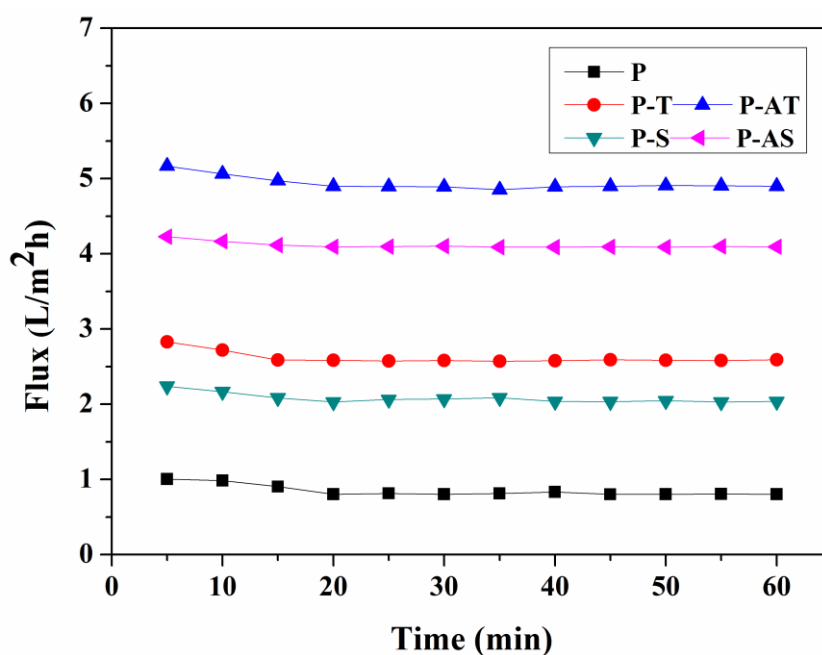


Figure 5.10 BSA Flux of the membranes

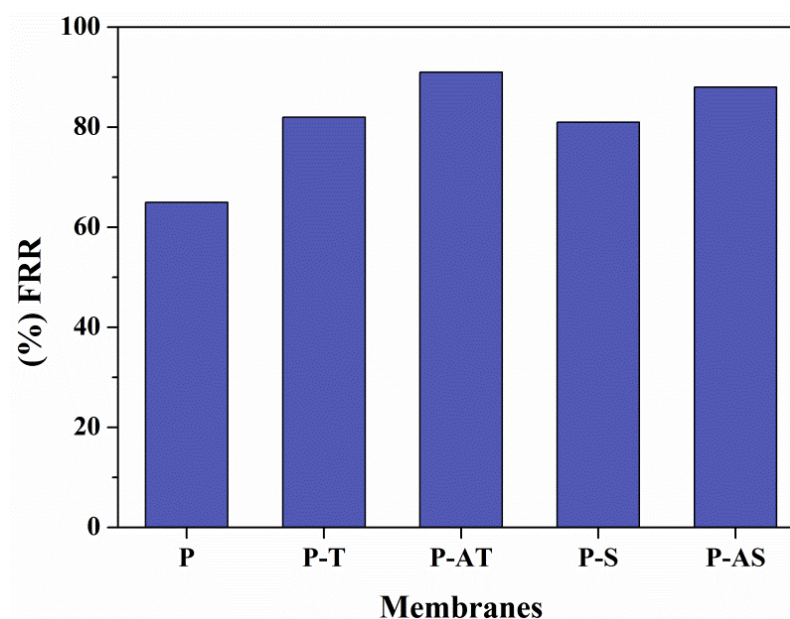
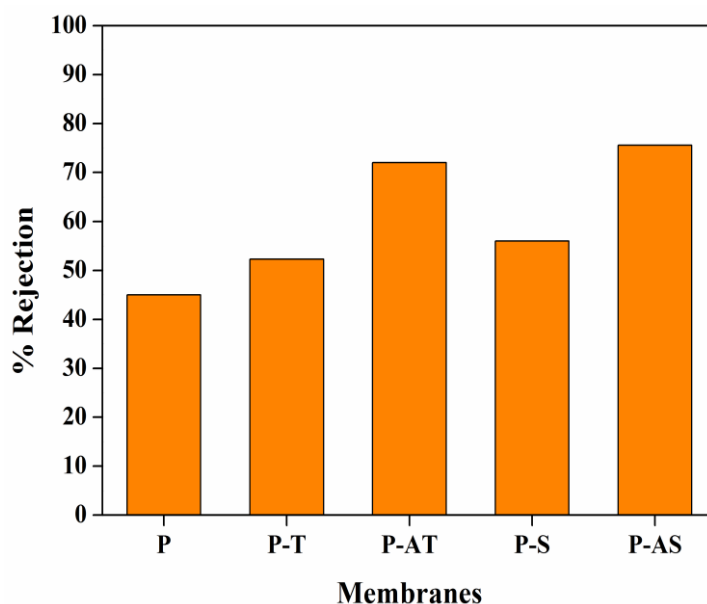


Figure 5.11 % FRR of the membranes

5.4.2.6 Heavy metal ion rejection by membranes

Figure 5.12 Heavy metal ion rejection by the membranes for Cd^{2+} metal ions

The heavy metal ion rejection by the membranes for Cd^{2+} is shown in Figure 5.12. The nanocomposite membranes showed better rejection than the pristine membrane. The maximum rejection by the membranes for Cd^{2+} was shown by P-AT and P-AS membranes which exhibited a rejection of 72% and 75.6% respectively.

This is due to the presence of amine groups in the membranes where the Cd^{2+} metal ions have tendency to chelate with the $-\text{NH}_2$ groups present on the membranes, hence contributing towards higher rejection.

5.5 CONCLUSIONS

In this chapter, nano TiO_2 and nano SiO_2 were used as additives into the polysulfone membranes. Nano- TiO_2 and nano- SiO_2 were functionalized with amine groups using APTES, which was confirmed by FTIR. Addition of TiO_2 and SiO_2 improved the properties of PSf membranes. However both nano TiO_2 and nano SiO_2 showed similar effects on membrane performance. The aminated forms of nano- TiO_2 and nano- SiO_2 further improved the membrane performance in terms of permeation, antifouling ability and hydrophilicity. The membranes containing aminated nanocomposites, P-AT and P-AS showed rejection of 72% and 75.6% for Cd^{2+} metal ions.

CHAPTER 6

PREPARATION OF PANI-TiO₂ NANOCOMPOSITE POLYSULFONE HOLLOW FIBER MEMBRANES FOR DYE REMOVAL APPLICATION

Abstract

This chapter explores the preparation of PSf hollow fiber membranes with PANI-TiO₂ nanocomposites as additives. The chapter gives insight as how PANI-TiO₂ and the air gap distance during fabrication affect the properties and performance of the membranes. The synthesized hollow fiber membranes can also be used as a potential candidate for the dye removal, showing maximum rejection of 81.5% and 96.5% for Reactive Black-5 and Reactive Orange 16 respectively.

6.1 INTRODUCTION

Membrane separation methods using hollow fiber membranes is one among the emerging technologies in the past few decades (Feng et al. 2013). Hollow fiber membranes have been used for several applications such as waste water treatment, dye rejection, gas separation etc, due to their selectivity and good productivity (Chen et al. 2015, Feng et al. 2013). Hollow fiber membranes have been preferred over other membrane configurations due to their high membrane surface area to module volume, mechanical property and easy handling (Chen et al. 2015). Immersion precipitation process provides asymmetric hollow fiber membranes which are used for separation process and also exhibit characteristic features more advantageous than flat sheet membranes (Tsai et al. 2006). The main advantages of hollow fibers over flat sheet membranes are high productivity per unit volume and self supporting nature of hollow fibers. The high productivity is due to the high surface area to volume ratio of the hollow fibers. Since the hollow fibers are self supporting, it simplifies the fabrication of the permeation cell whereas the flat sheet membranes require spacers or porous supports during permeation (Chanda and Roy 2008, Khulbe et al. 2007).

Polysulfone (PSf) is one among the excellent polymeric materials used for hollow fiber membrane fabrication (Korminouri et al. 2015). The properties of the hollow fiber membranes can be tailored through surface modification techniques such as polymer coating, photo grafting, using plasma etc. (Macanas et al. 2010). Hollow fiber membranes with additives are being fabricated in order to have required membrane morphology and desired properties (Chen et al. 2015). Adding inorganic nanoparticles into the polymer dope solution to prepare nanocomposite hollow fiber

membranes has been an interesting approach to improve separation properties, having advantages of both nanoparticles and organic membranes and also due to its simple operation process. Preparation of polyaniline (PANI) composites with inorganic nanoparticles has gained attraction in the recent years to improve the activity (Salem et al. 2009). PANI-TiO₂ nanocomposites exhibit properties which are combined of PANI and TiO₂, which are otherwise difficult to achieve with individual components (Salem et al. 2009).

Dyes have been extensively used in textile industries and has become a source of water contamination (Salem et al. 2009, Wei et al. 2013). Reactive dyes are usually found in higher concentrations in textile industry effluents due to their low degree of fixation to fibers such as cotton, viscose (Mondal and De 2016). There are various reports in the recent years where PANI-TiO₂ nanocomposites are effectively used for dye removal. Liu et al. (2014) prepared PANI coated TiO₂/SiO₂ nanofiber membranes, which were used for the degradation of methyl orange dye. The membranes showed enhanced photocatalytic activity under visible light due to the synergetic effect of TiO₂ and PANI. Debnath et al. (2015) synthesized PANI coated TiO₂ nanocomposite and was used as a catalyst for photodegradation of Eosin Yellow (EY) and Naphthol blue black (NBB) dye. The catalyst showed 99.85% and 99.74% degradation for EY and NBB dyes respectively under optimum conditions. Jeong et al. (2014) prepared PANI-TiO₂ nanocomposites and were used for antibacterial activity and for photocatalysis of Methylene Blue (MB) dye under visible light. The synergy between PANI and TiO₂ contributed towards higher charge separation in turn enhancing MB degradation.

In this research, polysulfone nanocomposite hollow fiber membranes were prepared with PANI-coated TiO₂ nanotubes as additives. Hollow fibers were fabricated with different concentration of PANI-TiO₂ nanocomposites and their effect on the performance of the membranes was evaluated. The air gap distance was also varied during membrane fabrication and its effect on membranes was evaluated. The hollow fiber nanocomposite membranes were investigated for rejection of reactive dyes namely Reactive Black 5 (RB-5) and Reactive Orange 16 (RO-16).

6.2 EXPERIMENTAL

6.2.1 Materials

Polysulfone (PSf Udel-P3500), TiO₂ nanoparticles, aniline (99.5%) were purchased from Sigma Aldrich Co. Bangalore, India. Bovine Serum Albumin (BSA), Reactive Black 5, Reactive Orange 16 were purchased from Sigma Aldrich Co. Malaysia. N-methyl-2-pyrrolidone (NMP) was purchased from Merck Malaysia, Ltd. Ammonium peroxydisulfate (APS) was purchased from Central Drug House (CDH), New Delhi. Hydrochloric acid (HCl) was purchased from Merck India, Ltd.

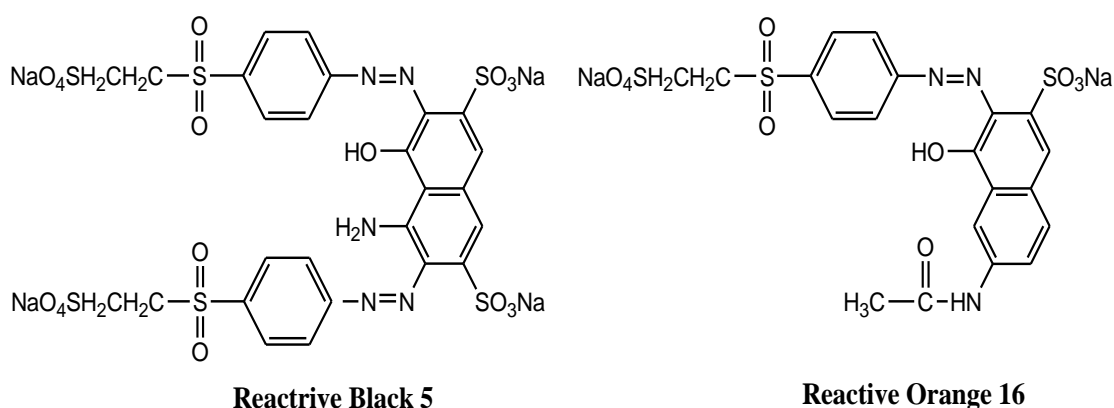


Figure 6.1 Structures of Reactive Black 5 and Reactive Orange 16

6.2.2 Preparation of PANI coated TiO₂ nanotubes

PANI coated TiO₂ nanotubes were synthesized as reported earlier in section 3.2.2 of CHAPTER 3 (Pereira et al. 2015). Initially TiO₂ nanotubes were prepared from TiO₂ nanoparticles and then the TiO₂ nanotubes obtained were surface coated with PANI. In brief, TiO₂ nanotubes were coated with PANI by chemical oxidative polymerization (Lokesh et al. 2008). 2.5 mL of aniline was first added to 500 mL of 2M HCl solution. Then 2.5 g of TiO₂ nanotubes dispersed in 25 mL of water, were added to the above solution and then stirred for two hours. Polymerization of aniline was carried out with the addition of 5.7 g of Ammonium peroxydisulfate (APS) to the above suspension. The product formed was isolated by centrifugation, followed by washing with HCl and water. The product was dried for 24 h at 80°C to obtain a yield of 7 g of PANI coated TiO₂.

6.2.3 Membrane Preparation

PSf which was used as the base polymer for the hollow fibers was initially dried in oven at 50°C for 24 h to remove any moisture present. First the PANI coated TiO₂ nanotubes were dispersed in desired amount of NMP taken in a Scott bottle. TiO₂-PANI nanocomposites were dispersed in NMP by sonication for 30 min with frequency of 40 kHz using Ultrasonic bath (Ultrasonic Cleaner DC-150H). The mixture was then stirred at 27°C with an overhead stirrer and polymer PSf was added to the solution. The solution was stirred until complete dissolution of the polymer was achieved (Zulhairun and Ismail 2014). Thus obtained homogenous dope solutions were degassed using the ultrasonic bath to remove trapped air bubbles (Dzinun et al. 2015). The neat PSf dope solution which did not contain any PANI-TiO₂ nanocomposite was prepared in a similar way without the addition of PANI-TiO₂. The composition of the dope solutions is given in Table 6.1. The viscosity of the dope solutions was recorded using Basic viscometer (Model: EW-98965-40, COLE PARMER, 20-2 million centipoises). The hollow fiber membranes were prepared by dry-wet spinning methods. The homogenous spinning dope solutions and bore fluid were extruded through the spinneret to obtain the hollow fibers membranes. The spinning conditions are summarized in Table 6.2. The hollow fiber membranes obtained were labeled as per the codes given in Table 6.1. The hollow fibers were immersed in water for 1 day to remove the residual solvent. Then the fibers were post-treated using glycerol aqueous solutions (glycerol: water; 10:90 wt. %) for 24 h to prevent the pore collapse (Ren and McCutcheon 2015). Finally the hollow fiber membranes were air dried for 2 days at room temperature before further use.

Table 6.1 Composition of the dope solutions

Membrane Code	Polysulfone (%)	PANI-TiO ₂ (wt. %)	Air gap between the spinneret and the bath	Flow rate (Dope/Bore liquid)
P-A	20	0	5 cm	5/5
P-B	20	0	10 cm	5/5
P-0.5-A	20	0.5	5 cm	5/5
P-0.5-B	20	0.5	10 cm	5/5
P-1.0-A	20	1.0	5 cm	5/5
P-1.0-B	20	1.0	10 cm	5/5

Table 6.2 Spinning conditions for hollow fiber membranes

Dope composition	PSf/PANI-TiO ₂ /NMP PSf/NMP (For Neat)
Dope Extrusion Rate (DER)	5 mL/min
Bore fluid	Distilled water
Bore Extrusion Rate (BER)	5/4 mL/min
Air gap	5 cm and 10 cm
Spinneret Dimension (o.d/i.d)	1.15/0.55 (mm)

6.3 CHARACTERIZATION

6.3.1 Characterization of PANI coated TiO₂ nanotubes

PANI coating on TiO₂ was confirmed by Fourier Transform Infrared spectroscopy (FTIR) and X-ray Diffraction (XRD). PANI coated TiO₂ nanotubes were also characterized by Transmission Electron Microscope (TEM). SHIMADZU

ATR-FTIR spectrophotometer was used to record the FTIR spectra. XRD measurements were recorded using Rigaku Miniflex 600 with Cu radiation. The morphology of PANI coated TiO₂ nanotubes was observed using TEM (JEOL JEM-2100).

6.3.2 Characterization of membranes

6.3.2.1 Membrane Morphology

The morphology of the hollow fiber membranes was inspected by observing the cross sectional images using Scanning Electron Microscope (SEM, TM 3000, Hitachi). The membrane samples were immersed in liquid nitrogen, frozen and then broken. The membrane samples were placed on a metal holder and sputtered with gold under vacuum for electron conductivity.

6.3.2.2 Porosity and pore size of membranes

The overall porosity (ϵ) of the hollow fibers was evaluated by gravimetry method (Kumar et al. 2013) using the equation 3.1 mentioned in section 3.3.2.3 of CHAPTER 3.

The pore size (r_m) of the membranes was calculated using Guerout-Elford-Ferry equation (equation 3.2), as explained in section 3.3.2.3 of CHAPTER 3.

6.3.2.3 Water Uptake study

The water uptake ability of the hollow fibers was determined by immersing the hollow fibers in distilled water for 5 hours. Then the membranes were removed from water, and the wet weight was noted immediately after blotting the surface water. The hollow fiber membranes were then dried and the dry weight was noted. The water uptake capacity of the hollow fiber membranes was calculated using the relation

$$\% \text{ water uptake} = \left(\frac{W_w - W_d}{W_w} \right) \times 100 \dots \dots \text{eqn 5.1}$$

where, W_w and W_d are weights of the wet and dry membrane samples respectively.

6.3.2.4 Contact Angle of membranes

The contact angle between water and external surface of the hollow fibers was measured using contact angle goniometer (Model: OCA 15EC, Dataphysics). To

minimize the experimental error, for each sample, the values were taken as an average of 10 contact angles measured at different locations on the hollow fibers.

6.3.2.5 Atomic Force Microscopy of membranes

The AFM studies on hollow fibers were conducted using SPM Atomic Force Microscopy. The membrane surfaces were analyzed as explained in section 3.3.2.2 of CHAPTER 3.

6.3.2.6 Pure Water Flux measurements

The pure water flux of the membranes was measured using bench scale cross flow filtration set up. The membrane modules for the filtration studies were prepared by potting the membranes with the help of epoxy resin and hardener (Kajekar et al. 2015). Five membranes of 16 cm length were assembled into each module. Distilled water was circulated through the set up. The membranes were compacted at a transmembrane pressure (TMP) of 3 bars for 30 min prior to further measurements. Then the pure water (J_{w1}) was collected on the lumen side at TMP of 2 bars.

$$J_{w1} = \frac{Q}{A \Delta t} \dots \dots \text{eqn 5.2}$$

where, Q is the pure water collected (L) for time Δt (h), A is the membrane surface area (m^2).

6.3.2.7 Antifouling studies

The fouling experiments were carried out with BSA as a model foulant. BSA solution was prepared by dissolving BSA in distilled water at a concentration of 800 ppm. The BSA solution was filtered through the membranes and the BSA flux was collected to evaluate the BSA rejection by the membranes. After the BSA filtration, the membranes were thoroughly rinsed and washed with water and the water flux (J_{w2}) of the membranes was measured.

The fouling resistance by the membranes was calculated using the formula

$$\text{FRR (\%)} = \frac{J_{w2}}{J_{w1}} \times 100 \dots \dots \text{eqn 5.3}$$

The BSA rejection by the membranes was evaluated using the equation

$$\%R = \left(1 - \frac{C_p}{C_f} \right) \times 100 \dots \dots \text{eqn 5.4}$$

where, C_p (mg/mL) is the concentration of BSA in the permeate and C_f (mg/mL) is the concentration of BSA in the feed solution.

6.3.2.8 Dye Rejection

The dye removal performance of the nanocomposite hollow fibers was studied using Reactive Black-5 and Reactive Orange-16 dyes. The aqueous solutions of RB-5 and RO-16 were prepared at a concentration of 10 ppm. The molecular structures of RB-5 and RO-16 are given in Figure 5.1 (Chen et al. 2015). The dye rejection studies of the hollow fiber membranes were carried out on the same cross flow filtration set up, under similar conditions (Wei et al. 2013) as that for permeation studies. The concentration of dyes in the aqueous solutions were analyzed using UV-Vis spectrophotometer (HACH, Model: DR 5000) at a wavelength of maximum absorption for each dye (Akbari et al. 2007). The dye rejection by the membranes was investigated in terms of % rejection, given by the formula,

$$\%Rejection = \left(1 - \frac{C_f}{C_i}\right) \times 100 \dots eqn 5.5$$

where, C_i and C_f are the initial and final concentrations of the dyes in the aqueous solutions.

6.4 RESULTS AND DISCUSSIONS

6.4.1 PANI coated TiO₂ nanotubes characteristics

PANI coated TiO₂ nanotubes characteristics confirmed the PANI coating on TiO₂. The characterization of PANI coating on TiO₂ along with their characteristic peaks of FTIR and XRD, TEM images are explained in section 3.4.1 in CHAPTER 3. From TEM it was found that PANI coated TiO₂ nanotubes had diameter in the range of 40-50 nm.

6.4.2 Membrane Morphology

The SEM cross-sectional images of hollow fiber membranes are shown in Figure 6.2, Figure 6.3 and Figure 6.4. It was found that the finger like projections were formed beneath both inner and outer surfaces of the hollow fibers with thin spongy layer sandwiched between them (Zhang and Wang 2014). The addition of

PANI-TiO₂ nanotubes and change in spinning parameters like air gap distance brought about change in membrane morphology (Sengur et al. 2015). It was observed

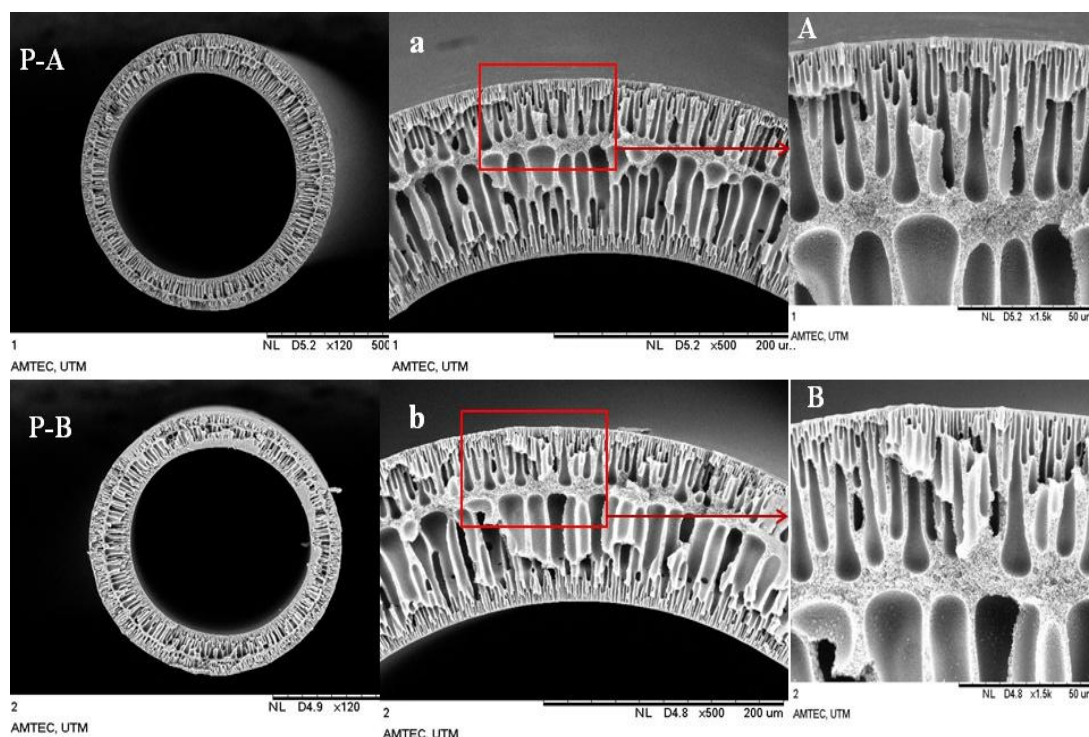


Figure 6.2 SEM Cross sectional images of P-A and P-B (A and B are magnified images of a and b respectively)

that pristine polysulfone hollow fibers showed more porous nature in the skin layer and also elongated pores whereas the porous nature in the skin was decreased with the addition of PANI-TiO₂.

Table 6.3 Viscosity of dope solutions

Dope solutions of	Viscosity (mPas)
P-A, P-B	1661.9
P-0.5-A, P-0.5-B	1752.4
P-1.0-A, P-1.0-B	1876.5

The viscosity of the polymer dope solution increased with the increase in PANI-TiO₂ content in the dope solution as seen in Table 6.3. The viscosity of the dope solution affects the rheological property during liquid-liquid demixing which in

turn affects the membrane morphology. During the phase inversion process, an increase in dope solution viscosity, decreases the mass transfer rate, preventing the formation of macroporous structure. Hence the length of the finger like projections decreased (Dzinun et al. 2015).

Difference in morphology beneath the outer surface of hollow fibers was also observed, when the air gap distance was varied for same composition of the dope solutions. With the increase in air gap distance, the depth of the finger like projections is reduced. The outer surface appeared denser with porous nature as the air gap distance was increased from 5 cm to 10 cm. This was more prominently visible in the case of P-1.0-A and P-1.0-B membranes. Similar results were also observed and reported by (Sengur et al. 2015, Shi et al. 2013).

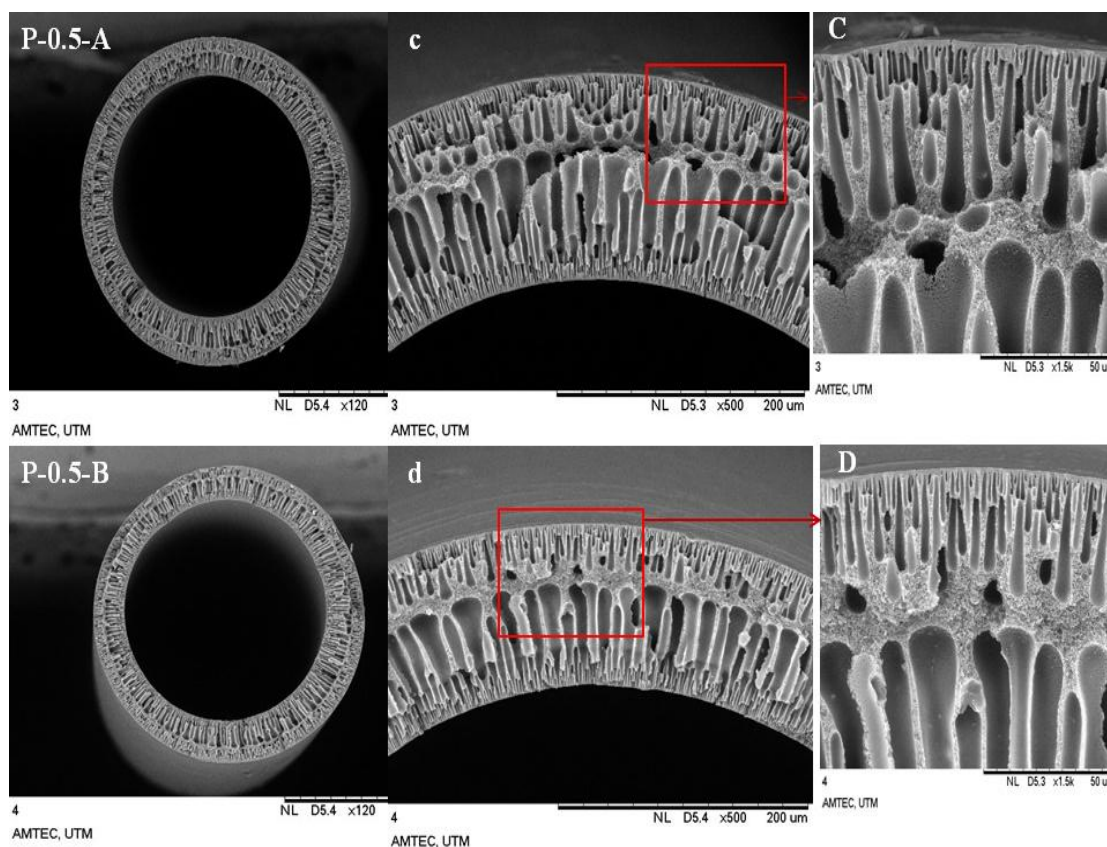


Figure 6.3 SEM Cross sectional images of P-0.5-A and P-0.5-B (C and D are magnified images of c and d respectively)

In dry-wet spinning method, the hollow fiber undergoes two coagulation paths. First is the “non convective” type in the air gap region, then the rapid exchange of solvents taking place as the fiber enters the coagulation bath. As the air gap distance is increased, the external surface of the fiber is more in contact with air and undergoes humid-induced phase separation for a longer time and then a delayed phase inversion in the coagulation bath. Whereas when the air gap is reduced, the time delay causing the phase inversion process is reduced, since the fiber enters the coagulation bath faster, as a result, more and longer finger like projections are produced (Chung and Hu 1997).

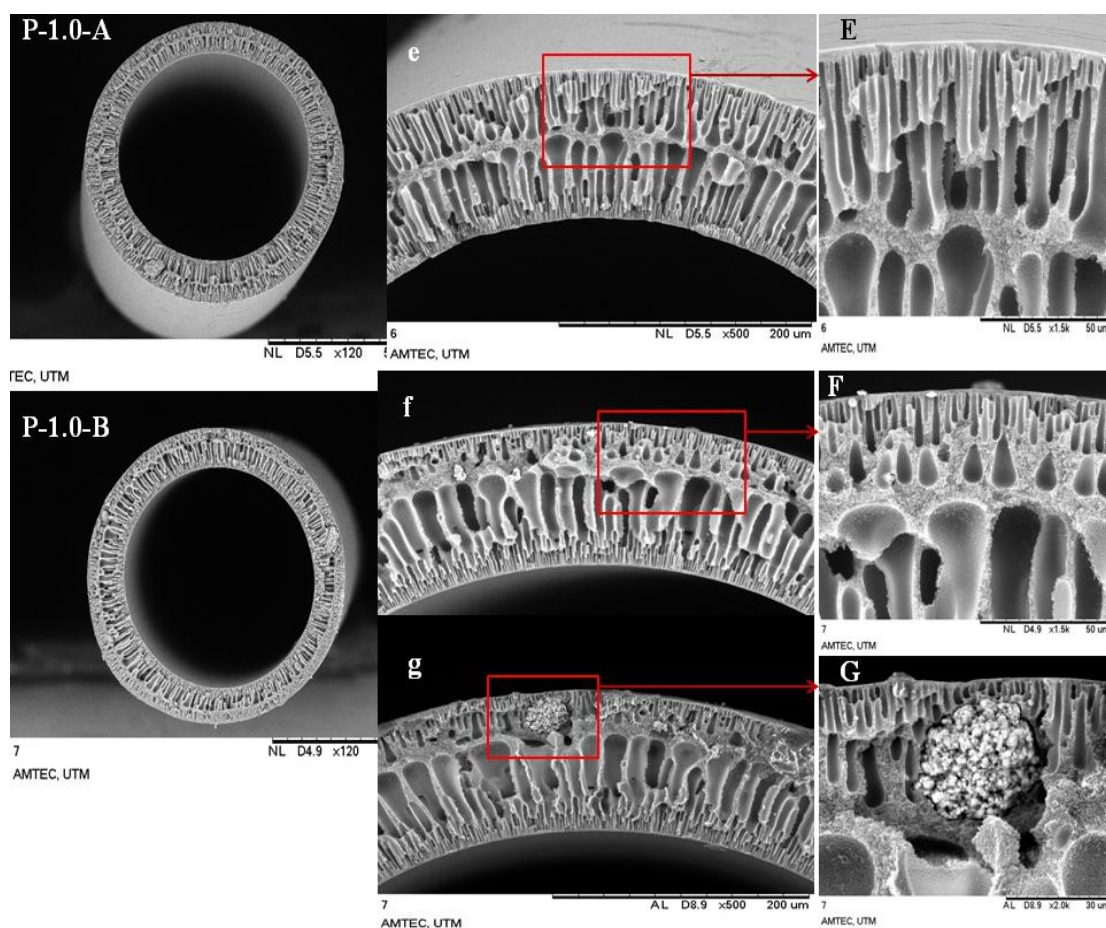


Figure 6.4 SEM Cross sectional images of P-1.0-A and P-1.0-B (E, F and G are magnified images of e, f and g respectively)

At higher content of PANI-TiO₂ in the hollow fibers i.e., at 1.0 wt.%, agglomeration of PANI-TiO₂ was observed as shown in Figure 6.4 (g ad G). The

agglomeration of PANI-TiO₂ in membrane was further confirmed by elemental mapping and EDX spectrum (Figure 6.5 and Figure 6.6). However lower content of PANI-TiO₂ did not show any such agglomeration.



Figure 6.5 Elemental Mapping of P-1.0-B membrane

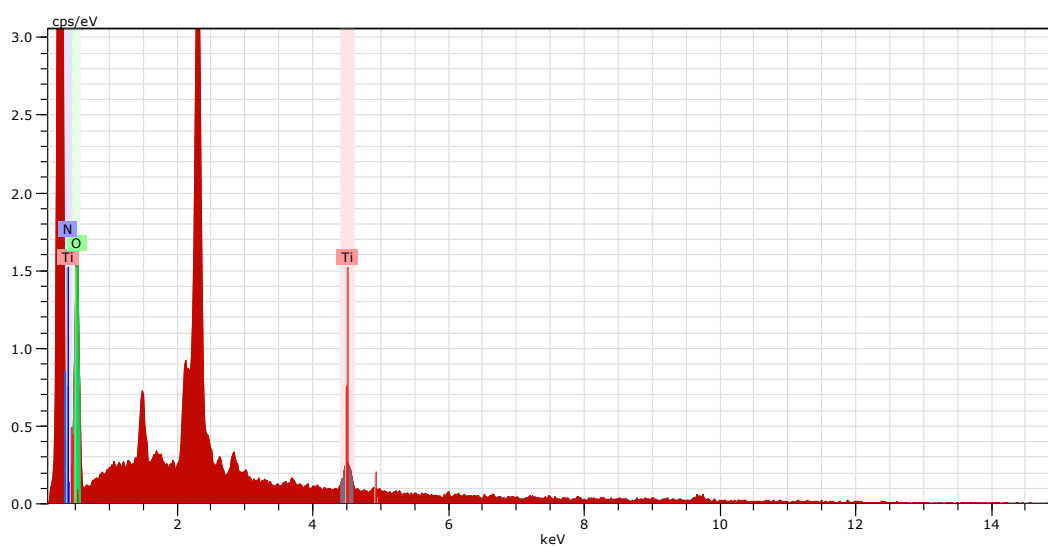


Figure 6.6 EDX of P-1.0-B membrane

6.4.3 Porosity, pore size and water uptake of membranes

The porosity and pore size of the membranes is given in Table 6.4. The porosity of the hollow fibers decreased with the inclusion of PANI-TiO₂ nanocomposites. This is because the viscosity of the polymer solutions increased with the addition of PANI-TiO₂, where the out diffusion of solvent is more favored than in diffusion of non-solvent, leading to decreased porosity (Sengur et al. 2015). However at 1.0 wt.% of PANI-TiO₂, the porosity increased. This increase is due to the hydrophilicity of PANI-TiO₂ membranes at 1.0 wt.% where the presence of higher PANI-TiO₂ would attract more water flow into the membrane, leading to higher porosity (Dzinun et al. 2015).

Table 6.4 Porosity and pore size of membranes

Membranes	Porosity (%)	Pore size (nm)
P-A	38.94	5.45
P-B	35.8	8.37
P-0.5-A	34.38	4.12
P-0.5-B	28.61	6.19
P-1.0-A	41.47	1.88
P-1.0-B	37.97	3.57

The water uptake by membranes is shown in Figure 6.7. Membrane water uptake depends on the porosity of the membranes. The water uptake by membranes decreases and then increases for 1.0 wt.% of PANI-TiO₂ membranes. The water uptake values are consistent with porosity values, where the porosity is found to first decrease and then increase.

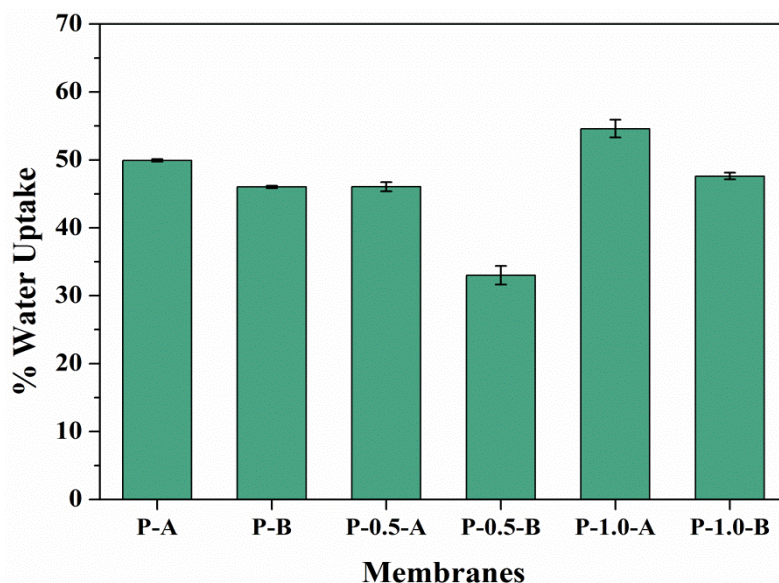


Figure 6.7 Water Uptake by membranes

6.4.4 Contact Angle of membranes

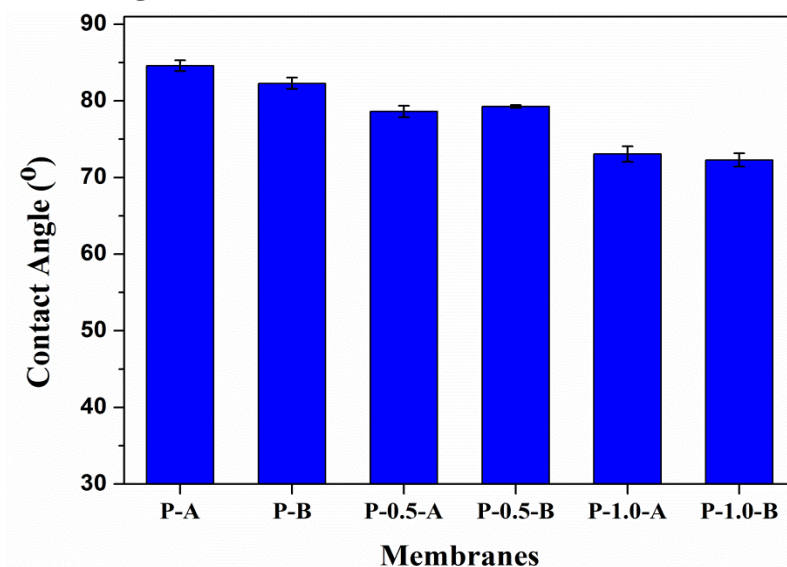


Figure 6.8 Contact angle of membranes

The contact angle of membranes is shown in Figure 6.8. The neat hollow fiber membranes P-A and P-B, showed a contact angle of 84.54° and 82.27° respectively, indicating that the membranes were hydrophobic in nature. The contact angle of the membranes P-0.5-A and P-0.5-B, reduced, exhibiting contact angle of 78.60° for P-0.5-A membrane and 79.26° for P-0.5-B membrane. The membranes P-1.0-A and P-1.0-B which contained 1.0 wt.% of PANI-TiO₂ showed even lower contact angle of

73.05° and 72.28° respectively. This reduction of contact angle is attributed to the addition of PANI-TiO₂ nanotubes, which are hydrophilic in nature. Hence PANI-TiO₂ nanocomposites were able to reduce the hydrophobicity of the polysulfone membranes. The variation in air gap did not affect the contact angle of the membranes. The membranes with same composition but with different air gaps showed nearly the same contact angle values.

6.4.5 Surface roughness of membranes

The surface topography of hollow fiber membranes was studied using AFM. The three-dimensional and two-dimensional scans of the hollow fibers P-A, P-0.5-A, P-1.0-A are shown in Figure 6.9. It was observed that the surface roughness of the membranes increased with the increase in addition of PANI-TiO₂. This may be due to the reason that neat PSf, which did not contain any PANI-TiO₂ resulted in the smooth surface. Whereas in the case of P-0.5-A and P-1.0-A membranes, the presence of PANI-TiO₂ on the surface of hollow fibers would give rise to nodules or lumps on surface, which may be due to the presence of agglomerated PANI-TiO₂, contributing to the increase in surface roughness. The trend was further supported by the surface roughness parameters measured in terms of mean roughness (R_a) and root mean surface roughness (R_q) as given in Table 6.5.

Table 6.5 Surface roughness parameters of membranes

Membranes	R_a (nm)	R_q (nm)
P-A	10.7	12.5
P-0.5-A	13.8	16.9
P-1.0-A	30.0	37.1

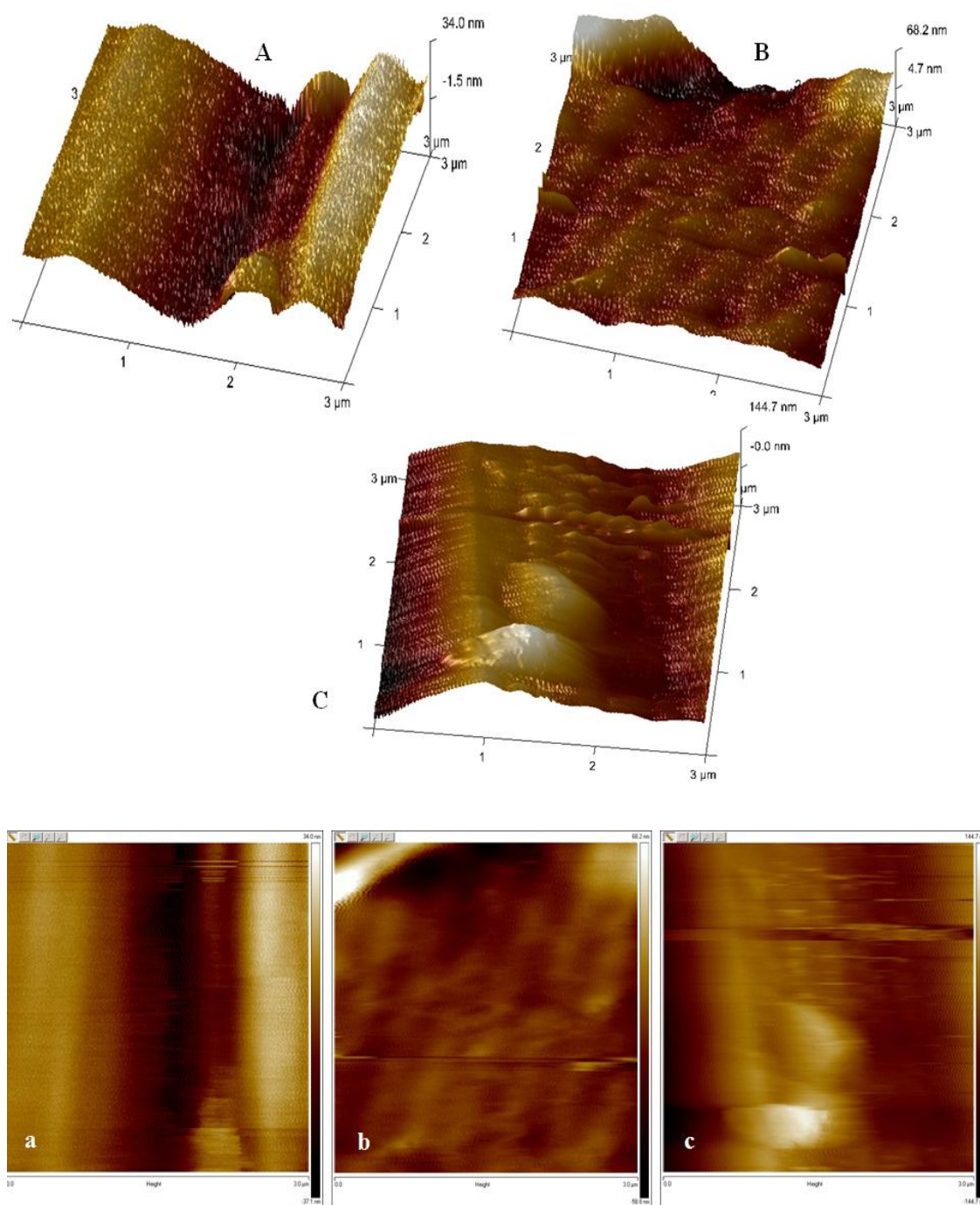


Figure 6.9 Three-dimensional scans of A) P-A B) P-0.5-A C) P-1.0-A and two-dimensional scans of a) P-A b) P-0.5-A c) P-1.0-A

6.4.6 Permeation Studies

Figure 6.10 displays the PWF of the membranes measured at 0.1 MPa. There are two main trends observed in the pure water flux of the membranes. First one is that the membranes which were fabricated with higher residence time in air exhibited higher PWF. As reported by Sengur et al. (2015) membranes with higher air residence time have greater permeation rate. The pore size of the membranes fabricated with higher air gap, were greater than that of the membranes prepared with lower air gaps (Table 6.4). Therefore the membranes P-B, P-0.5-B and P-1.0-B exhibited high flux than the corresponding P-A, P-0.5-A and P-1.0-A membranes.

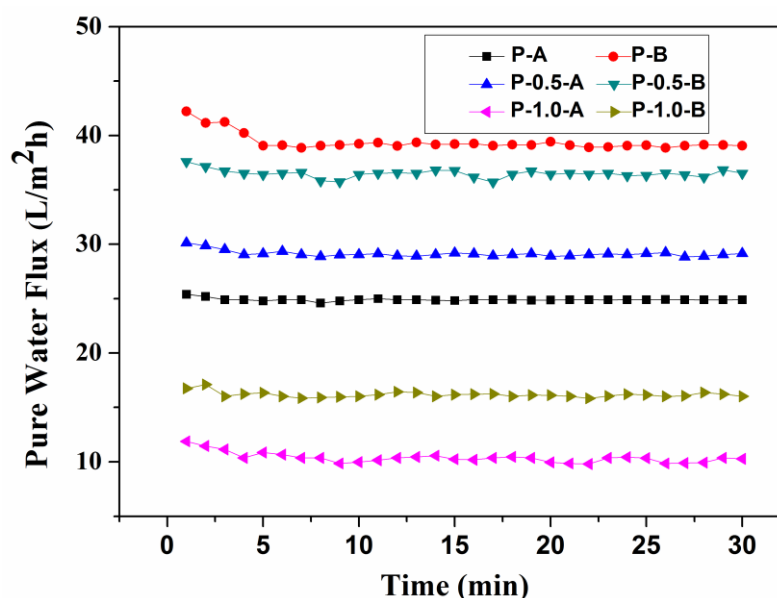


Figure 6.10 Pure water flux of membranes

Second trend is that the PWF of the membranes decreased with the increase in PANI-TiO₂ content in the membranes. This may be because the porosity and pore size of the membranes decreased with the increase in PANI-TiO₂ content in the membranes.

6.4.7 Antifouling property

The flux of the membranes during BSA filtration is given in Figure 6.11. The figure also shows the flux of the membranes for water before and after the BSA filtration. The antifouling ability of membranes was evaluated by calculating the FRR value for the hollow fiber membranes. The pristine membranes exhibited lower %

FRR values whereas the hollow fibers containing PANI-TiO₂ showed better % FRR values. Membrane P-1.0-B showed highest flux recovery ratio of 95% (Figure 6.12). Higher FRR indicates that in the presence of PANI-TiO₂, the BSA molecules did not remain adsorbed on the membrane surface after the BSA filtration. Thus the membranes containing PANI-TiO₂ exhibited antifouling nature.

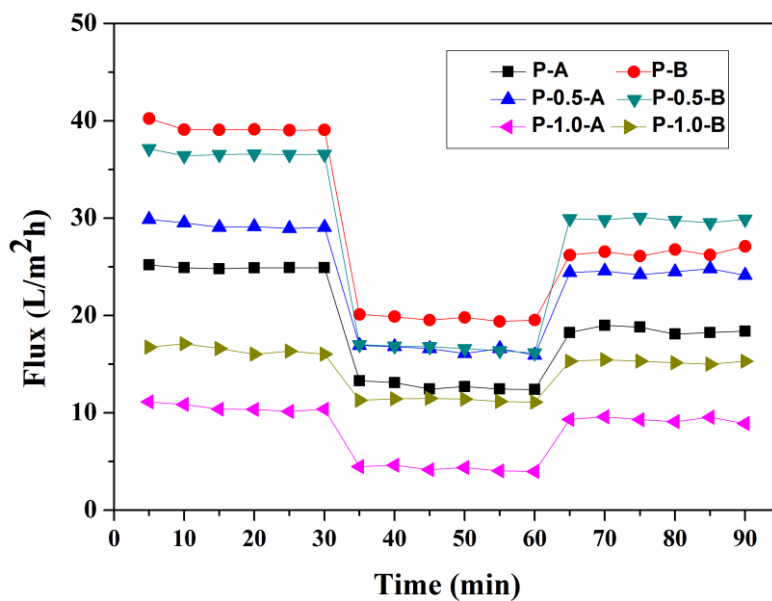


Figure 6.11 Flux of the membranes during BSA filtration

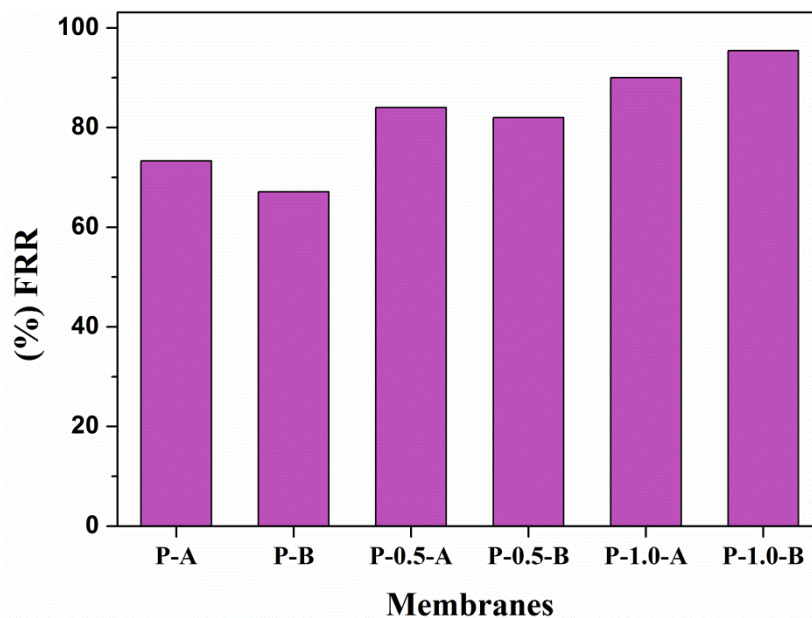


Figure 6.12 Flux Recovery Ratio (FRR) of membranes

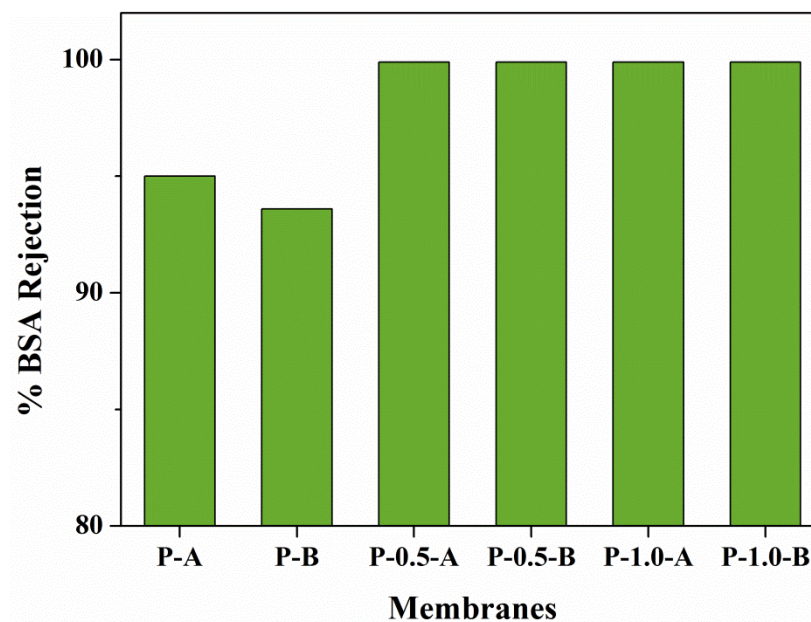


Figure 6.13 % BSA Rejection by membranes

The BSA rejection by the membranes was also evaluated. The hollow fibers containing PANI-TiO₂ showed 99% rejection for BSA molecules whereas pristine membranes P-A and P-B exhibited rejection of 95% and 93.6% respectively (Figure 6.13). This is because the nanocomposite hollow fibers had pore size smaller than that of the BSA molecules, resulting in almost complete rejection.

6.4.8 Dye removal by membranes

The dye rejection by the hollow fiber membranes is shown in Figure 6.14 and Figure 6.16. The membranes (P-1.0-A) showed a highest rejection of 81.5% for Reactive Black 5 and maximum of 96.5% for Reactive Orange 16. The pristine hollow fiber membranes, P-A and P-B showed least rejection for both the dyes.

The rejection of dyes by the hollow fibers increases with the increase in PANI-TiO₂ content in the membranes. The PANI-TiO₂ incorporated hollow fibers have NH⁺ centers from PANI, due to which there is electrostatic interaction between polyaniline and dye anions (Ahmed et al. 2012). Reactive Black 5 and Reactive orange 16 are anionic dyes, which dissociate in aqueous to give sulfonic acid groups. As a result of this, dyes get adsorbed on the membranes. Therefore higher the content of PANI-TiO₂ in the membranes, higher will be the rejection. Also it was observed that, 'A' membranes (P-A, P-0.5-A and P-1.0-A) showed higher rejection than their

corresponding 'B' membranes (P-B, P-0.5-B and P-1.0-B) for both the dyes. This is because the membranes P-B, P-0.5-B and P-1.0-B had pore size greater than their corresponding 'A' membranes (Table 6.4). Figure 6.15 and 6.17 display the digital images of dye permeate after filtration of dyes Reactive Black 5 and Reactive Orange 16 through the hollow fiber membranes.

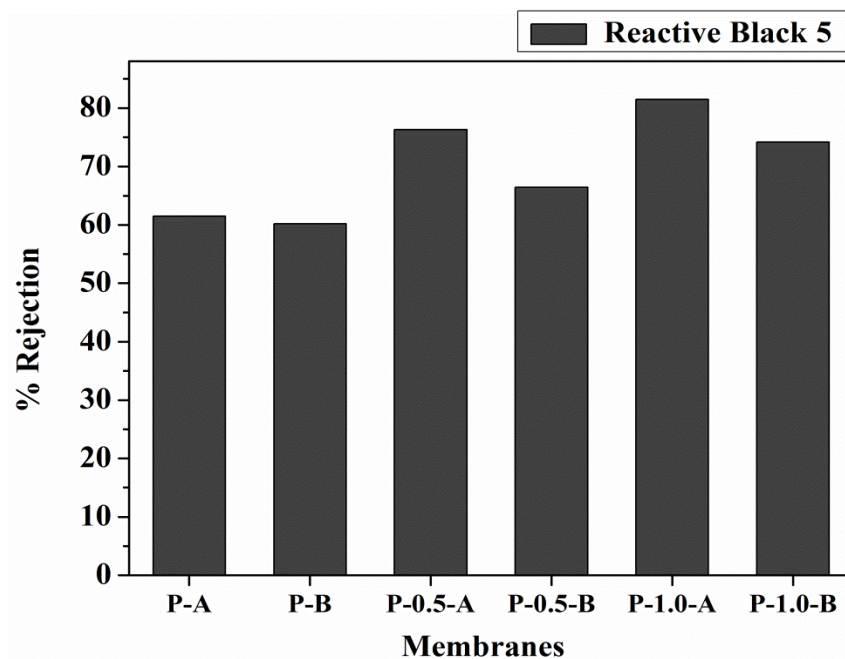


Figure 6.14 Dye Rejection by membranes for Reactive Black 5

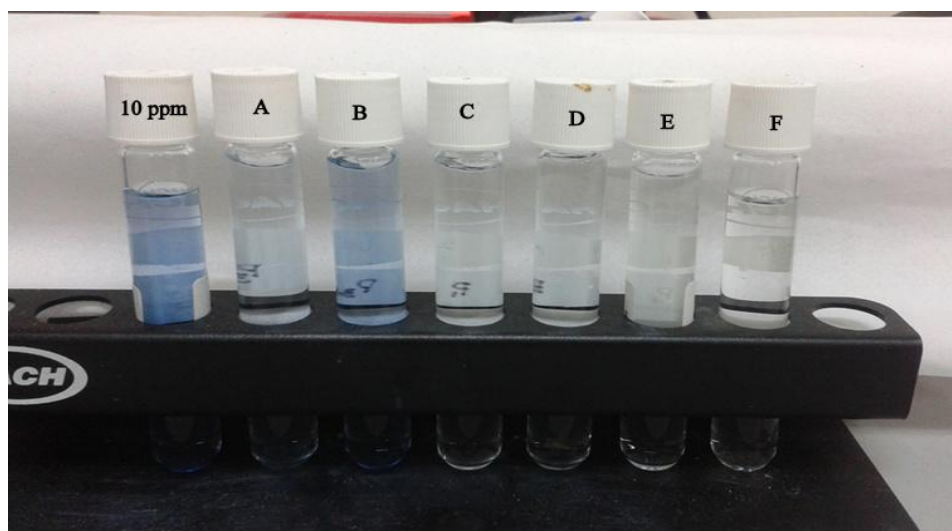


Figure 6.15 Images showing rejection of Reactive Black 5 by membranes A) P-A B) P-B C) P-0.5-A D) P-0.5-B E) P-1.0-A F) P-1.0-B

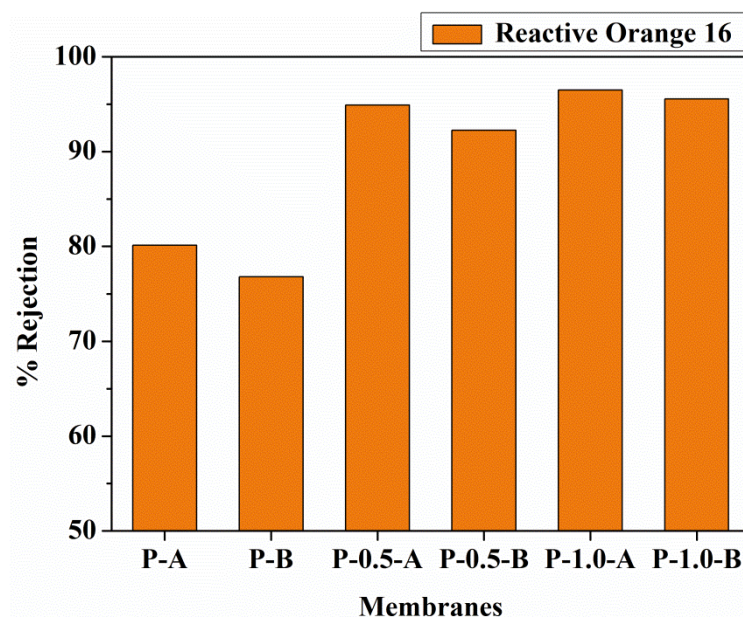


Figure 6.16 Dye Rejection by membranes for Reactive Orange 16

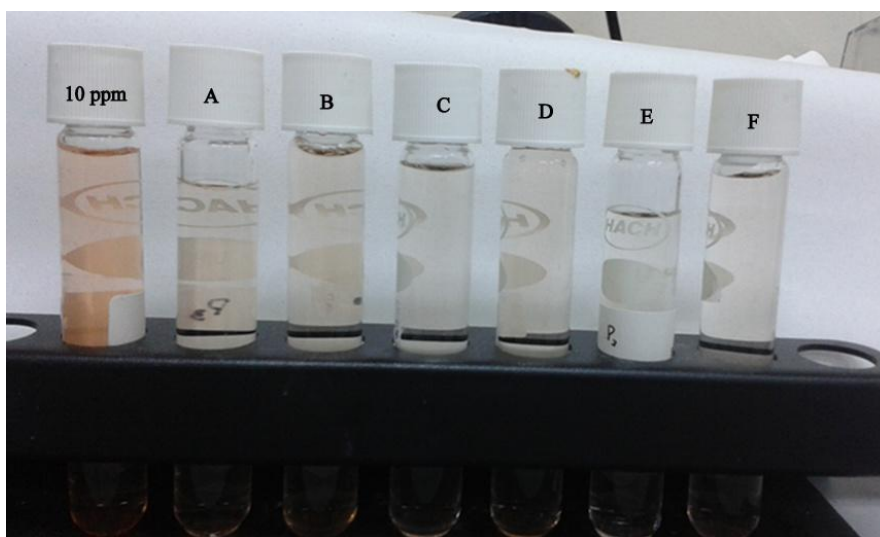


Figure 6.17 Images showing rejection of Reactive Orange 16 by membranes A) P-A
B) P-B C) P-0.5-A D) P-0.5-B E) P-1.0-A F) P-1.0-B

6.5 CONCLUSIONS

Polysulfone hollow fiber membranes with different amount of PANI-TiO₂ nanocomposites were fabricated. The air gap distance was also varied during fabrication for each composition. The PANI-TiO₂ content and air gap distance affected the morphology, permeation properties of the membranes. With the higher

content of PANI-TiO₂ nanocomposite and higher air gap distance, finger-like projections in the membranes decreased. The antifouling ability and hydrophilicity of the membranes increased with the addition of PANI-TiO₂. The membrane (P-1.0-A) showed a maximum rejection of 81.5% and 96.5% for Reactive Black 5 and Reactive Orange 16 dyes respectively. Thus the PANi-TiO₂ nanocomposite hollow fiber membranes, can be used for dye removal from aqueous solutions by suitably varying the air gap distance and PANI-TiO₂ content.

CHAPTER 7

SUMMARY AND CONCLUSIONS

Abstract

This chapter summarizes the entire work in brief and draws a comparison between in house synthesized membranes in terms of their properties and performance. It also lists the major conclusions drawn from the work.

7.1 SUMMARY

- A total of twenty seven membranes (5 series) with different compositions were prepared in this research work
- Among the twenty seven membranes, twenty one were flat sheet membranes and six were hollow fiber membranes
- Different nanomaterials based on Polyaniline and TiO₂ were synthesized in this work which include Polyaniline nanofibers, Polyaniline coated TiO₂, sulfated TiO₂ and aminated TiO₂
- The morphology of the prepared membranes was studied using SEM, AFM
- The performance of the prepared membranes was evaluated by examining the water permeation property, surface hydrophilicity, water uptake capacity antifouling study
- The synthesized membranes were subjected to water purification with respect to heavy metal ion rejection and dye removal. Following are the important results obtained
 1. The PVDF membrane containing 1.0 wt. % of PANI nanofibers showed a maximum rejection of 98.52% and 97.38% for Pb²⁺ and Cd²⁺ respectively during Polymer Enhanced Ultrafiltration Process (PEUF)
 2. The membrane containing 1.0 wt.% of PANI-TiO₂ exhibited a rejection of 83.75% and 73.41% during the PUEF process and 68% and 53.78% during UF respectively.
 3. A maximum of 90.4% rejection was obtained for Methylene Blue (MB) for the membrane having 2.0 wt% of S-TiO₂ under UV light radiation.
 4. The hollow fiber membrane, P-1.0-A dye rejection of 81.5% and 96.5% for Reactive Black 5 and Reactive Orange 16 dyes respectively.
 5. Polysulfone membranes (P-AS) was successful in removing Cd²⁺ metal ions up to 75.6% from aqueous solutions

The performance of all the prepared membranes in terms of PWF, contact angle and antifouling ability (% FRR) are compared below. The five series of membranes are named as follows

Table 7.1 Membrane series

Membrane series name	Membranes
M-0-4	M-0, M-1, M-2, M-3, M-4
P-0.1.5	P-0, P-0.05, P-0.5, P-1.0, P-1.5
S-0-2.0	S-0, S-0.05, S-0.5, S-1.0, S-1.5, S-2.0
P-Aminated	P, P-T, P-AT, P-S, P-AS
HF	P-A, P-B, P-0.5-A, P-0.5-B, P-1.0-A, P-1.0-B

Figure 7.1 shows the PWF of ultrafiltration membranes measured at 2 MPa. It shows that the PVDF membranes containing PANI nanofibers showed highest PWF. This may be due to the larger pore size of the membranes. The hollow fiber PSf membranes containing PANI-TiO₂ showed higher flux than flat sheet PSf membranes containing PANI-TiO₂. This proves that the hollow fiber membranes have greater productivity than the flat sheet membranes.

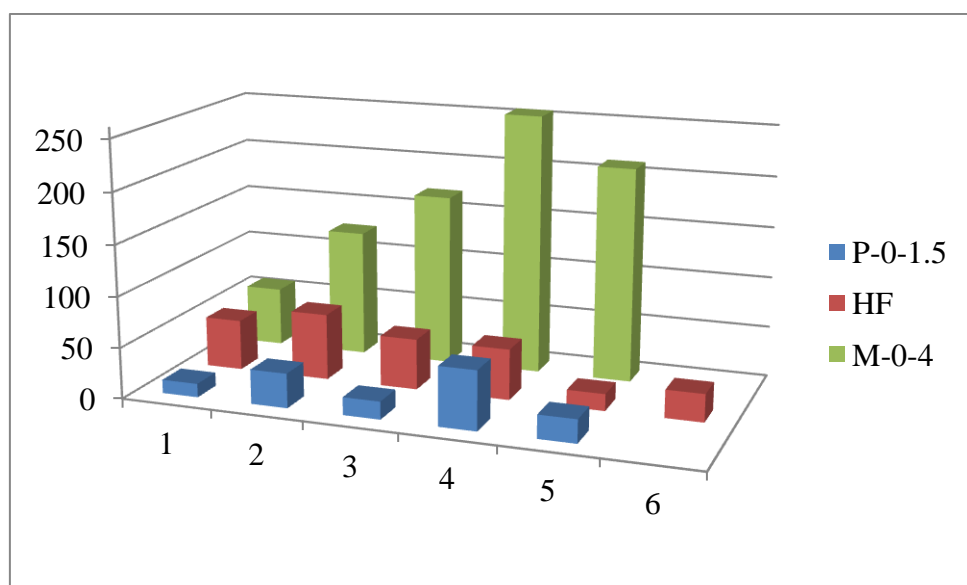


Figure 7.1 PWF (L/m²h) of UF membranes at 0.2 MPa

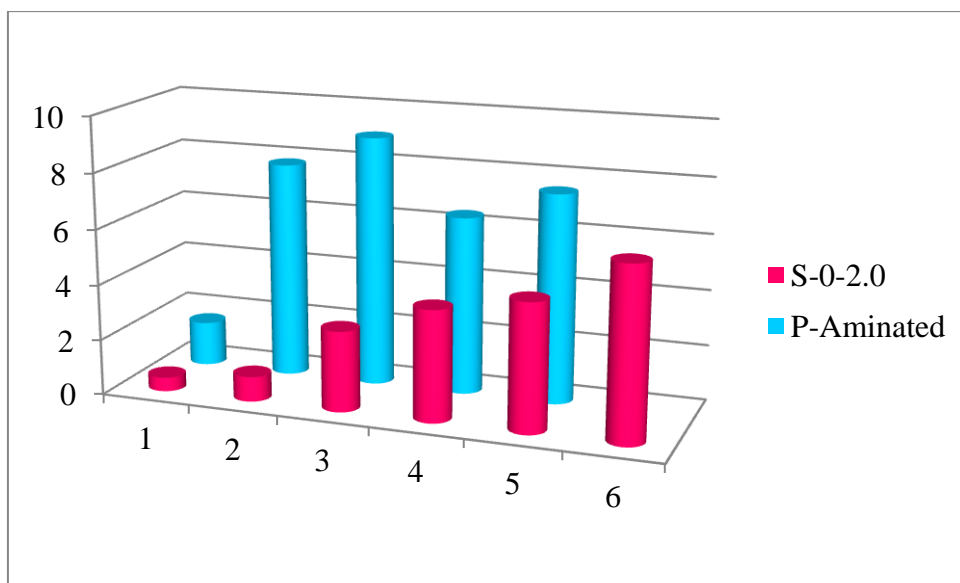


Figure 7.2 PWF (L/m²h) of NF membranes at 0.6 MPa

Figure 7.2 gives the PWF of NF membranes measured at 6 MPa. The neat PSf membranes in both the series showed lower flux. P-Aminated series showed higher flux because in this series all the membranes contained 1.0 wt.% of nanoparticles whereas in the case of S-0-2.0 series, nanoparticles were added in increasing concentrations from 0.05 to 2.0 wt.% However the flux of the membranes of P-aminated series was higher than the highest composition (2.0 wt.% of S-TiO₂) of S-0-2.0 series.

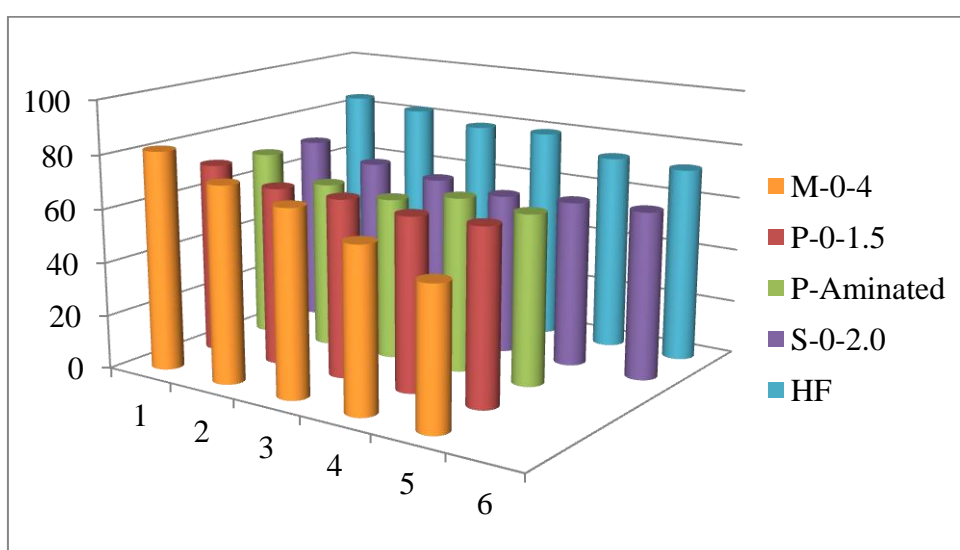


Figure 7.3 Contact Angle (in degrees) of membranes

Figure 7.3 shows the contact angle of all the synthesized membranes. All the series of membranes showed decrease in the contact angle values with the addition of nanomaterials in the membranes. The lowest contact angle was shown by M-4 membrane of M-0-4 series, containing 1.5 wt.% of PANI nanofibers.

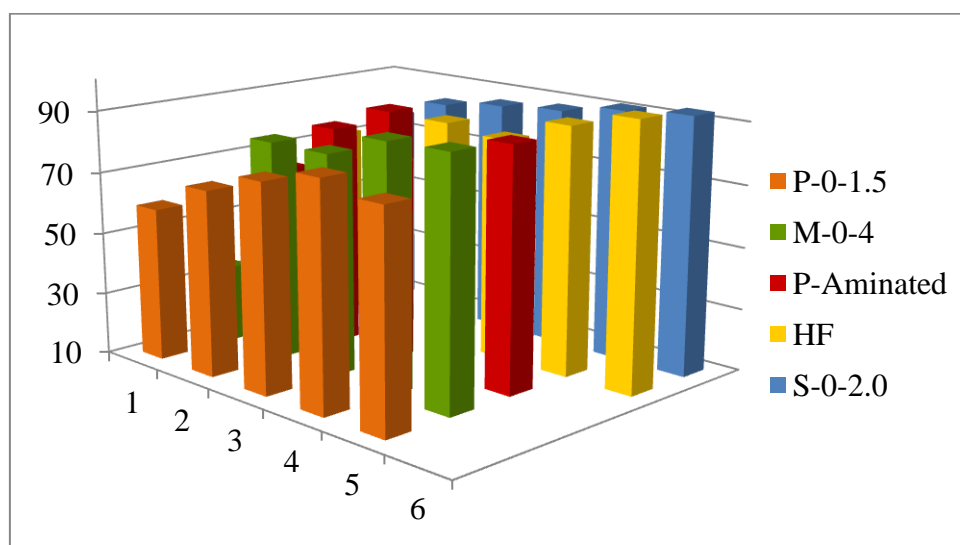


Figure 7.4 % FRR of the membranes

The antifouling ability of the membranes was studied by measuring the % FRR values for the membranes. All the membrane series showed an increasing trend in the % FRR values. Among all the membranes, the hollow fibre membrane containing 1.0 wt.% of PANI-TiO₂ showed highest flux recovery ratio of 95.46%

7.2 CONCLUSIONS

The major conclusions of the present work are listed below

- ✓ The addition of PANI and TiO₂ nanocomposites improve the properties and performance of the PVDF and PSf membranes
- ✓ There exists threshold content for the nanomaterials in the membranes beyond which the nanomaterials agglomerate in the membranes
- ✓ The change in spinning parameters like air gap distance during hollow fibre membrane fabrication brings about change in membrane morphology and performance. Lower the air gap distance, better is the performance of the membrane

- ✓ The well performed membranes in this research work can be used for the heavy metal ion removal and dye removal from aqueous solutions under suitable conditions

The nanocomposite membranes prepared in this work can be subjected to further studies of heavy metal ion removal using some other metal ions and removal of few other dyes. Also the different nanomaterials and the nanocomposites prepared in this work can serve as a guiding path for preparing new membranes with novel applications.

LIST OF PUBLICATIONS

Pereira, V. R., Isloor, A. M., Bhat, U. K. and Ismail, A. F. (2014). "Preparation and antifouling properties of PVDF ultrafiltration membranes with polyaniline (PANI) nanofibers and hydrolysed PSMA (H-PSMA) as additives." *Desalination*, 351, 220-227.

Pereira, V. R., Isloor, A. M., Al Ahmed, A. and Ismail, A. (2015). "Preparation, characterization and the effect of PANI coated TiO₂ nanocomposites on the performance of polysulfone ultrafiltration membranes." *New J. Chem.*, 39, 703-712.

Pereira, V. R., Isloor, A. M., Bhat, U. K., Ismail, A., Obaid, A. and Fun, H.-K. (2015). "Preparation and performance studies of polysulfone-sulfated nano-titania (S-TiO₂) nanofiltration membranes for dye removal." *RSC Adv.*, 5, 53874-53885.

Pereira, V. R., Isloor, A. M. and Ismail, A. "Preparation of PANI-TiO₂ nanocomposite polysulfone hollow fibre membranes for dye removal." Communicated to *Sep. Purif. Technol.*

Pereira, V. R., Isloor, A. M. and Ismail, A. "Preparation and characterization of Polysulfone membranes containing TiO₂, SiO₂ and 3-Aminopropyltriethoxysilane (APTES) modified TiO₂ and SiO₂ nanocomposites" Communicated to *J. Membr. Sci.*

LIST OF CONFERENCES ATTENDED

Attended International Conference on Natural Polymers & Biomaterials (ICNP 2012), Mahatma Gandhi University, Kottayam, India.

Presented a poster on a research paper titled "Preparation of PVDF Ultrafiltration membranes with Polyaniline (PANI) nanofibers and Hydrolysed PSMA (H-PSMA) as additives" at 13th Eurasia International Conference on Chemical Sciences (2014) at Indian Institute of Science, Bangalore, India.

REFERENCES

Abdal-Hay, A., Mousa, H. M., Khan, A., Vanegas, P. and Lim, J. H. (2014). "TiO₂ nanorods coated onto nylon 6 nanofibers using hydrothermal treatment with improved mechanical properties." *Colloids Surf.,A*, 457, 275-281.

Ahmed, S. M., El-Dib, F. I., El-Gendy, N. S., Sayed, W. M. and El-Khodary, M. (2012). "A kinetic study for the removal of anionic sulphonated dye from aqueous solution using nano-polyaniline and Baker's yeast." *Arabian J. Chem.*

Akbari, A., Desclaux, S., Rouch, J. and Remigy, J. (2007). "Application of nanofiltration hollow fibre membranes, developed by photografting, to treatment of anionic dye solutions." *J. Membr. Sci.*, 297, 243-252.

Aluigi, A., Rombaldoni, F., Tonetti, C. and Jannoke, L. (2014). "Study of Methylene Blue adsorption on keratin nanofibrous membranes." *J. Hazard. Mater.*, 268, 156-165.

Aminabhavi, T. M. and Patil, M. B. (2010). "Nanocomposite membranes of poly (vinyl alcohol) loaded with polyaniline-coated TiO₂ and TiO₂ nanoparticles for the pervaporation dehydration of aqueous mixtures of 1, 4-dioxane and tetrahydrofuran." *Des. Monomers Polym.*, 13, 497-508.

Arantes, T. M., Pinto, A. H., Leite, E. R., Longo, E. and Camargo, E. R. (2012). "Synthesis and optimization of colloidal silica nanoparticles and their functionalization with methacrylic acid." *Colloids Surf., A*, 415, 209-217.

Arthanareeswaran, G., Thanikaivelan, P. and Raajenthiren, M. (2008). "Fabrication and Characterization of CA/PSf/SPEEK Ternary Blend Ultrafiltration Membranes." *Ind. Eng. Chem. Res.*, 47, 1488-1494.

Bhaiswar, J. B., Salunkhe, M. Y. and Dongre, S. P. (2013). "Synthesis, Characterization and Thermal, Electrical study of CdS-Polyaniline Nanocomposite via Oxidation Polymerization." *Int. J. Sci. Res. Public*, 3, 1-4.

Chanda, M. and Roy, S. K. (2008). *Industrial polymers, specialty polymers, and their applications*. CRC Press.

Chen, Y., Hu, X., Hu, X., Zhang, S. and Zhang, Y. (2015). "Polymeric hollow fiber membranes prepared by dual pore formation mechanism." *Mater. Lett.*, 143, 315-318.

Cheng, F., Sajedin, S. M., Kelly, S. M., Lee, A. F. and Kornherr, A. (2014). "UV-stable paper coated with APTES-modified P25 TiO₂ nanoparticles." *Carbohydr. Polym.*, 114, 246-252.

Cheng, X. Q., Shao, L. and Lau, C. H. (2015). "High flux polyethylene glycol based nanofiltration membranes for water environmental remediation." *J. Membr. Sci.*, 476, 95-104.

Chung, T. S. and Hu, X. (1997). "Effect of air-gap distance on the morphology and thermal properties of polyethersulfone hollow fibers." *J. Appl. Polym. Sci.*, 66, 1067-1077.

Daraei, P., Madaeni, S. S., Ghaemi, N., Salehi, E., Khadivi, M. A., Moradian, R. and Astinchap, B. (2012). "Novel polyethersulfone nanocomposite membrane prepared by PANI/Fe₃O₄ nanoparticles with enhanced performance for Cu(II) removal from water." *J. Membr. Sci.*, 415-416, 250-259.

Debnath, S., Ballav, N., Nyoni, H., Maity, A. and Pillay, K. (2015). "Optimization and mechanism elucidation of the catalytic photo-degradation of the dyes Eosin Yellow (EY) and Naphthol blue black (NBB) by a polyaniline-coated titanium dioxide nanocomposite." *Appl. Catal. B.*, 163, 330-342.

Dzinun, H., Othman, M. H. D., Ismail, A., Puteh, M. H., Rahman, M. A. and Jaafar, J. (2015). "Morphological study of co-extruded dual-layer hollow fiber membranes incorporated with different TiO₂ loadings." *J. Membr. Sci.*, 479, 123-131.

Dzinun, H., Othman, M. H. D., Ismail, A. F., Puteh, M. H., Rahman, M. A. and Jaafar, J. (2015). "Photocatalytic degradation of nonylphenol by immobilized TiO₂ in dual layer hollow fibre membranes." *Chem. Eng. J. (Lausanne)*, 269, 255-261.

Eisazadeh, A., Eisazadeh, H. and Kassim, K. A. (2013). "Removal of Pb (II) using polyaniline composites and iron oxide coated natural sand and clay from aqueous solution." *Synth. Met.*, 171, 56-61.

Emadzadeh, D., Lau, W. J., Matsuura, T., Rahbari-Sisakht, M. and Ismail, A. F. (2014). "A novel thin film composite forward osmosis membrane prepared from PSf–TiO₂ nanocomposite substrate for water desalination." *Chem. Eng. J. (Lausanne)*, 237, 70-80.

Fan, Z., Wang, Z., Duan, M., Wang, J. and Wang, S. (2008). "Preparation and characterization of polyaniline/polysulfone nanocomposite ultrafiltration membrane." *J. Membr. Sci.*, 310, 402-408.

Fan, Z., Wang, Z., Sun, N., Wang, J. and Wang, S. (2008). "Performance improvement of polysulfone ultrafiltration membrane by blending with polyaniline nanofibers." *J. Membr. Sci.*, 320, 363-371.

Feng, C., Khulbe, K., Matsuura, T. and Ismail, A. (2013). "Recent progresses in polymeric hollow fiber membrane preparation, characterization and applications." *Sep. Purif. Technol.*, 111, 43-71.

Fradj, A. B., Hamouda, S. B., Ouni, H., Lafi, R., Gzara, L. and Hafiane, A. (2014). "Removal of methylene blue from aqueous solutions by poly (acrylic acid) and poly (ammonium acrylate) assisted ultrafiltration." *Sep. Purif. Technol.*, 133, 76-81.

Gambhire, A., Lande, M., Arbad, B., Rathod, S., Gholap, R. and Patil, K. (2011). "Degradation of methylene blue via photocatalysis of transition metal-loaded sulfated TiO₂." *Mater. Chem. Phys.*, 125, 807-812.

Gradzik, B., El Fray, M. and Wisniewska, E. (2011). "Surface modification of TiO₂ and SiO₂ nanoparticles for application in polymeric nanocomposites." *Chemik*, 65, 621-626.

Haddadine-Rahmoun, N., Amrani, F., Arrighi, V. and Cowie, J. M. G. (2008). "Interpolymer complexation in hydrolysed poly(styrene-co-maleic anhydride)/poly(styrene-co-4-vinylpyridine)." *Eur. Polym. J.*, 44, 821-831.

Hamid, N., Ismail, A. F., Matsuura, T., Zularisam, A., Lau, W. J., Yuliwati, E. and Abdullah, M. S. (2011). "Morphological and separation performance study of polysulfone/titanium dioxide (PSF/TiO₂) ultrafiltration membranes for humic acid removal." *Desalination*, 273, 85-92.

Han, Y.-G., Kusunose, T. and Sekino, T. (2009). "A study of conductive elastomer composites reinforced with sulfonic acid doped polyaniline coated titanium dioxide." *J. Ceram Process Res.*, 10, 208-211.

Hsieh, H. (1996). *Inorganic membranes for separation and reaction*. Elsevier.

Huang, H., Qu, X., Ji, X., Gao, X., Zhang, L., Chen, H. and Hou, L. (2013). "Acid and multivalent ion resistance of thin film nanocomposite RO membranes loaded with silicalite-1 nanozeolites." *J. Mater. Chem. A*, 1, 11343-11349.

Huang, J.-H., Zhou, C.-F., Zeng, G.-M., Li, X., Niu, J., Huang, H.-J., Shi, L.-J. and He, S.-B. (2010). "Micellar-enhanced ultrafiltration of methylene blue from dye wastewater via a polysulfone hollow fiber membrane." *J. Membr. Sci.*, 365, 138-144.

Huang, J. and Kaner, R. B. (2004). "Nanofiber formation in the chemical polymerization of aniline: a mechanistic study." *Angew. Chem. Int. Ed. Engl.*, 43, 5817-21.

Jeong, W.-H., Amna, T., Ha, Y.-M., Hassan, M. S., Kim, H.-C. and Khil, M.-S. (2014). "Novel PANI nanotube-TiO₂ composite as efficient chemical and biological disinfectant." *Chem. Eng. J. (Lausanne)*, 246, 204-210.

Jyothi, M., Nayak, V., Padaki, M., Balakrishna, R. G. and Soontarapa, K. (2016). "Aminated polysulfone/TiO₂ composite membranes for an effective removal of Cr (VI)." *Chem. Eng. J. (Lausanne)*, 283, 1494-1505.

Kajekar, A. J., Dodamani, B., Isloor, A. M., Karim, Z. A., Cheer, N. B., Ismail, A. and Shilton, S. J. (2015). "Preparation and characterization of novel PSf/PVP/PANI-nanofiber nanocomposite hollow fiber ultrafiltration membranes and their possible applications for hazardous dye rejection." *Desalination*, 365, 117-125.

Katoch, A., Burkhart, M., Hwang, T. and Kim, S. S. (2012). "Synthesis of polyaniline/TiO₂ hybrid nanoplates via a sol-gel chemical method." *Chem. Eng. J. (Lausanne)*, 192, 262-268.

Khulbe, K. C., Feng, C. and Matsuura, T. (2007). *Synthetic polymeric membranes: characterization by atomic force microscopy*, Springer Science & Business Media.

Kim, J.-H., Kim, S.-K., Nam, K. and Kim, D.-W. (2012). "Composite proton conducting membranes based on Nafion and sulfonated SiO₂ nanoparticles." *J. Membr. Sci.*, 415-416, 696-701.

Kim, J. and Bruggenb, B. V. D. (2010). "The use of nanoparticles in polymeric and ceramic membrane structures: Review of manufacturing procedures and performance improvement for water treatment." *Environ. Pollut.*, 158, 2335-2349.

Korminouri, F., Rahbari-Sisakht, M., Matsuura, T. and Ismail, A. (2015). "Surface modification of polysulfone hollow fiber membrane spun under different air-gap lengths for carbon dioxide absorption in membrane contactor system." *Chem. Eng. J. (Lausanne)*, 264, 453-461.

Krishnakumar, B. and Swaminathan, M. (2011). "Solvent free synthesis of quinoxalines, dipyridophenazines and chalcones under microwave irradiation with sulfated Degussa titania as a novel solid acid catalyst." *J. Mol. Catal. A: Chem.*, 350, 16-25.

Kumar, R., Isloor, A. M., Ismail, A., Rashid, S. A. and Ahmed, A. A. (2013). "Permeation, antifouling and desalination performance of TiO₂ nanotube incorporated PSf/CS blend membranes." *Desalination*, 316, 76-84.

Kumar, R., Isloor, A. M., Ismail, A. F. and Matsuura, T. (2013). "Synthesis and characterization of novel water soluble derivative of Chitosan as an additive for polysulfone ultrafiltration membrane." *J. Membr. Sci.*, 440, 140-147.

Kumar, R., Isloor, A. M., Ismail, A. F., Rashid, S. A. and Matsuura, T. (2013). "Polysulfone–Chitosan blend ultrafiltration membranes: preparation, characterization, permeation and antifouling properties." *RSC Adv.*, 3, 7855.

Kumar, R., Ismail, A., Kassim, M. and Isloor, A. M. (2013). "Modification of PSf/PIAM membrane for improved desalination applications using Chitosan coagulation media." *Desalination*, 317, 108-115.

Lalia, B. S., Kochkodan, V., Hashaikheh, R. and Hilal, N. (2013). "A review on membrane fabrication: Structure, properties and performance relationship." *Desalination*, 326, 77-95.

Li, H., Lin, Y., Luo, Y., Yu, P. and Hou, L. (2011). "Relating organic fouling of reverse osmosis membranes to adsorption during the reclamation of secondary effluents containing methylene blue and rhodamine B." *J. Hazard. Mater.*, 192, 490-499.

Li, N. N., Fane, A. G., Ho, W. W. and Matsuura, T. (2011). *Advanced membrane technology and applications*. John Wiley & Sons, New Jersey.

Li, Y., Yu, Y., Wu, L. and Zhi, J. (2013). "Processable polyaniline/titania nanocomposites with good photocatalytic and conductivity properties prepared via peroxo-titanium complex catalyzed emulsion polymerization approach." *Appl. Surf. Sci.*, 273, 135-143.

Liang, X., Su, Y., Yang, Y. and Qin, W. (2012). "Separation and recovery of lead from a low concentration solution of lead(II) and zinc(II) using the hydrolysis production of poly styrene-co-maleic anhydride." *J. Hazard. Mater.*, 203-204, 183-187.

Liao, Y., Yu, D.-G., Wang, X., Chain, W., Li, X.-G., Hoek, E. M. and Kaner, R. B. (2013). "Carbon nanotube-templated polyaniline nanofibers: synthesis, flash welding and ultrafiltration membranes." *Nanoscale*, 5, 3856-3862.

Liu, Z., Miao, Y.-E., Liu, M., Ding, Q., Tjiu, W. W., Cui, X. and Liu, T. (2014). "Flexible polyaniline-coated TiO₂/SiO₂ nanofiber membranes with enhanced visible-light photocatalytic degradation performance." *J. Colloid Interface Sci.*, 424, 49-55.

Lokesh, B. G., Rao, K. S. V. K., Reddy, K. M., Rao, K. C. and Rao, P. S. (2008). "Novel nanocomposite membranes of sodium alginate filled with polyaniline-coated titanium dioxide for dehydration of 1,4-dioxane/water mixtures." *Desalination*, 233, 166-172.

Macanas, J., Ouyang, L., Bruening, M. L., Muñoz, M., Remigy, J.-C. and Lahitte, J.-F. (2010). "Development of polymeric hollow fiber membranes containing catalytic metal nanoparticles." *Catal. Today*, 156, 181-186.

Maheswari, P., Barghava, P. and Mohan, D. (2013). "Preparation, morphology, hydrophilicity and performance of poly (ether-ether- sulfone) incorporated cellulose acetate ultrafiltration membranes." *J. Polym. Res.*, 20, 1-17.

Mahlambi, M. M., Mahlangu, O. T., Vilakati, G. D. and Mamba, B. B. (2014). "Visible light photodegradation of Rhodamine B dye by two forms of Carbon-Covered Alumina Supported TiO₂/Polysulfone membranes." *Ind. Eng. Chem. Res.*, 53, 5709-5717.

Martín, A., Arsuaga, J. M., Roldán, N., De Abajo, J., Martínez, A. and Sotto, A. (2015). "Enhanced ultrafiltration PES membranes doped with mesostructured functionalized silica particles." *Desalination*, 357, 16-25.

Martínez, A., González, C., Porras, M. and Gutiérrez, J. M. (2005). "Nano-sized latex particles obtained by emulsion polymerization using an amphiphilic block copolymer as surfactant." *Colloids Surf., A*, 270-271, 67-71.

Min, M., Shen, L., Hong, G., Zhu, M., Zhang, Y., Wang, X., Chen, Y. and Hsiao, B. S. (2012). "Micro-nano structure poly(ether sulfones)/poly(ethyleneimine) nanofibrous affinity membranes for adsorption of anionic dyes and heavy metal ions in aqueous solution." *Chem. Eng. J. (Lausanne)*, 197, 88-100.

Misdan, N., Lau, W. J. and Ismail, A. F. (2012). "Seawater Reverse Osmosis (SWRO) desalination by thin-film composite membrane—Current development, challenges and future prospects." *Desalination*, 287, 228-237.

Moghimifar, V., Raisi, A. and Aroujalian, A. (2014). "Surface modification of polyethersulfone ultrafiltration membranes by corona plasma-assisted coating TiO₂ nanoparticles." *J. Membr. Sci.*, 461, 69-80.

Mohamed, M. M. and Al-Esaimi, M. M. (2006). "Characterization, adsorption and photocatalytic activity of vanadium-doped TiO₂ and sulfated TiO₂ (rutile) catalysts: degradation of methylene blue dye." *J. Mol. Catal. A: Chem.*, 255, 53-61.

Mohapatra, P. and Parida, K. (2006). "Photocatalytic activity of sulfate modified titania 3: decolorization of methylene blue in aqueous solution." *J. Mol. Catal. A: Chem.*, 258, 118-123.

Mondal, M. and De, S. (2016). "Treatment of textile plant effluent by hollow fiber nanofiltration membrane and multi-component steady state modeling." *Chem. Eng. J. (Lausanne)*, 285, 304-318.

Mozia, S., Toyoda, M., Tsumura, T., Inagaki, M. and Morawski, A. W. (2007). "Comparison of effectiveness of methylene blue decomposition using pristine and carbon-coated TiO₂ in a photocatalytic membrane reactor." *Desalination*, 212, 141-151.

Mulder, M. (1996). *Basic principles of membrane technology*. Springer Science & Business Media, The Netherlands.

Nagendran, A., Vijayalakshmi, A., Arockiasamy, D. L., Shobana, K. H. and Mohan, D. (2008). "Toxic metal ion separation by cellulose acetate/sulfonated poly(ether

imide) blend membranes: Effect of polymer composition and additive." *J. Hazard. Mater.*, 155, 477-485.

Nair, A. K., Isloor, A. M., Kumar, R. and Ismail, A. F. (2013). "Antifouling and performance enhancement of polysulfone ultrafiltration membranes using CaCO₃ nanoparticles." *Desalination*, 322, 69-75.

Nasirian, S. and Milani Moghaddam, H. (2014). "Hydrogen gas sensing based on polyaniline/anatase titania nanocomposite." *Int. J. Hydrogen Energy*, 39, 630-642.

Ng, L. Y., Mohammad, A. W., Leo, C. P. and Hilal, N. (2013). "Polymeric membranes incorporated with metal/metal oxide nanoparticles: A comprehensive review." *Desalination*, 308, 15-33.

Oh, S., Kang, T., Kim, H., Moon, J., Hong, S. and Yi, J. (2007). "Preparation of novel ceramic membranes modified by mesoporous silica with 3-aminopropyltriethoxysilane (APTES) and its application to Cu²⁺ separation in the aqueous phase." *J. Membr. Sci.*, 301, 118-125.

Padaki, M., Isloor, A. M., Belavadi, G. and Prabhu, K. N. (2011). "Preparation, Characterization and Performance Study of Poly(isobutylene-alt-maleic anhydride) [PIAM] and Polysulfone [PSf] Composite Membranes before and after Alkali Treatment." *Ind. Eng. Chem. Res.*, 50, 6528-6534.

Padaki, M., Isloor, A. M. and Wanichapichart, P. (2011). "Polysulfone/N-phthaloylchitosan novel composite membranes for salt rejection application." *Desalination*, 279, 409-414.

Pang, Z., Fu, J., Luo, L., Huang, F. and Wei, Q. (2014). "Fabrication of PA6/TiO₂/PANI composite nanofibers by electrospinning–electrospraying for ammonia sensor." *Colloids Surf., A*, 461, 113-118.

Peng, J., Su, Y., Chen, W., Shi, Q. and Jiang, Z. (2010). "Effects of coagulation bath temperature on the separation performance and antifouling property of poly (ether sulfone) ultrafiltration membranes." *Ind. Eng. Chem. Res.*, 49, 4858-4864.

Pereira, V. R., Isloor, A. M., Bhat, U. K. and Ismail, A. F. (2014). "Preparation and antifouling properties of PVDF ultrafiltration membranes with polyaniline (PANI) nanofibers and hydrolysed PSMA (H-PSMA) as additives." *Desalination*, 351, 220-227.

Pereira, V. R., Isloor, A. M., Al Ahmed, A. and Ismail, A. (2015). "Preparation, characterization and the effect of PANI coated TiO₂ nanocomposites on the performance of polysulfone ultrafiltration membranes." *New J. Chem.*, 39, 703-712.

Pereira, V. R., Isloor, A. M., Bhat, U. K., Ismail, A., Obaid, A. and Fun, H.-K. (2015). "Preparation and performance studies of polysulfone-sulfated nano-titania (S-TiO₂) nanofiltration membranes for dye removal." *RSC Adv.*, 5, 53874-53885.

Porter, M. C. (1989). "Handbook of industrial membrane technology." Noyes Publication.

Qin, A., Li, X., Zhao, X., Liu, D. and He, C. (2015). "Preparation and characterization of nano-chitin whisker reinforced PVDF membrane with excellent antifouling property." *J. Membr. Sci.*, 480, 1-10.

Rabiee, H., Farahani, M. H. D. A. and Vatanpour, V. (2014). "Preparation and characterization of emulsion poly (vinyl chloride)(EPVC)/TiO₂ nanocomposite ultrafiltration membrane." *J. Membr. Sci.*, 472, 185-193.

Radoičić, M. B., Milošević, M. V., Miličević, D. S., Suljovrujić, E. H., Ćirić-Marjanović, G. N., Radetić, M. M. and Šaponjić, Z. V. (2015). "Influence of TiO₂

nanoparticles on formation mechanism of PANI/TiO₂ nanocomposite coating on PET fabric and its structural and electrical properties." *Surf. Coat. Technol.*, 278, 38-47.

Rahimpour, A., Jahanshahi, M., Mollahosseini, A. and Rajaeian, B. (2012). "Structural and performance properties of UV-assisted TiO₂ deposited nanocomposite PVDF/SPES membranes." *Desalination*, 285, 31-38.

Rajesh, S., Senthilkumar, S., Jayalakshmi, A., Nirmala, M., Ismail, A. and Mohan, D. (2013). "Preparation and performance evaluation of poly (amide-imide) and TiO₂ nanoparticles impregnated polysulfone nanofiltration membranes in the removal of humic substances." *Colloids Surf., A*, 418, 92-104.

Razali, N. F., Mohammad, A. W., Hilal, N., Leo, C. P. and Alam, J. (2013). "Optimisation of polyethersulfone/polyaniline blended membranes using response surface methodology approach." *Desalination*, 311, 182-191.

Razmjou, A., Mansouri, J. and Chen, V. (2011). "The effects of mechanical and chemical modification of TiO₂ nanoparticles on the surface chemistry, structure and fouling performance of PES ultrafiltration membranes." *J. Membr. Sci.*, 378, 73-84.

Razmjou, A., Mansouri, J. and Chen, V. (2011). "The effects of mechanical and chemical modification of TiO₂ nanoparticles on the surface chemistry, structure and fouling performance of PES ultrafiltration membranes." *J. Membr. Sci.*, 378, 73-84.

Ren, J. and Mccutcheon, J. R. (2015). "Polyacrylonitrile supported thin film composite hollow fiber membranes for forward osmosis." *Desalination*, 372, 67-74.

Richard, W. B. (2004). "Membrane technology and applications." *John Wiley & Sons Ltd.*

Salem, M. A., Al-Ghonemiy, A. F. and Zaki, A. B. (2009). "Photocatalytic degradation of Allura red and Quinoline yellow with Polyaniline/TiO₂ nanocomposite." *Appl. Catal. B*, 91, 59-66.

Sengur, R., De Lannoy, C.-F., Turken, T., Wiesner, M. and Koyuncu, I. (2015). "Fabrication and characterization of hydroxylated and carboxylated multiwalled carbon nanotube/polyethersulfone (PES) nanocomposite hollow fiber membranes." *Desalination*, 359, 123-140.

Shannon, M. A., Bohn, P. W., Elimelech, M., Georgiadis, J. G., Marinas, B. J. and Mayes, A. M. (2008). "Science and technology for waterpurification in the coming decades." *Nature*, 452, 301-310.

Shao, L., Cheng, X. Q., Liu, Y., Quan, S., Ma, J., Zhao, S. Z. and Wang, K. Y. (2013). "Newly developed nanofiltration (NF) composite membranes by interfacial polymerization for Safranin O and Aniline blue removal." *J. Membr. Sci.*, 430, 96-105.

Shi, F., Ma, Y., Ma, J., Wang, P. and Sun, W. (2012). "Preparation and characterization of PVDF/TiO₂ hybrid membranes with different dosage of nano-TiO₂." *J. Membr. Sci.*, 389, 522-531.

Shi, F., Ma, Y., Ma, J., Wang, P. and Sun, W. (2013). "Preparation and characterization of PVDF/TiO₂ hybrid membranes with ionic liquid modified nano-TiO₂ particles." *J. Membr. Sci.*, 427, 259-269.

Shi, H., Liu, F. and Xue, L. (2013). "Fabrication and characterization of antibacterial PVDF hollow fibre membrane by doping Ag-loaded zeolites." *J. Membr. Sci.*, 437, 205-215.

Singh, R. (2006). *Hybrid Membrane Systems for Water Purification: Technology, Systems Design and Operations*. Elsevier.

Song, H., Jo, Y., Kim, S.-Y., Lee, J. and Kim, C. (2014). "Characteristics of ultrafiltration membranes fabricated from polysulfone and polymer-grafted silica nanoparticles: Effects of the particle size and grafted polymer on the membrane performance." *J. Membr. Sci.*, 466, 173-182.

Song, H. J. and Kim, C. K. (2013). "Fabrication and properties of ultrafiltration membranes composed of polysulfone and poly(1-vinylpyrrolidone) grafted silica nanoparticles." *J. Membr. Sci.*, 444, 318-326.

Subramanian, S. and Seeram, R. (2013). "New directions in nanofiltration applications — Are nanofibers the right materials as membranes in desalination?" *Desalination*, 308, 198-208.

Teli, S. B., Molina, S., Calvo, E. G., Lozano, A. E. and De Abajo, J. (2012). "Preparation, characterization and antifouling property of polyethersulfone–PANI/PMA ultrafiltration membranes." *Desalination*, 299, 113-122.

Teli, S. B., Molina, S., Sotto, A., Calvo, E. G. and Abajo, J. D. (2013). "Fouling Resistant Polysulfone–PANI/TiO₂ Ultrafiltration Nanocomposite Membranes." *Ind. Eng. Chem. Res.*, 52, 9470-9479.

Teli, S. B., Molina, S., Sotto, A., Calvo, E. G. A. and Abajob, J. D. (2013). "Fouling Resistant Polysulfone–PANI/TiO₂ Ultrafiltration Nanocomposite Membranes." *Ind. Eng. Chem. Res.*, 52, 9470-9479.

Tsai, C.-H., Lin, H.-J., Tsai, H.-M., Hwang, J.-T., Chang, S.-M. and Chen-Yang, Y.-W. (2011). "Characterization and PEMFC application of a mesoporous sulfonated

silica prepared from two precursors, tetraethoxysilane and phenyltriethoxysilane." *Int. J. Hydrogen Energy*, 36, 9831-9841.

Tsai, H., Chen, H., Lee, K. and Lai, J. (2006). "Study of the separation properties of chitosan/polysulfone composite hollow-fiber membranes." *Desalination*, 193, 129-136.

Vatanpour, V., Madaeni, S. S., Rajabi, L., Zinadini, S. and Derakhshan, A. A. (2012). "Boehmite nanoparticles as a new nanofiller for preparation of antifouling mixed matrix membranes." *J. Membr. Sci.*, 401-402, 132-143.

Vilakati, G. D., Hoek, E. M. and Mamba, B. B. (2014). "Probing the mechanical and thermal properties of polysulfone membranes modified with synthetic and natural polymer additives." *Polym. Test.*, 34, 202-210.

Wang, B., Liu, C., Yin, Y., Yu, S., Chen, K., Liu, P. and Liang, B. (2013). "Double template assisting synthesized core-shell structured titania/polyaniline nanocomposite and its smart electrorheological response." *Compos. Sci. Technol.*, 86, 89-100.

Wang, P., Ma, J., Shi, F., Ma, Y., Wang, Z. and Zhao, X. (2013). "Behaviors and Effects of Differing Dimensional Nanomaterials in Water Filtration Membranes through the Classical Phase Inversion Process: A Review." *Ind. Eng. Chem. Res.*, 52, 10355-10363.

Wei, X., Kong, X., Sun, C. and Chen, J. (2013). "Characterization and application of a thin-film composite nanofiltration hollow fiber membrane for dye desalination and concentration." *Chem. Eng. J. (Lausanne)*, 223, 172-182.

Wu, H., Mansouri, J. and Chen, V. (2013). "Silica nanoparticles as carriers of antifouling ligands for PVDF ultrafiltration membranes." *J. Membr. Sci.*, 433, 135-151.

Wu, H., Tang, B. and Wu, P. (2014). "Development of novel SiO₂-GO nanohybrid/polysulfone membrane with enhanced performance." *J. Membr. Sci.*, 451, 94-102.

Xie, S., Gan, M., Ma, L., Li, Z., Yan, J., Yin, H., Shen, X., Xu, F., Zheng, J. and Zhang, J. (2014). "Synthesis of polyaniline-titania nanotube arrays hybrid composite via self-assembling and graft polymerization for supercapacitor application." *Electrochim. Acta*, 120, 408-415.

Yan, L., Li, Y. S. and Xiang, C. B. (2005). "Preparation of poly(vinylidene fluoride)(pvdf) ultrafiltration membrane modified by nano-sized alumina (Al₂O₃) and its antifouling research." *Polymer*, 46, 7701-7706.

Yan, L., Li, Y., Xiang, C. and Xianda, S. (2006). "Effect of nano-sized Al₂O₃ -particle addition on PVDF ultrafiltration membrane performance." *J. Membr. Sci.*, 276, 162-167.

Yang, Y., Zhang, H., Wang, P., Zheng, Q. and Li, J. (2007). "The influence of nano-sized TiO₂ fillers on the morphologies and properties of PSF UF membrane." *J. Membr. Sci.*, 288, 231-238.

Yi, X., Yu, S., Shi, W., Wang, S., Sun, N., Jin, L. and Ma, C. (2013). "Estimation of fouling stages in separation of oil/water emulsion using nano-particles Al₂O₃/TiO₂ modified PVDF UF membranes." *Desalination*, 319, 38-46.

Yuliwati, E., Ismail, A. F., Matsuura, T., Kassim, M. A. and Abdullah, M. S. (2011). "Effect of modified PVDF hollow fiber submerged ultrafiltration membrane for refinery wastewater treatment." *Desalination*, 283, 214-220.

Zeng, G.-M., Li, X., Huang, J.-H., Zhang, C., Zhou, C.-F., Niu, J., Shi, L.-J., He, S.-B. and Li, F. (2011). "Micellar-enhanced ultrafiltration of cadmium and methylene blue in synthetic wastewater using SDS." *J. Hazard. Mater.*, 185, 1304-1310.

Zhan, C., Chen, F., Yang, J., Dai, D., Cao, X. and Zhong, M. (2014). "Visible light responsive sulfated rare earth doped TiO₂ fumed SiO₂ composites with mesoporosity: Enhanced photocatalytic activity for methyl orange degradation." *J. Hazard. Mater.*, 267, 88-97.

Zhang, G., Lu, S., Zhang, L., Meng, Q., Shen, C. and Zhang, J. (2013). "Novel polysulfone hybrid ultrafiltration membrane prepared with TiO₂-g-HEMA and its antifouling characteristics." *J. Membr. Sci.*, 436, 163-173.

Zhang, J., Zhang, Y., Chen, Y., Du, L., Zhang, B., Zhang, H., Liu, J. and Wang, K. (2012). "Preparation and characterization of novel polyethersulfone hybrid ultrafiltration membranes bending with modified halloysite nanotubes loaded with silver nanoparticles." *Ind. Eng. Chem. Res.*, 51, 3081-3090.

Zhang, X., Wang, Y., You, Y., Meng, H., Zhang, J. and Xu, X. (2012). "Preparation, performance and adsorption activity of TiO₂ nanoparticles entrapped PVDF hybrid membranes." *Appl. Surf. Sci.*, 263, 660-665.

Zhang, X., Wang, Y., Liu, Y., Xu, J., Han, Y. and Xu, X. (2014). "Preparation, performances of PVDF/ZnO hybrid membranes and their applications in the removal of copper ions." *Appl. Surf. Sci.*, 316, 333-340.

Zhang, Y. and Wang, R. (2014). "Novel method for incorporating hydrophobic silica nanoparticles on polyetherimide hollow fiber membranes for CO₂ absorption in a gas-liquid membrane contactor." *J. Membr. Sci.*, 452, 379-389.

Zhang, Y. and Liu, P. (2015). "Polysulfone (PSF) composite membrane with micro-reaction locations (MRLs) made by doping sulfated TiO₂ deposited on SiO₂ nanotubes (STSNs) for cleaning wastewater." *J. Membr. Sci.*, 493, 275-284.

Zhao, C., Xu, X., Chen, J. and Yang, F. (2013). "Effect of graphene oxide concentration on the morphologies and antifouling properties of PVDF ultrafiltration membranes." *Journal of Environmental Chemical Engineering*, 1, 349-354.

Zhao, S., Wang, Z., Wang, J., Yang, S. and Wang, S. (2011). "PSf/PANI nanocomposite membrane prepared by in situ blending of PSf and PANI/NMP." *J. Membr. Sci.*, 376, 83-95.

Zhao, S., Wang, Z., Wei, X., Tian, X., Wang, J., Yang, S. and Wang, S. (2011). "Comparison study of the effect of PVP and PANI nanofibers additives on membrane formation mechanism, structure and performance." *J. Membr. Sci.*, 385-386, 110-122.

Zhao, S., Wang, Z., Wei, X., Zhao, B., Wang, J., Yang, S. and Wang, S. (2011). "Performance improvement of polysulfone ultrafiltration membrane using PANiEB as both pore forming agent and hydrophilic modifier." *J. Membr. Sci.*, 385-386, 251-262.

Zhao, S., Wang, Z., Wei, X., Zhao, B., Wang, J., Yang, S. and Wang, S. (2012). "Performance Improvement of Polysulfone Ultrafiltration Membrane Using Well-Dispersed Polyaniline–Poly(vinylpyrrolidone) Nanocomposite as the Additive." *Ind. Eng. Chem. Res.*, 51, 4661-4672.

Zhao, S., Yan, W., Shi, M., Wang, Z., Wang, J. and Wang, S. (2015). "Improving permeability and antifouling performance of polyethersulfone ultrafiltration membrane by incorporation of ZnO-DMF dispersion containing nano-ZnO and polyvinylpyrrolidone." *J. Membr. Sci.*, 478, 105-116.

Zhao, Y.-F., Zhu, L.-P., Yi, Z., Zhu, B.-K. and Xu, Y.-Y. (2013). "Improving the hydrophilicity and fouling-resistance of polysulfone ultrafiltration membranes via surface zwitterionization mediated by polysulfone-based triblock copolymer additive." *J. Membr. Sci.*, 440, 40-47.

Zhao, Y.-F., Zhang, P.-B., Sun, J., Liu, C.-J., Yi, Z., Zhu, L.-P. and Xu, Y.-Y. (2015). "Versatile antifouling polyethersulfone filtration membranes modified via surface grafting of zwitterionic polymers from a reactive amphiphilic copolymer additive." *J. Colloid Interface Sci.*, 448, 380-388.

Zheng, L., Su, Y., Wang, L. and Jiang, Z. (2009). "Adsorption and recovery of methylene blue from aqueous solution through ultrafiltration technique." *Sep. Purif. Technol.*, 68, 244-249.

Zou, J., Gao, J. and Wang, Y. (2009). "Synthesis of highly active H₂O₂-sensitized sulfated titania nanoparticles with a response to visible light." *J. Photochem. Photobiol. A*, 202, 128-135.

Zulhairun, A. and Ismail, A. (2014). "The role of layered silicate loadings and their dispersion states on the gas separation performance of mixed matrix membrane." *J. Membr. Sci.*, 468, 20-30.

BIODATA

VALEEN RASHMI PEREIRA

Email: valeenrashmipereira@gmail.com

Phone No: +91-7795792198

Educational Qualification

M. Sc. in General Chemistry from NIT, Karnataka (National Institute of Technology, Karnataka-NITK) (2010-2012)

B.Sc. (Physics, Chemistry, Mathematics) from St. Aloysius College, Mangalore (2007-2010)

Research Publications

Pereira, V. R., Isloor, A. M., Bhat, U. K. and Ismail, A. F. (2014). "Preparation and antifouling properties of PVDF ultrafiltration membranes with polyaniline (PANI) nanofibers and hydrolysed PSMA (H-PSMA) as additives." *Desalination*, 351, 220-227.

Pereira, V. R., Isloor, A. M., Al Ahmed, A. and Ismail, A. (2015). "Preparation, characterization and the effect of PANI coated TiO₂ nanocomposites on the performance of polysulfone ultrafiltration membranes." *New Journal of Chemistry*, 39, 703-712.

Pereira, V. R., Isloor, A. M., Bhat, U. K., Ismail, A., Obaid, A. and Fun, H.-K. (2015). "Preparation and performance studies of polysulfone-sulfated nano-titania (S-TiO₂) nanofiltration membranes for dye removal." *RSC Advances*, 5, 53874-53885.

Additional academic achievements/experience

- ✓ Worked as a research student intern for two months (from August-October 2015) at Advanced Membrane Technology Research Centre (AMTEC), Universiti Teknologi Malaysia, Skudai, Johor, Malaysia
- ✓ Conducted laboratory practical classes for B.Tech and M.Sc students for 5 semesters at NITK Surathkal

- ✓ Worked as summer intern for 2 months in 2011 and 2012 at Jawaharlal Nehru Centre for Advanced Scientific Research (JNCASR), Bangalore
- ✓ Participated and presented papers in 3 International and national conferences
- ✓ II Rank holder in B.Sc. (Physical Sciences) Examination held in April-May 2010
- ✓ Best Outgoing Student of 2005 batch (10th Std) from Sri Mahalingeshwara English Medium School, Surathkal
- ✓ Have worked and handled instruments such as FTIR spectrophotometer, UV-visible spectrophotometer, Contact Angle Analyzer
- ✓ Have volunteered and been part of the core organizing committee for an international conference and a national symposium organized at NITK, Department of Chemistry

Personal Details

Address for correspondence	303, Mangaladhama Apartments Old Post Office Road, Surathkal-575014, Mangalore, Karnataka, India
Email Id	valeenrashmipereira@gmail.com
Contact No:	+91-7795792198
Sex	Female
Date of birth	27 July, 1989
Nationality	Indian
Languages known	English, Hindi, Kannada, Konkani
References	
1. Dr. Arun M. Isloor Associate Professor, Department of Chemistry NITK Surathkal, Karnataka, India. Contact No: +91 – 9448523990 Email: isloor@yahoo.com	2. Dr. A. Nithyananda Shetty Professor Department of Chemistry NITK Surathkal, Karnataka, India. Contact No:+91-9448779922 Email: nityashreya@gmail.com

